Univerzita Karlova v Praze

Matematicko-fyzikální fakulta

DIPLOMOVÁ PRÁCE

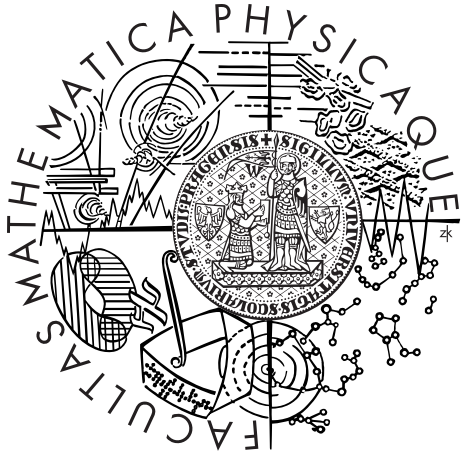

Mark Dostalík

Vliv materiálových parametrů na stabilitu termální konvekce

Katedra geofyziky

Vedoucí diplomové práce:	doc. RNDr. Ctirad Matyska, DrSc.
Studijní program:	Fyzika
Studijní obor:	Matematické a počítačové modelování ve fyzice a technice

Praha 2016

Charles University in Prague

Faculty of Mathematics and Physics

MASTER THESIS

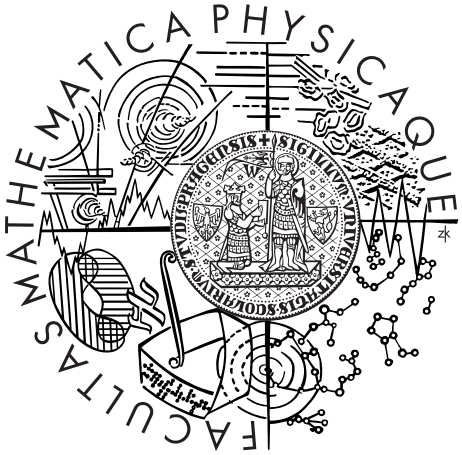

Mark Dostalík

Influence of material parameters on stability of thermal convection

Department of Geophysics

Supervisor of the master thesis:	doc. RNDr. Ctirad Matyska, DrSc.
Study programme:	Physics
Specialization:	Mathematical Modelling in Physics and Technology

Prague 2016

I declare that I carried out this master thesis independently, and only with the cited sources, literature and other professional sources.

I understand that my work relates to the rights and obligations under the Act No. 121/2000 Coll., the Copyright Act, as amended, in particular the fact that the Charles University in Prague has the right to conclude a license agreement on the use of this work as a school work pursuant to Section 60 paragraph 1 of the Copyright Act.

In ..... on ..... Author signature

I would like to thank my supervisor, doc. RNDr. Ctirad Matyska, DrSc., for introducing me to the topic of my thesis, for his valuable advice and remarks and his helpfulness throughout the writing of this thesis. I thank my advisor, Mgr. Vít Průša, PhD., for his patient guidance, encouragement and for all the time he invested in the supervision. Lastly, I am thankful to my family for their support during the completion of this thesis.

Název práce: Vliv materiálových parametrů na stabilitu termální konvekce

Autor: Mark Dostalík

Katedra: Katedra geofyziky

Vedoucí bakalářské práce: doc. RNDr. Ctirad Matyska, DrSc., katedra geofyziky

Abstrakt:

Diplomová práce je zaměřena na zkoumání Rayleigh-Bénardova problému v rozšířené konfiguraci aproximující podmínky v zemském plášti. Cílem práce je vyhodnocení vlivu hloubkově a teplotně závislých materiálových parametrů, disipace, adiabatického zahřívání/ochlazování a teplotních zdrojů na kvalitativní charakter termální konvekce. Identifikujeme kritické hodnoty bezrozměrných veličin, které určují počátek konvekce a charakterizujeme dominantní konvekční vzorce v mezně superkritickém stavu. Tyto problémy jsou řešeny aplikací lineární teorie stability a slabě nelineární analýzy. Nalezený charakter konvekce se podstatně liší od standardního případu Rayleigh-Bénardovy konvekce.

Klíčová slova: Rayleigh-Bénardova konvekce, Boussinesqova aproximace, lineární teorie stability, slabě nelineární analýza, Čebyševova spektrální metoda

Title: Influence of material parameters on stability of thermal convection

Author: Mark Dostalík

Department: Department of Geophysics

Supervisor of the master thesis: doc. RNDr. Ctirad Matyska, DrSc., Department of Geophysics

Abstract:

The thesis is focused on the investigation of Rayleigh-Bénard problem in an extended setting approximating the conditions in the Earth's mantle. The aim is to evaluate the influence of depth- and temperature- dependent material parameters, dissipation, adiabatic heating/cooling and heat sources on the qualitative characteristics of thermal convection. We identify the critical values of dimensionless parameters that determine the onset of convection and characterize the dominating convection patterns in marginally supercritical states. These issues are addressed by the application of linear stability analysis and weakly non-linear analysis. It has been found that the character of convection differ substantially from the standard case of Rayleigh-Bénard convection.

Keywords: Rayleigh-Bénard convection, Boussinesq approximation, linear stability analysis, weakly non-linear analysis, Chebyshev spectral method

Contents

Chapter 1

Introduction

Rayleigh-Bénard convection represents a flow of a fluid in a horizontal layer heated from below. The standard system of equations governing thermal convection reads

$$\operatorname{div} \mathbf{v} = 0,$$

$$\frac{1}{Pr}\left[\frac{\partial \mathbf{v}}{\partial t} + (\mathbf{v}\cdot\nabla)\,\mathbf{v}\right] = -Ra(T-T_0)\mathbf{e}_{\hat{z}} - \nabla\Pi + \Delta\mathbf{v},$$

$$\frac{\partial T}{\partial t} = \Delta T - \mathbf{v}\cdot\nabla T,$$

where the unknowns are the velocity $\mathbf{v}$, temperature T and pressure Π. The reference temperature is denoted by T_0 and dimensionless numbers arising from scaling by Pr and Ra. This system is derived from the basic laws of conservation by using the *classical Boussinesq approximation* which assumes that the material coefficients – thermal conductivity, thermal expansivity and dynamical viscosity – are constant. Moreover, the classical derivation neglects dissipation, adiabatic heating/cooling and heat sources.

However, in geophysics the material properties such as thermal conductivity, thermal expansivity and dynamic viscosity are are pressure- and temperature-dependent which makes the classical results inapplicable. Our aim is to investigate the Rayleigh-Bénard problem using the *extended Boussinesq approximation* which assumes non-constant material coefficients and also retains the effects of dissipation, adiabatic heating/cooling and heat sources.

More specifically, the presented thesis aims at

- the identification of the critical values of dimensionless parameters that determine the onset of convection,
- the characterization of dominating convection patterns in marginally supercritical states.

These issues are addressed by the application of

- linear stability analysis,
- weakly non-linear analysis.

In the rest of this introductory chapter we present the basic equations describing the Rayleigh-Bénard problem and introduce the methods of linear stability analysis and weakly non-linear analysis.

The second chapter concerns the onset of instability in both cases of the classical and extended Boussinesq approximation. We develop a numerical method for finding the critical threshold of instability and compare the numerical results with the analytical solutions which are known for the classical case. We then analyse the results for the extended Boussinesq approximation and compare them with the classical case.

In the third chapter we treat the convection in the slightly supercritical regime again in both cases of the Boussinesq aprroximation and compare the two. We quantify the evolution of convection numerically extending the model from the previous chapter.

The study of Rayleigh-Bénard problem in the case of the extended Boussinesq approximation is geophysically motivated – we are interested in thermal convection occurring in the Earth's mantle. Let us then begin with the fundamental laws of conservation describing transfer of heat in the Earth's mantle.

1.1 Basic hydrodynamic equations

See Matyska and Yuen (2007) for details in this and the following section.

By $\mathbf{x} = (x, y, z)$ we denote the spatial coordinates, by t we denote time. The operators $\{\nabla, \mathrm{div}, \Delta\}$ are defined as usual and are always taken with respect to the spatial coordinates only.

The fundamental conservation laws of continuum mechanics are as follows

Equation of continuity

$$\frac{\partial \varrho}{\partial t} + \mathrm{div}(\varrho \mathbf{v}) = 0, \tag{1.1}$$

where ϱ is the density and $\mathbf{v}$ is the velocity of motion.

Equation of motion

$$\frac{\partial(\varrho \mathbf{v})}{\partial t} + \mathrm{div}(\varrho \mathbf{v} \otimes \mathbf{v}) = \varrho \mathbf{b} + \mathrm{div}\, \mathbb{T},$$

where $\mathbf{b}$ is the body force density and $\mathbb{T}$ is the Cauchy stress tensor. In our case we consider non-rotating Earth model – there will be only gravitational force per unit mass $\mathbf{g}$ acting as the body force density. Further, we consider the Newtonian fluid, i.e.

$$\mathbb{T} = -p\mathbb{I} + \lambda(\mathrm{div}\, \mathbf{v})\mathbb{I} + 2\mu\mathbb{D}(\mathbf{v}),$$

where p is the pressure, λ and μ are viscosity coefficients (depending on p and T in general) and $\mathbb{D}(\mathbf{v}) = \frac{1}{2}\left[\nabla\mathbf{v} + (\nabla\mathbf{v})^T\right]$ is the symmetric velocity gradient. We can then rewrite the equation of motion (using the equation of continuity) in the form

$$\varrho\left[\frac{\partial\mathbf{v}}{\partial t} + (\mathbf{v}\cdot\nabla)\,\mathbf{v}\right] = \varrho\mathbf{g} - \nabla p + \nabla\left(\lambda\,\mathrm{div}\,\mathbf{v}\right) + \mathrm{div}\left(2\mu\mathbb{D}\right). \tag{1.2}$$

Heat equation

$$\varrho T\left[\frac{\partial s}{\partial t} + (\mathbf{v}\cdot\nabla)\,s\right] = \mathrm{div}(k\nabla T) + \lambda(\mathrm{div}\,\mathbf{v})^2 + 2\mu\mathbb{D}:\mathbb{D} + Q,$$

where T is the absolute temperature, s is the entropy per unit mass, k is the thermal conductivity and Q are the volumetric heat sources. The term $\mathrm{div}(k\nabla T)$ describes conduction of heat and the term $[\lambda(\mathrm{div}\,\mathbf{v})^2 + 2\mu\mathbb{D}:\mathbb{D}]$ describes the dissipation.

If we assume that there is a reference hydrostatic state characterized by $\mathbf{v} \equiv \mathbf{0}$, the hydrostatic pressure p_0, hydrostatic density ϱ_0 and hydrostatic gravity acceleration $\mathbf{g}_0$ are according to (1.2) related by the equation

$$\nabla p_0 = \varrho_0\mathbf{g}_0. \tag{1.3}$$

Moreover, if pressure deviations $\Pi = p - p_0$ are negligible in the heat equation, the transfer of heat in a homogeneous material (i.e. entropy may be considered as a function of only p and T) is then described by

$$\varrho c_p\frac{\partial T}{\partial t} = \mathrm{div}(k\nabla T) - \varrho c_p\mathbf{v}\cdot\nabla T - \varrho v^{\hat{r}}\alpha T g + \lambda(\mathrm{div}\,\mathbf{v})^2 + 2\mu\mathbb{D}:\mathbb{D} + Q, \tag{1.4}$$

where c_p is the isobaric specific heat, α is the thermal expansion coefficient and v_r denotes the radial component of velocity. The left-hand side of (1.4) represents local changes of heat balance, the second (third) term on the right-hand side describes advection of heat (adiabatic heating/cooling).

We must add to the balance equations the *equation of state* which we write in the form

$$\varrho = \varrho(p, T). \tag{1.5}$$

1.2 Boussinesq approximation

It is understood that buoyancy, and hence gravity, is responsible for the appearance of convection cells. The essence of the Boussinesq approximation thus lies in neglecting the variation of density everywhere except in the buoyancy that drives the motion.

If we neglect density changes caused by the pressure deviations $\Pi = p - p_0$, we may linearize the state equation with respect to the temperature deviations $T - T_0$, where T_0 is a reference temperature, and write

$$\varrho = \varrho_0\left[1 - \alpha(T - T_0)\right]. \tag{1.6}$$

The influence of hydrostatic pressure on density is thus hidden in a spatial dependence of the reference density ϱ_0.

Since the reference density ϱ_0 is assumed to be a time-independent function, considering only the largest term in the equation of continuity, i.e. neglecting thermal expansion, we arrive at the simplified equation

$$\operatorname{div}(\varrho_0 \mathbf{v}) = 0. \tag{1.7}$$

Putting (1.3) and (1.6) into (1.2) yields

$$\varrho_0 \left[\frac{\partial \mathbf{v}}{\partial t} + (\mathbf{v} \cdot \nabla)\, \mathbf{v} \right] = -\varrho_0 \alpha (T - T_0) \mathbf{g}_0 - \nabla \Pi + \nabla(\lambda \operatorname{div} \mathbf{v}) + \operatorname{div}(2\mu \mathbb{D}), \tag{1.8}$$

where we neglected the thermal expansion on the left-hand side, i.e., the changes of the inertial force due to the thermal expansion, and the quadratic term $\varrho_0 \alpha (T - T_0)(\mathbf{g} - \mathbf{g}_0)$ and the self-gravitation term $\varrho_0(\mathbf{g} - \mathbf{g}_0)$ on the right-hand side.

We simplify the heat equation by replacing ϱ by ϱ_0 , i.e.

$$\varrho_0 c_p \frac{\partial T}{\partial t} = \operatorname{div}(k \nabla T) - \varrho_0 c_p \mathbf{v} \cdot \nabla T - \varrho_0 v^{\hat{r}} \alpha T g + \lambda (\operatorname{div} \mathbf{v})^2 + 2\mu \mathbb{D} : \mathbb{D} + Q. \tag{1.9}$$

The system of equations (1.7)-(1.9) is referred to as the *anelastic liquid approximation* of the conservation laws. For our purposes, it is common to neglect compressibility in the equation of continuity (1.1) and to replace it by incompressible model (where ϱ_0 is now constant). The obtained system of equations is then usually called the *extended Boussinesq approximation*

$$\operatorname{div} \mathbf{v} = 0, \tag{1.10}$$

$$\varrho_0 \left[\frac{\partial \mathbf{v}}{\partial t} + (\mathbf{v} \cdot \nabla)\, \mathbf{v} \right] = -\varrho_0 \alpha (T - T_0) \mathbf{g}_0 - \nabla \Pi + \operatorname{div}(2\mu \mathbb{D}), \tag{1.11}$$

$$\varrho_0 c_p \frac{\partial T}{\partial t} = \operatorname{div}(k \nabla T) - \varrho_0 c_p \mathbf{v} \cdot \nabla T - \varrho_0 v^{\hat{r}} \alpha T g + 2\mu \mathbb{D} : \mathbb{D} + Q. \tag{1.12}$$

Further substantial simplification of the studied system of equations can be obtained by setting the reference density ϱ_0, the reference gravitational acceleration $\mathbf{g}_0$ and the material coefficients α, c_p, k and μ to be constant. Moreover, dissipation term $2\mu \mathbb{D} : \mathbb{D}$, adiabatic heating/cooling term $\varrho_0 v^{\hat{r}} \alpha T g$ and the heat sources Q are not taken into account. We then arrive at the system of equations called the *classical Boussinesq approximation*

$$\operatorname{div} \mathbf{v} = 0, \tag{1.13}$$

$$\varrho_0 \left[\frac{\partial \mathbf{v}}{\partial t} + (\mathbf{v} \cdot \nabla)\, \mathbf{v} \right] = -\varrho_0 \alpha (T - T_0) \mathbf{g}_0 - \nabla \Pi + \mu \Delta \mathbf{v}, \tag{1.14}$$

$$\frac{\partial T}{\partial t} = \kappa \Delta T - \mathbf{v} \cdot \nabla T, \tag{1.15}$$

where $\kappa = k / \varrho_0 c_p$ is the thermal diffusivity.

1.3 Linear stability analysis

The second chapter concerns the initial onset of instability studied via the dynamics of small perturbations to the basic flow. We explain the method of linear stability analysis used for finding the threshold of instability on a model example following the approach presented in Chandrasekhar (1961).

Let us consider an abstract evolution equation for unknown function $\mathbf{u}$

$$\frac{\partial \mathbf{u}}{\partial t} = \mathcal{L}(\lambda)\mathbf{u} + \mathcal{N}(\mathbf{u}, \mathbf{u}),$$

where $\mathcal{L}$ is a linear operator, $\mathcal{N}$ is a quadratic operator and $\lambda \in \mathbb{R}$ is a control parameter. Let us also assume that appropriate boundary conditions are imposed on $\mathbf{u}$.

We find the *basic flow*[1] $\mathbf{u}_0$, i.e. time-independent solution of the governing equations fulfilling the corresponding boundary conditions. For simplicity let us assume that $\mathbf{u}_0 \equiv \mathbf{0}$.

We subject the basic flow to small perturbations and substitute the resulting forms into the governing equations. Specifically, we set

$$\mathbf{u} = \mathbf{u}_0 + \mathbf{u}',$$

where $\mathbf{u}'$ is the perturbation. The substitution then yields

$$\frac{\partial \mathbf{u}'}{\partial t} = \mathcal{L}(\lambda)\mathbf{u}' + \mathcal{N}(\mathbf{u}', \mathbf{u}'), \tag{1.16}$$

where we used the fact that $\mathbf{u}_0 \equiv \mathbf{0}$.

Now, we linearize the resulting equation with respect to the perturbations, i.e. we neglect the quadratic term $\mathcal{N}(\mathbf{u}', \mathbf{u}')$. Then we study the linearized system

$$\frac{\partial \mathbf{u}'}{\partial t} = \mathcal{L}(\lambda)\mathbf{u}', \tag{1.17}$$

via the *normal mode analysis*. We consider the perturbation $\mathbf{u}'$ in the form

$$\mathbf{u}'(t, \mathbf{x}) = \tilde{\mathbf{u}}'(\mathbf{x})e^{\sigma t},$$

where $\sigma \in \mathbb{C}$ which upon substitution into (1.17) yields the eigenvalue problem

$$\boxed{\sigma\tilde{\mathbf{u}}' = \mathcal{L}(\lambda)\tilde{\mathbf{u}}'.} \tag{1.18}$$

Solving this eigenvalue problem determines the (un)stability of the basic flow for a specific value of a control parameter λ. Indeed, if there is for a fixed value of λ an eigenvalue with $\operatorname{Re}\sigma > 0$, then the corresponding eigenmode grows in time and the basic flow is said to be linearly unstable. If all of the eigenvalues are

[1] We are also going to use the term the *reference state* as in our case the basic flow is indeed the reference state mentioned above.

such that $\mathrm{Re}\,\sigma < 0$, then the perturbations decay and the basic flow is said to be linearly stable. The largest value of λ for which the basic flow is stable represents the sought critical threshold of instability.

Let us mention that the normal modes of the perturbations can be further decomposed considering the boundary conditions on $\mathbf{u}$. If $\mathbf{u}$ is periodic in horizontal coordinates x, y, say, we can write the perturbation in the form[2]

$$\mathbf{u}'(t, \mathbf{x}) = \tilde{\mathbf{u}}'(z) e^{\mathrm{i}(a_x x + a_y y) + \sigma t},$$

where a_x, a_y are corresponding wave-numbers.

1.4 Weakly non-linear analysis

For larger perturbations, non-linear effects become important. By neglecting non-linear terms (describing the interaction of the perturbations with themselves) linear stability analysis is restricted to the regime in which the amplitude of perturbations is very small.

Therefore for supercritical values of the control parameter (in our case the Rayleigh number), linear analysis can't say anything about the behaviour of the flow in the limit $t \to \infty$ due to the fact that the amplitude of perturbations A obeys

$$\frac{\mathrm{d}A}{\mathrm{d}t} = \sigma A,$$

where σ is the coefficient that accounts for the growth rate – it is negative below the threshold (damping effect) and positive beyond (amplifying effect). In other words $A(t) = \exp(\sigma t)$, as was stated in the preceding, and the perturbation grows quickly for $\mathrm{Re}\,\sigma > 0$.

In the third chapter we thus show in detail, following the works of Cross (1980) and Fujimura (1997), that the amplitude A of the unstable mode ($\mathrm{Re}\,\sigma > 0$), when all the other modes are damped, is in fact for supercritical values of Ra governed by the *amplitude equation* (also known as *Stuart-Landau equation*)

$$\boxed{\frac{\mathrm{d}A}{\mathrm{d}t} = \sigma A + \Lambda A^3,} \tag{1.19}$$

where Λ is a negative coefficient coming from quadratic non-linearities that weren't neglected opposed to the linear stability analysis. We can see that for $t \to \infty$ the solution of (1.19) for an arbitrary initial condition converges to $A^* \equiv \pm\sqrt{\sigma/\Lambda}$, i.e. we obtain a supercritical pitchfork bifurcation.

[2]Note that we use the notation i for the imaginary unit. This shouldn't be confused with the summation index i used especially in the third chapter concerning the weakly non-linear analysis.

Chapter 2

The onset of convection

In this chapter we follow the work of Chandrasekhar (1961) in deriving the critical threshold of instability. The numerical model (see 2.1.5) which was build on Chandrasekhar's approach is compared to the analytical results for classical Boussinesq approximation. We use the numerical model for finding the critical Rayleigh numbers in the case of extended Boussinesq approximation.

2.1 Classical Boussinesq approximation

Let us introduce dimensionless variables (denoted by the stars) by means of the relations

$$\mathbf{x} = d\mathbf{x}^*, \quad t = \frac{d^2}{\kappa}t^*, \quad \mathbf{v} = \frac{\kappa}{d}\mathbf{v}^*, \quad \Pi = \frac{\mu\kappa}{d^2}\Pi^*, \quad T = T_s + (T_b - T_s)T^*,$$

where d is characteristic length (thickness of the convecting layer).

The dimensionless form of the classical Boussinesq approximation (1.13) - (1.15) then reads

$$\operatorname{div}^* \mathbf{v}^* = 0, \tag{2.1}$$

$$\frac{1}{Pr}\left[\frac{\partial \mathbf{v}^*}{\partial t^*} + (\mathbf{v}^* \cdot \nabla^*)\,\mathbf{v}^*\right] = Ra(T^* - T_0^*)\mathbf{e}_{\hat{r}} - \nabla^*\Pi^* + \Delta^*\mathbf{v}^*, \tag{2.2}$$

$$\frac{\partial T^*}{\partial t^*} = \Delta^* T^* - \mathbf{v}^* \cdot \nabla^* T^*, \tag{2.3}$$

where we introduced the dimensionless numbers

$$\textit{Prandtl number} \qquad Pr = \frac{\mu}{\varrho_0 \kappa}$$

$$\textit{Rayleigh number} \qquad Ra = \frac{\varrho_0 \alpha (T_b - T_s) g_0 d^3}{\mu\kappa}.$$

We now rewrite equations (2.1) - (2.3) in Cartesian coordinates (x^*, y^*, z^*), where x^* and y^* are dimensionless horizontal coordinates and z^* denotes dimensionless

depth, $z^* \in [0,1]$, $z = 0$ at the surface and $z = 1$ at the bottom of the convecting layer. The new system of equations reads (from now on we omit denoting the dimensionless variables by the star, unless misunderstanding may arise)

$$\operatorname{div} \mathbf{v} = 0, \tag{2.4}$$

$$\frac{1}{Pr}\left[\frac{\partial \mathbf{v}}{\partial t} + (\mathbf{v}\cdot\nabla)\,\mathbf{v}\right] = -Ra(T - T_0)\mathbf{e}_{\hat{z}} - \nabla\Pi + \Delta\mathbf{v}, \tag{2.5}$$

$$\frac{\partial T}{\partial t} = \Delta T - \mathbf{v}\cdot\nabla T. \tag{2.6}$$

We assume that in the reference state the fluid is in quiescent state, i.e. $\mathbf{v} \equiv \mathbf{0}$, and the temperature is only function of depth, i.e. $T_0 = T_0(z)$. Equation (2.6) in the reference state then reads

$$0 = \frac{\mathrm{d}^2 T_0}{\mathrm{d}z^2}. \tag{2.7}$$

We can see quite easily that the solution of this equation fulfilling the boundary conditions $T_0(0) = 0$ and $T_0(1) = 1$ is

$$T_0 = z.$$

Let us now assume that the reference state is perturbed slightly. We denote these perturbations of velocity, temperature and pressure by $\mathbf{v}$, θ and π, respectively. The perturbed state is then described by the quantities denoted by the prime

$$\begin{aligned}
\mathbf{v}' &= \mathbf{0} + \mathbf{v} = \mathbf{v},\\
T' &= T_0 + \theta,\\
\Pi' &= 0 + \pi = \pi.
\end{aligned}$$

Putting these expressions into equations (2.4) - (2.6) yields (with the aid of (2.7))

$$\operatorname{div} \mathbf{v} = 0, \tag{2.8}$$

$$\frac{1}{Pr}\left[\frac{\partial \mathbf{v}}{\partial t} + (\mathbf{v}\cdot\nabla)\mathbf{v}\right] = -Ra\theta\mathbf{e}_{\hat{z}} - \nabla\pi + \Delta\mathbf{v}, \tag{2.9}$$

$$\frac{\partial \theta}{\partial t} = \Delta\theta - v^{\hat{z}}\frac{\mathrm{d}T_0}{\mathrm{d}z} - \mathbf{v}\cdot\nabla\theta. \tag{2.10}$$

After neglecting the non-linear terms we obtain

$$\operatorname{div} \mathbf{v} = 0, \tag{2.11}$$

$$\frac{1}{Pr}\frac{\partial \mathbf{v}}{\partial t} = -Ra\theta\mathbf{e}_{\hat{z}} - \nabla\pi + \Delta\mathbf{v}, \tag{2.12}$$

$$\frac{\partial \theta}{\partial t} = \Delta\theta - v^{\hat{z}}\frac{\mathrm{d}T_0}{\mathrm{d}z}. \tag{2.13}$$

Let us now apply the operator div to equation (2.12). We get

$$0 = -Ra\frac{\partial \theta}{\partial z} - \Delta\pi. \tag{2.14}$$

Applying of the operator Δ to equation (2.12) yields

$$\frac{1}{Pr}\frac{\partial}{\partial t}(\Delta \mathbf{v}) = -Ra\Delta\theta \mathbf{e}_{\hat{z}} - \nabla(\Delta\pi) + \Delta(\Delta\mathbf{v}). \tag{2.15}$$

Putting the expression $\Delta\pi$ from (2.14) into (2.15) further yields

$$\frac{1}{Pr}\frac{\partial}{\partial t}(\Delta \mathbf{v}) = Ra \begin{bmatrix} \frac{\partial^2\theta}{\partial x\partial z} \\ \frac{\partial^2\theta}{\partial y\partial z} \\ -\frac{\partial^2\theta}{\partial x^2} - \frac{\partial^2\theta}{\partial y^2} \end{bmatrix} + \Delta(\Delta\mathbf{v}). \tag{2.16}$$

Let us go back to equation (2.12) again and apply the operator curl to it. With the aid of the identity $\operatorname{curl}\nabla\varphi = 0$, we obtain

$$\frac{1}{Pr}\frac{\partial}{\partial t}(\operatorname{curl}\mathbf{v}) = Ra \begin{bmatrix} -\frac{\partial\theta}{\partial y} \\ \frac{\partial\theta}{\partial x} \\ 0 \end{bmatrix} + \Delta(\operatorname{rot}\mathbf{v}). \tag{2.17}$$

We now express z-components from equations (2.16) and (2.17). We also add the equation (2.13), where we substitute the known reference temperature T_0. Our final system of equations reads

$$\frac{1}{Pr}\frac{\partial}{\partial t}(\Delta v^{\hat{z}}) = -Ra\left(\frac{\partial^2\theta}{\partial x^2} + \frac{\partial^2\theta}{\partial y^2}\right) + \Delta(\Delta v^{\hat{z}}), \tag{2.18}$$

$$\frac{1}{Pr}\frac{\partial\eta^{\hat{z}}}{\partial t} = \Delta\eta^{\hat{z}}, \tag{2.19}$$

$$\frac{\partial\theta}{\partial t} = \Delta\theta - v^{\hat{z}}, \tag{2.20}$$

where we used the notation $\boldsymbol{\eta} \equiv \operatorname{curl}\mathbf{v}$ ($\boldsymbol{\eta}$ is called the vorticity).

We will now consider the perturbations in the form of normal modes

$$\begin{aligned} \mathbf{v}(t,\mathbf{x}) &= \tilde{\mathbf{v}}(z)\exp\left[\mathrm{i}(a_x x + a_y y) + \sigma t\right], \\ \boldsymbol{\eta}(t,\mathbf{x}) &= \tilde{\boldsymbol{\eta}}(z)\exp\left[\mathrm{i}(a_x x + a_y y) + \sigma t\right], \\ \theta(t,\mathbf{x}) &= \tilde{\theta}(z)\exp\left[\mathrm{i}(a_x x + a_y y) + \sigma t\right]. \end{aligned}$$

The system (2.18) - (2.20) can then be transformed into

$$\frac{\sigma}{Pr}\left(\frac{\mathrm{d}^2}{\mathrm{d}z^2} - a^2\right)\tilde{v}^{\hat{z}} = a^2 Ra\tilde{\theta} + \left(\frac{\mathrm{d}^2}{\mathrm{d}z^2} - a^2\right)^2 \tilde{v}^{\hat{z}}, \tag{2.21}$$

$$\frac{\sigma}{Pr}\tilde{\eta}^{\hat{z}} = \left(\frac{\mathrm{d}^2}{\mathrm{d}z^2} - a^2\right)\tilde{\eta}^{\hat{z}}, \tag{2.22}$$

$$\sigma\tilde{\theta} = \left(\frac{\mathrm{d}^2}{\mathrm{d}z^2} - a^2\right)\tilde{\theta} - \tilde{v}^{\hat{z}}, \tag{2.23}$$

where we used the notation $a^2 = a_x^2 + a_y^2$.

2.1.1 Boundary conditions

Boundary conditions for the perturbed quantities $\tilde{v}^{\hat{z}}$, $\tilde{\eta}^{\hat{z}}$ a $\tilde{\theta}$ will be needed.

From prescribed boundary conditions for temperature T we see, that boundary conditions for perturbation θ must fulfil

$$\theta|_{z=0,1} = 0,$$

This yields

$$\tilde{\theta}\Big|_{z=0,1} = 0. \tag{2.24}$$

We will consider impermeable boundaries for velocity $\mathbf{v}$ (also called *no-penetration* boundary condition), i.e.

$$v^{\hat{z}}\big|_{z=0,1} = 0.$$

This again yields

$$\tilde{v}^{\hat{z}}\big|_{z=0,1} = 0. \tag{2.25}$$

Since our equations are at least of the fourth order for velocity, we need more boundary conditions for this quantity. In what follows we will be considering two cases of boundary conditions: *free-slip* and *no-slip* boundary conditions. Both cases yield different critical values of Rayleigh number Ra and wave-number a.

For free-slip boundary condition we are able to derive Ra_{crit} (and corresponding critical wave-number) analytically, which will be shown below. In this case $Ra_{\text{crit}} = \frac{27}{4}\pi^4$ and $a_{\text{crit}} = \frac{\pi}{\sqrt{2}}$.

For no-slip boundary condition the analytical technique is slightly more complicated and in the end yields a transcendental equation whose solution is the critical value of Ra. In this case we can only proceed by solving this equation numerically. Specifically for no-slip condition $Ra_{\text{crit}} \approx 1707.762$ and $a_{\text{crit}} \approx 3.117$ (see Chandrasekhar, 1961).

We will only show the analytical method for free-slip boundary condition. However, we will treat both cases later on when investigating the numerical way of finding the critical values of Ra and a.

Free-slip

This boundary condition can be expressed as $\mathbb{T}\mathbf{n} - (\mathbb{T}\mathbf{n} \cdot \mathbf{n})\mathbf{n} = \mathbf{0}$, where $\mathbf{n}$ is the unit outer normal vector, in our case $\mathbf{n} = \pm\mathbf{e}_{\hat{z}}$. For the stress tensor we have $\mathbb{T} = -p\mathbb{I} + 2\mu\mathbb{D}(\mathbf{v})$. Put all together, the boundary condition can be written as

$$\begin{bmatrix} \mu\left(\frac{\partial v^{\hat{x}}}{\partial z} + \frac{\partial v^{\hat{z}}}{\partial x}\right) \\ \mu\left(\frac{\partial v^{\hat{y}}}{\partial z} + \frac{\partial v^{\hat{z}}}{\partial y}\right) \\ 0 \end{bmatrix} = \begin{bmatrix} 0 \\ 0 \\ 0 \end{bmatrix}.$$

Equality of the first two components yields

$$\frac{\partial v^{\hat{x}}}{\partial z} + \frac{\partial v^{\hat{z}}}{\partial x} = 0, \quad \frac{\partial v^{\hat{y}}}{\partial z} + \frac{\partial v^{\hat{z}}}{\partial y} = 0.$$

From no-penetration condition we know that

$$\left.\frac{\partial v^{\hat{z}}}{\partial x}\right|_{z=0,1} = \left.\frac{\partial v^{\hat{z}}}{\partial y}\right|_{z=0,1} = 0.$$

Hence,

$$\left.\frac{\partial v^{\hat{x}}}{\partial z}\right|_{z=0,1} = \left.\frac{\partial v^{\hat{y}}}{\partial z}\right|_{z=0,1} = 0. \tag{2.26}$$

We also know that the velocity field is divergence-free, i.e. $\operatorname{div} \mathbf{v} = 0$. Differentiating this equation with respect to z yields

$$\frac{\partial^2 v^{\hat{x}}}{\partial x \partial z} + \frac{\partial^2 v^{\hat{y}}}{\partial y \partial z} + \frac{\partial^2 v^{\hat{z}}}{\partial z^2} = 0$$

Combining this with (2.26), we arrive at

$$\left.\frac{\partial^2 v^{\hat{z}}}{\partial z^2}\right|_{z=0,1} = 0.$$

And thus,

$$\left.\frac{\mathrm{d}^2 \tilde{v}^{\hat{z}}}{\mathrm{d}z^2}\right|_{z=0,1} = 0. \tag{2.27}$$

Since we are interested in the analytical solution in the case of free-slip boundary conditions, we are going to need more boundary conditions on $\tilde{v}^{\hat{z}}$ as we shall see below (see section 2.1.3). Let us use equation (2.21) to obtain these conditions by setting the boundary values for z and also by using boundary conditions (2.24), (2.25) and (2.27). We obtain

$$\left.\frac{\mathrm{d}^4 \tilde{v}^{\hat{z}}}{\mathrm{d}z^4}\right|_{z=0,1} = 0. \tag{2.28}$$

Following this pattern we could easily show that all the even derivatives of $\tilde{v}^{\hat{z}}$ vanish on the boundaries. Let us mention that this is true for the classical case only and not for the extended Boussinesq approximation.

It remains to take care of the boundary conditions for z-component of vorticity. By definition

$$\eta^{\hat{z}} = \frac{\partial v^{\hat{y}}}{\partial x} - \frac{\partial v^{\hat{x}}}{\partial y}.$$

Hence by using (2.26) it follows that

$$\left.\frac{\partial \eta^{\hat{z}}}{\partial z}\right|_{z=0,1} = 0,$$

And thus,

$$\left.\frac{\mathrm{d}\tilde{\eta}^{\hat{z}}}{\mathrm{d}z}\right|_{z=0,1} = 0. \tag{2.29}$$

Let us note that we obtained boundary conditions (2.24), (2.25), (2.27) and (2.29) by only using the fact that the velocity field is divergence-free. That means we can use these boundary conditions for extended Boussinesq approximation too (since in that case $\operatorname{div}\mathbf{v} = 0$ still holds). However, condition (2.28) holds for classical Boussinesq approximation only.

No-slip

In this case we can write the condition as $\mathbf{v}\cdot\mathbf{t} = 0$ on the boundary, where $\mathbf{t}$ is an arbitrary vector tangent to the boundary. This means that

$$v^{\hat{x}}\big|_{z=0,1} = v^{\hat{y}}\big|_{z=0,1} = 0,$$

which also yields

$$\left.\frac{\partial v^{\hat{x}}}{\partial x}\right|_{z=0,1} = \left.\frac{\partial v^{\hat{y}}}{\partial y}\right|_{z=0,1} = 0. \tag{2.30}$$

After using the continuity equation we obtain

$$\left.\frac{\partial v^{\hat{z}}}{\partial z}\right|_{z=0,1} = 0,$$

A hence,

$$\left.\frac{\mathrm{d}\tilde{v}^{\hat{z}}}{\mathrm{d}z}\right|_{z=0,1} = 0. \tag{2.31}$$

For no-slip boundary condition we are not going to solve (2.33) analytically. Four boundary conditions for $\tilde{v}^{\hat{z}}$ are sufficient for solving the onset of convection numerically and hence we don't need more boundary conditions.

It remains to find the boundary conditions for z-component of vorticity. From definition of vorticity and (2.30) we easily arrive at

$$\eta^{\hat{z}}\big|_{z=0,1} = 0,$$

and thus,

$$\tilde{\eta}^{\hat{z}}\big|_{z=0,1} = 0. \tag{2.32}$$

Again, conditions (2.24), (2.25), (2.31) and (2.32) can be applied in the case of extended Boussinesq approximation too because the condition $\operatorname{div}\mathbf{v} = 0$ is still valid.

2.1.2 The principle of the exchange of stabilities

The number σ in (2.33) is in general complex, i.e. $\sigma = \sigma_{\mathrm{Re}} + \mathrm{i}\sigma_{\mathrm{Im}}$. Let us show that in our case the so called *principle of the exchange of stabilities* is valid, i.e. $\sigma \in \mathbb{R}$ (see Chandrasekhar (1961) for details on the terminology).

First of all, applying the operator

$$\mathcal{P} \equiv \frac{\mathrm{d}^2}{\mathrm{d}z^2} - a^2 - \sigma$$

to the equation (2.21) yields

$$\frac{\sigma}{Pr}\left(\frac{\mathrm{d}^2}{\mathrm{d}z^2} - a^2\right)\mathcal{P}\tilde{v}^{\hat{z}} = a^2 Ra\mathcal{P}\tilde{\theta} + \left(\frac{\mathrm{d}^2}{\mathrm{d}z^2} - a^2\right)^2 \mathcal{P}\tilde{v}^{\hat{z}}.$$

We see from (2.23) that the expression $\mathcal{P}\tilde{\theta}$ can be substituted by $\tilde{v}^{\hat{z}}$ and this leads to

$$\frac{\sigma}{Pr}\left(\frac{\mathrm{d}^2}{\mathrm{d}z^2} - a^2\right)\mathcal{P}\tilde{v}^{\hat{z}} = a^2 Ra\tilde{v}^{\hat{z}} + \left(\frac{\mathrm{d}^2}{\mathrm{d}z^2} - a^2\right)^2 \mathcal{P}\tilde{v}^{\hat{z}},$$

which can be further written as

$$\left(\frac{\mathrm{d}^2}{\mathrm{d}z^2} - a^2\right)\left(\frac{\mathrm{d}^2}{\mathrm{d}z^2} - a^2 - \frac{\sigma}{Pr}\right)\left(\frac{\mathrm{d}^2}{\mathrm{d}z^2} - a^2 - \sigma\right)\tilde{v}^{\hat{z}} = -a^2 Ra\tilde{v}^{\hat{z}}. \tag{2.33}$$

Let us now denote

$$f \equiv \left(\frac{\mathrm{d}^2}{\mathrm{d}z^2} - a^2\right)\left(\frac{\mathrm{d}^2}{\mathrm{d}z^2} - a^2 - \frac{\sigma}{Pr}\right)\tilde{v}^{\hat{z}}.$$

Multiplying equation (2.33) by complex conjugate $\overline{f}$ and integrating the resulting equation with respect to z over the whole layer yields

$$\int_0^1 \left[\left(\frac{\mathrm{d}^2}{\mathrm{d}z^2} - a^2 - \sigma\right) f\right]\overline{f}\,\mathrm{d}z = -a^2 Ra\int_0^1 \tilde{v}^{\hat{z}}\overline{f}\,\mathrm{d}z. \tag{2.34}$$

Integrating by parts and using the boundary conditions on $\tilde{v}^{\hat{z}}$ we derive

$$-\int_0^1 \left(\left|\frac{\mathrm{d}f}{\mathrm{d}z}\right|^2 + (a^2+\sigma)|f|^2\right)\mathrm{d}z = \\ -a^2 Ra\int_0^1 \left(\left|\frac{\mathrm{d}^2\tilde{v}^{\hat{z}}}{\mathrm{d}z^2}\right|^2 + \left(2a^2 + \frac{\overline{\sigma}}{Pr}\right)\left|\frac{\mathrm{d}\tilde{v}^{\hat{z}}}{\mathrm{d}z}\right|^2 + a^2\left(a^2 + \frac{\overline{\sigma}}{Pr}\right)|\tilde{v}^{\hat{z}}|^2\right)\mathrm{d}z.$$

The imaginary part of the last equation reads

$$\sigma_{\mathrm{Im}}\int_0^1 \left(|f|^2 + \frac{a^2 Ra}{Pr}\left(\left|\frac{\mathrm{d}\tilde{v}^{\hat{z}}}{\mathrm{d}z}\right|^2 + a^2|\tilde{v}^{\hat{z}}|^2\right)\right)\mathrm{d}z = 0,$$

which indicates that $\sigma_{\mathrm{Im}} = 0$ and thus $\sigma \in \mathbb{R}$ indeed.

2.1.3 The onset of convection analytically

This section concerns the free-slip boundary conditions only.

Since σ is real, the marginal state is characterized by $\sigma = 0$. Let us investigate equation (2.22) first. Substitution by $\sigma = 0$ yields

$$0 = \left(\frac{\mathrm{d}^2}{\mathrm{d}z^2} - a^2\right)\tilde{\eta}^{\hat{z}}, \tag{2.35}$$

with boundary conditions

$$\left.\frac{\mathrm{d}\tilde{\eta}^{\hat{z}}}{\mathrm{d}z}\right|_{z=0,1} = 0.$$

We can check easily that there is no non-trivial solution of the stated problem and thus in the marginal state the z-component of vorticity always disappears.

Let us return to equation (2.33). Substitution by $\sigma = 0$ yields an eigenvalue problem

$$\left(\frac{\mathrm{d}^2}{\mathrm{d}z^2} - a^2\right)^3 \tilde{v}^{\hat{z}} = -a^2 Ra\, \tilde{v}^{\hat{z}}, \tag{2.36}$$

with boundary conditions

$$\tilde{v}^{\hat{z}}\big|_{z=0,1} = \left.\frac{\mathrm{d}^2\tilde{v}^{\hat{z}}}{\mathrm{d}z^2}\right|_{z=0,1} = \left.\frac{\mathrm{d}^4\tilde{v}^{\hat{z}}}{\mathrm{d}z^4}\right|_{z=0,1} = 0.$$

It follows from the boundary conditions (let us remember that all the even derivatives of $\tilde{v}^{\hat{z}}$ vanish on the boundaries) that we should seek the solution in the form

$$\tilde{v}^{\hat{z}}(z) = \sum_{n=1}^{+\infty} c_n \sin(n\pi z) \tag{2.37}$$

where $c_n \in \mathbb{R}$ for $n \in \mathbb{N}$. From equation (2.36) we then obtain condition for Rayleigh number

$$Ra = \frac{(a^2 + n^2\pi^2)^3}{a^2}. \tag{2.38}$$

For a fixed a, Ra attains its minimum for $n = 1$. We then have

$$Ra = \frac{(a^2 + \pi^2)^3}{a^2}. \tag{2.39}$$

Minimization of the last equation with respect to a yields the critical value of Rayleigh number $Ra_{\mathrm{crit}} = \frac{27}{4}\pi^4$. This minimum is attained for $a_{\mathrm{crit}} = \frac{\pi}{\sqrt{2}}$.

2.1.4 Cells

From z-components of velocity and vorticity we can derive horizontal components of velocity quite easily. Equation of continuity yields

$$\left(\frac{\partial^2}{\partial x^2} + \frac{\partial^2}{\partial y^2}\right) v^{\hat{x}} = -\frac{\partial^2 v^{\hat{z}}}{\partial x \partial z} - \frac{\partial \eta^{\hat{z}}}{\partial y},$$
$$\left(\frac{\partial^2}{\partial x^2} + \frac{\partial^2}{\partial y^2}\right) v^{\hat{y}} = -\frac{\partial^2 v^{\hat{z}}}{\partial y \partial z} + \frac{\partial \eta^{\hat{z}}}{\partial x}.$$

Normal modes analysis then yields

$$v^{\hat{x}} = \frac{\mathrm{i}}{a^2}\left(a_x \frac{\mathrm{d}\tilde{v}^{\hat{z}}}{\mathrm{d}z} + a_y \tilde{\eta}^{\hat{z}}\right) \exp\left[\mathrm{i}(a_x x + a_y y) + \sigma t\right],$$

$$v^{\hat{y}} = \frac{\mathrm{i}}{a^2}\left(a_y \frac{\mathrm{d}\tilde{v}^{\hat{z}}}{\mathrm{d}z} - a_x \tilde{\eta}^{\hat{z}}\right) \exp\left[\mathrm{i}(a_x x + a_y y) + \sigma t\right].$$

And this remains valid for the extended Boussinesq approximation too.

We show later that for Ra greater than the critical value $\tilde{\eta}^{\hat{z}}$ vanishes. This is valid for both classical and extended Boussinesq approximations. Hence, in this case we can simplify the relations above by setting $\tilde{\eta}^{\hat{z}} = 0$. That will be useful for investigating the slightly supercritical behaviour of convection in the third chapter.

In the simplest case of infinite longitudinal convective cells (so called *single rolls*) we can further simplify the expression above to obtain (we assume that the y-component of velocity is zero: $a_x = a$, $a_y = 0$)

$$v^{\hat{x}} = \frac{\mathrm{i}}{a}\frac{\mathrm{d}\tilde{v}^{\hat{z}}}{\mathrm{d}z}\exp\left[\mathrm{i}ax + \sigma t\right], \tag{2.40}$$

$$v^{\hat{y}} = 0, \tag{2.41}$$

$$v^{\hat{z}} = \tilde{v}^{\hat{z}}\exp\left[\mathrm{i}ax + \sigma t\right], \tag{2.42}$$

Note: Of course, we always consider real part of each component of velocity only.

2.1.5 Numerical solution

We found the critical values of Ra and a characterizing the onset of convection for classical Boussinesq approximation and free-slip boundary conditions. In the following sections we are going to investigate this problem for extended Boussinesq approximation. In this case we cannot use the analytical approach as before and we have to come up with a numerical model solving this problem. Let us now show how to solve the classical case numerically (for both cases of boundary conditions this time). This will also serve us as a benchmark for gauging our numerical model.

Let us return to equations (2.21)–(2.23). We shall write this system in the form of an eigenvalue problem

$$\sigma\mathcal{A}\begin{bmatrix}\tilde{v}^{\hat{z}}\\ \tilde{\eta}^{\hat{z}}\\ \tilde{\theta}\end{bmatrix} = \mathcal{B}\begin{bmatrix}\tilde{v}^{\hat{z}}\\ \tilde{\eta}^{\hat{z}}\\ \tilde{\theta}\end{bmatrix}, \tag{2.43}$$

where

$$\mathcal{A} = \begin{bmatrix}\frac{1}{Pr}\left(\frac{\mathrm{d}^2}{\mathrm{d}z^2} - a^2\right) & 0 & 0\\ 0 & \frac{1}{Pr} & 0\\ 0 & 0 & 1\end{bmatrix}, \quad \mathcal{B} = \begin{bmatrix}\left(\frac{\mathrm{d}^2}{\mathrm{d}z^2} - a^2\right)^2 & 0 & a^2 Ra\\ 0 & \left(\frac{\mathrm{d}^2}{\mathrm{d}z^2} - a^2\right) & 0\\ -1 & 0 & \left(\frac{\mathrm{d}^2}{\mathrm{d}z^2} - a^2\right)\end{bmatrix}.$$

For free-slip boundary condition it holds

$$\tilde{v}^{\hat{z}}\big|_{z=0,1} = \left.\frac{\mathrm{d}^2\tilde{v}^{\hat{z}}}{\mathrm{d}z^2}\right|_{z=0,1} = 0, \quad \left.\frac{\mathrm{d}\tilde{\eta}^{\hat{z}}}{\mathrm{d}z}\right|_{z=0,1} = 0, \quad \tilde{\theta}\Big|_{z=0,1} = 0,$$

while for no-slip we have

$$\tilde{v}^{\hat{z}}\big|_{z=0,1} = \left.\frac{\mathrm{d}\tilde{v}^{\hat{z}}}{\mathrm{d}z}\right|_{z=0,1} = 0, \quad \tilde{\eta}^{\hat{z}}\big|_{z=0,1} = 0, \quad \tilde{\theta}\Big|_{z=0,1} = 0.$$

Our goal is to find eigenvalues σ. If for specific Ra and a there exists a positive eigenvalue, then the perturbation grows in time and the state is unstable. On the other hand if all the eigenvalues are negative, the state is stable and the perturbations decay.

Let us first note that equation (2.22) has non-trivial solution only when $\sigma < 0$. Indeed, multiplying (2.22) by $\overline{\tilde{\eta}^{\hat{z}}}$ and integrating the resulting equation by parts (with the aid of either free-slip, or no-slip boundary conditions) yields

$$\begin{aligned}\frac{\sigma}{Pr}\int_0^1 |\tilde{\eta}^{\hat{z}}|^2\,\mathrm{d}z &= \int_0^1 \frac{\mathrm{d}^2\tilde{\eta}^{\hat{z}}}{\mathrm{d}z^2}\overline{\tilde{\eta}^{\hat{z}}}\,\mathrm{d}z - a^2\int_0^1 |\tilde{\eta}^{\hat{z}}|^2\,\mathrm{d}z \\ &= -\int_0^1 \left|\frac{\mathrm{d}\tilde{\eta}^{\hat{z}}}{\mathrm{d}z}\right|^2 \mathrm{d}z - a^2\int_0^1 |\tilde{\eta}^{\hat{z}}|^2\,\mathrm{d}z.\end{aligned}$$

Thus, for $\tilde{\eta}^{\hat{z}} \neq 0$ it must hold that $\sigma < 0$. This means that equation (2.22) won't affect the positive part of spectrum of (2.43). Hence, we can consider a simpler problem

$$\sigma\mathcal{A}\begin{bmatrix}\tilde{v}^{\hat{z}}\\ \tilde{\theta}\end{bmatrix} = \mathcal{B}\begin{bmatrix}\tilde{v}^{\hat{z}}\\ \tilde{\theta}\end{bmatrix}, \tag{2.44}$$

where

$$\mathcal{A} = \begin{bmatrix}\frac{1}{Pr}\left(\frac{\mathrm{d}^2}{\mathrm{d}z^2} - a^2\right) & 0\\ 0 & 1\end{bmatrix}, \quad \mathcal{B} = \begin{bmatrix}\left(\frac{\mathrm{d}^2}{\mathrm{d}z^2} - a^2\right)^2 & a^2Ra\\ -1 & \left(\frac{\mathrm{d}^2}{\mathrm{d}z^2} - a^2\right)\end{bmatrix}. \tag{2.45}$$

With free-slip boundary conditions

$$\tilde{v}^{\hat{z}}\big|_{z=0,1} = \left.\frac{\mathrm{d}^2\tilde{v}^{\hat{z}}}{\mathrm{d}z^2}\right|_{z=0,1} = 0, \quad \tilde{\theta}\Big|_{z=0,1} = 0,$$

or no-slip boundary conditions

$$\tilde{v}^{\hat{z}}\big|_{z=0,1} = \left.\frac{\mathrm{d}\tilde{v}^{\hat{z}}}{\mathrm{d}z}\right|_{z=0,1} = 0, \quad \tilde{\theta}\Big|_{z=0,1} = 0.$$

To solve the eigenvalue problem (2.44) numerically we need to discretize the differential operators $\mathcal{A}$ and $\mathcal{B}$. We used the *Chebyshev collocation method* which is a spectral method suitable for solving ODEs or PDEs to high accuracy on a simple domain when the data defining the problem are smooth enough. This is indeed our case (even for the extended Boussinesq approximation since we

consider smooth material parameters only, as we shall see below). Chebyshev spectral method is based on polynomial interpolation in unevenly spaced points. These are called Chebyshev points and on the interval $[-1, 1]$ are given by

$$x_j = \cos(j\pi/N), \qquad j = 0, 1, \ldots, N. \tag{2.46}$$

We use these points to construct the *Chebyshev differentiation matrices*. Given a function f defined on $[-1, 1]$, we set $\mathbf{f} = [f_0, f_1, \ldots f_N]^T$, where $f_j = f(x_j)$ for $j = 0, 1, \ldots, N$ and some $N \in \mathbb{N}$. We obtain a discrete derivative $\mathbf{g}$ by interpolating f in Chebyshev points and then setting $\mathbf{g}$ as the derivative of the interpolated polynomial in these points. This operation is linear and it can be represented by an $(N + 1) \times (N + 1)$ differentiation matrix $\mathbb{D}_N$:

$$\mathbf{g} = \mathbb{D}_N \mathbf{f}.$$

Differential equations can be then transformed into algebraic problems where the differential operators are approximated by the Chebyshev differentiation matrices $\mathbb{D}_N$. This can be easily implemented in MATLAB. The general formula for $\mathbb{D}_N$ as well as more thorough introduction to Chebyshev spectral method can be found in Trefethen (2001) or Boyd (2001). As an illustrative example consider the case when $N = 2$. We then have three Chebyshev points $x_0 = 1$, $x_1 = 0$ and $x_2 = -1$, and the interpolant is the quadratic

$$p(x) = \frac{1}{2}x(1 + x)f_0 + (1 + x)(1 - x)f_1 + \frac{1}{2}x(x - 1)f_2,$$

where $f_j = f(x_j)$ for $j = 0, 1, 2$. The derivative is a linear polynomial

$$p'(x) = (x + \frac{1}{2})f_0 - 2xf_1 + (x - \frac{1}{2})f_2,$$

and the Chebyshev differentiation matrix is then given by

$$\mathbb{D}_2 = \begin{bmatrix} 3/2 & -2 & 1/2 \\ 1/2 & 0 & -1/2 \\ -1/2 & 2 & -3/2 \end{bmatrix}.$$

What remains is incorporating the boundary conditions in the differentiation matrices. This is a slightly more complicated matter since we are not dealing with just simple homogeneous Dirichlet boundary conditions. For our computations we used the differentiation matrices `chebdif` and `cheb4c` from the work of Reddy and Weideman (2000). Problem (2.44) is a fourth-order problem with either hinged (free-slip case) or clamped (no-slip case) boundary conditions on $\tilde{v}^{\hat{z}}$.[1]

[1] We say that a fourth-order boundary value problem

$$u''''(x) = f(x, u, u', u'', u'''), \qquad x \in [a, b],$$

has *hinged* boundary conditions if

$$u|_{x=a,b} = u''|_{x=a,b} = 0,$$

or *clamped* boundary conditions if

$$u|_{x=a,b} = u'|_{x=a,b} = 0.$$

The eigenvalue problem for clamped boundary conditions can be solved using the differentiation matrices `chebdif` for the second derivatives and `cheb4c` for the fourth derivatives (see Reddy and Weideman (2000) for details). Solving the eigenvalue problem for hinged boundary conditions is more complicated and we used a different method than the one proposed in the referenced paper. By introducing a new variable

$$w = \left(\frac{\mathrm{d}^2}{\mathrm{d}z^2} - a^2\right)\tilde{v}^{\hat{z}},$$

we transformed our boundary value problem into a second-order system of differential equations with homogeneous Dirichlet boundary conditions

$$\tilde{v}^{\hat{z}}\big|_{z=0,1} = w|_{z=0,1} = \tilde{\theta}\Big|_{z=0,1} = 0.$$

This can be solved easily using just the differentiation matrix `chebdif` for the second derivatives. In both cases we obtain a generalized algebraic eigenvalue problem

$$\sigma\mathbb{A}\mathbf{u} = \mathbb{B}\mathbf{u}, \tag{2.47}$$

where matrices $\mathbb{A}$ and $\mathbb{B}$ are appropriately discretized versions of operators $\mathcal{A}$ and $\mathcal{B}$ and vector $\mathbf{u}$ is formed from values of $\tilde{v}^{\hat{z}}$ and θ (and w in case of free-slip boundary conditions) in the Chebyshev points. It should be mentioned that the differentiation matrices `chebdif` and `cheb4c` along with the vector of Chebyshev points were transformed from the reference interval $[-1, 1]$ to our case of $[0, 1]$.

Problem (2.47) was solved using the MATLAB's implemented function `eig`. Experimenting with the number N of Chebyshev points we settled on using the value $N = 40$. This value was used for all the computations in this paper. [2]

Free-slip

In Figure 2.1 we depicted the largest eigenvalues σ for $a \in [0, 10]$ with a step size of 0.2 and $Ra \in [100, 1300]$ with a step size of 40. Prandtl number was set to $Pr = 10^9$.

We can see that for the values of $a \approx 2$ and $Ra \approx 650$ the first positive eigenvalues emerge. Analysing this marginal area in more detail yields the critical values of wave-number and Rayleigh number very close to the analytical results. We can see that in Figure 2.2 where we depicted the values of σ for $a \in [2.210, 2.234]$ with a step size of 0.0005 and $Ra \in [657.50, 657.53]$ with a step size of 0.001. Again, Prandtl number was set to $Pr = 10^9$.

Figures 2.1 and 2.2 show the maximum eigenvalue for specific a and Ra. Even though that the shape of the marginal curve is apparent from the figures (it separates the negative part of the spectrum from the positive part), it is quantitatively more accessible to depict the curves of specific values of σ. This is shown in Figure 2.3 where we chose the values $\sigma = -5$ (green line), $\sigma = 0$ (gray line, the marginal curve) and $\sigma = 5$ (red line).

[2] The MATLAB code that was developed for all the computations in this thesis can be found in the Student Information System as an attachment of the thesis.

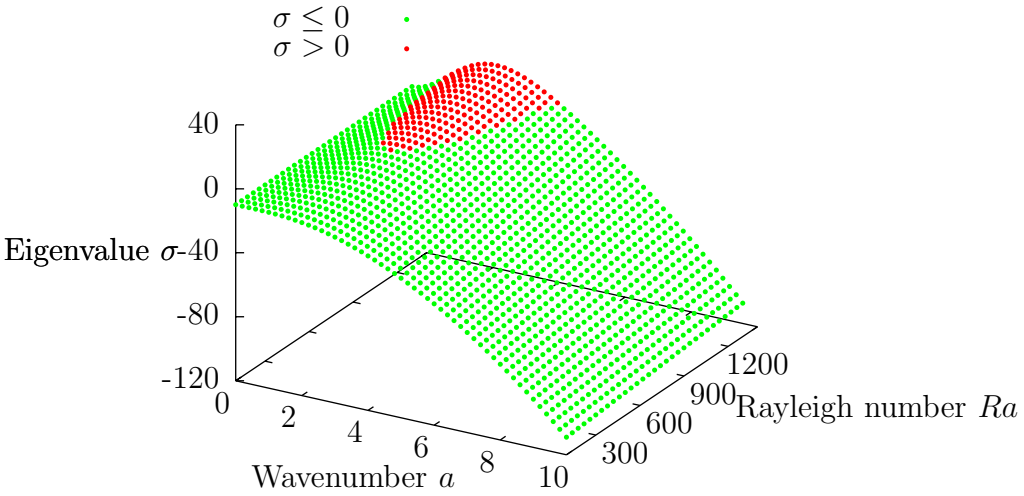

Figure 2.1: Spectrum for classical Boussinesq approximation and free-slip boundary condition

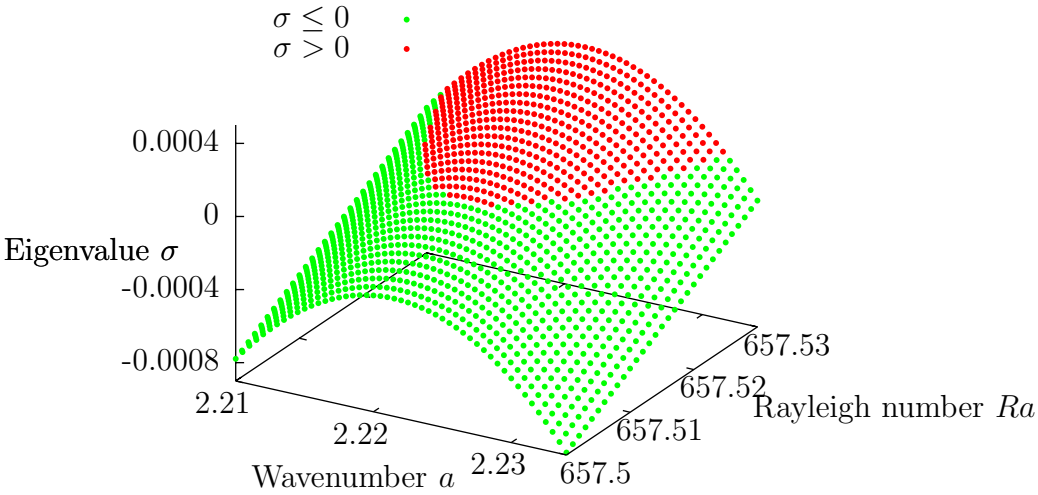

Figure 2.2: Magnification of spectrum near the critical point for classical Boussinesq approximation and free-slip boundary condition

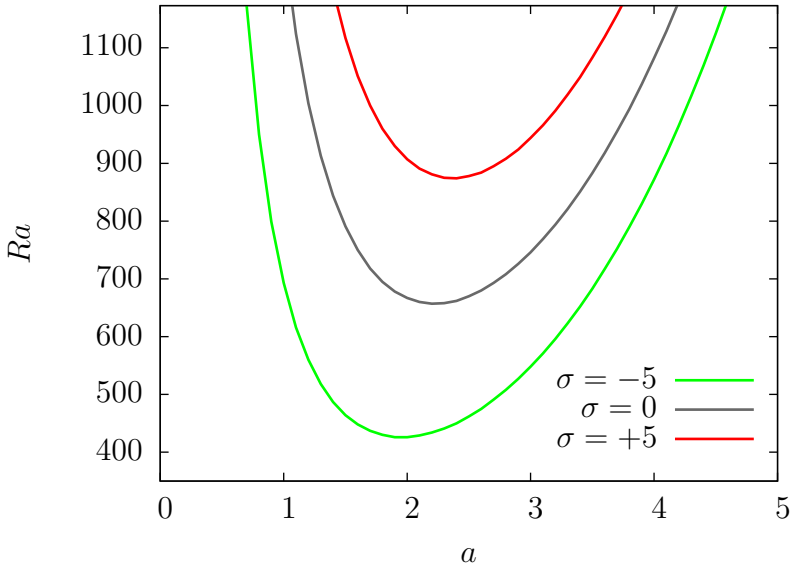

Figure 2.3: Curves for specific values of maximum eigenvalue σ, free-slip boundary condition

We know from the analytical solution of Rayleigh-Bénard problem that the critical values of wave-number and Rayleigh number are independent of Prandtl number. Let us first investigate if (and how) Prandtl number influences the numerically obtained critical values of a and Ra.[3] Table 2.1 shows critical values of a and Ra for several values of Pr. We can see that the difference is not very significant. However, for magnification of this size the spectrum is not as "smooth" as it appears in Figure 2.2 and we notice small defects from the shape of the marginal curve separating the negative and positive eigenvalues. Hence, we can't get more precise results than the values listed in Table 2.1.

Pr	Ra_{crit}	a_{crit}
0.1	657.5113643	2.22144
1	657.511364	2.22145
10	657.511364	2.22143
100	657.5113643	2.22145
1000	657.5113644	2.22144
10^9	657.5113644	2.22144
∞	657.5113644	2.22144

Table 2.1: The influence of Prandtl number on critical values of wave-number and Rayleigh number, free-slip boundary condition

Based on the results in Table 2.1 we set the numerically obtained critical values of wave-number and Rayleigh number to be $a_{\text{crit}} = 2.2214$ and $Ra_{\text{crit}} = 657.511364$. This gives a relative difference of approximately 1.867×10^{-5} and 7.293×10^{-10}

[3]We could also use the infinite Prandtl number approximation and thus simplify our eigenvalue problem (a common practice in geophysics where Prandtl number is very high, $Pr \approx 10^{20}$). However, for reasons that will be explained in the next chapter we keep Prandtl number finite. Nevertheless, for a comparison we include the case when $Pr \to \infty$.

compared to the critical values of wave-number and Rayleigh number obtained analytically.

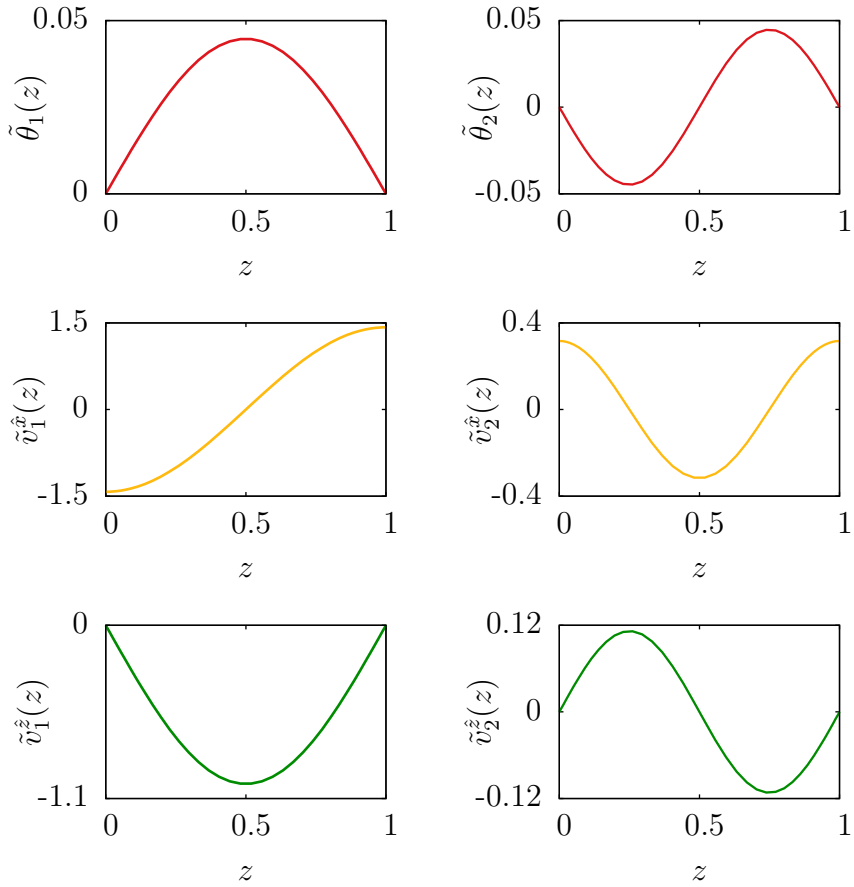

Figure 2.4: First two eigenfunctions for classical Boussinesq approximation and free-slip boundary condition in case of single rolls, $Pr = 10^9$, $Ra = 1000$, $a = a_{\text{crit}} = 2.2214$

Along with eigenvalues σ of problem (2.47) for specific values of a and Ra, we obtained eigenvectors $\mathbf{u}$ which can be transformed into eigenfunctions of (2.44) formed from $\tilde{v}^{\hat{z}}$ and $\tilde{\theta}$.

In the case of infinite longitudinal cells the y-component of velocity is zero. From (2.40) we can get the x-component of velocity for specific values of a and Ra from the computed $\tilde{v}^{\hat{z}}$. According to (2.40) the z-dependent part of $v^{\hat{x}}$ (which we denote by $\tilde{v}^{\hat{x}}$) reads

$$\tilde{v}^{\hat{x}} = \frac{\mathrm{i}}{a}\frac{\mathrm{d}\tilde{v}^{\hat{z}}}{\mathrm{d}z}.$$

This along with quantities $\tilde{v}^{\hat{z}}$ and $\tilde{\theta}$ form an eigenfunction of eigenvalue problem (3.3) formulated in the following chapter. We can see the functions depicted in Figure 2.4 where we plotted the imaginary part of $\tilde{v}^{\hat{x}}$ and used the normalization

$$\int_0^1 \left(Ra|\tilde{\theta}(z)|^2 + Pr^{-1}|\tilde{v}^{\hat{x}}(z)|^2 + Pr^{-1}|\tilde{v}^{\hat{z}}(z)|^2 \right) \mathrm{d}z = 1,$$

which will be useful later on for weakly non-linear analysis.

Numerically, we obtained the quantity $\tilde{v}^{\hat{x}}$ using the open-source package CHEBFUN for computing with functions in MATLAB. The discrete values of $\tilde{v}^{\hat{z}}$ and $\tilde{\theta}$ in Chebyshev points were first transformed into functions via the `polyfit` command. Differentiation and integration was than carried out by the `diff` and `sum` commands, respectively.

From the components of velocity and from the temperature of the most unstable mode we can depict velocity field and temperature field in the convecting layer. However, we do not yet know the real evolution in time for these quantities – the exponential evolution would cause enormous growth of magnitude and the assumption of non-linear perturbation terms being small would be violated. Taking into account the non-linear terms of the original problem will yield steady solution for slightly supercritical Rayleigh numbers. This will be done in the next chapter. As a result we will be able to depict the behaviour of convective cells for specific supercritical values of Ra.

No-slip

In Figure 2.5 we depicted eigenvalues σ for $a \in [0, 10]$ with a step size of 0.2 and $Ra \in [100, 3400]$ with a step size of 100. Prandtl number was set to $Pr = 10^9$.

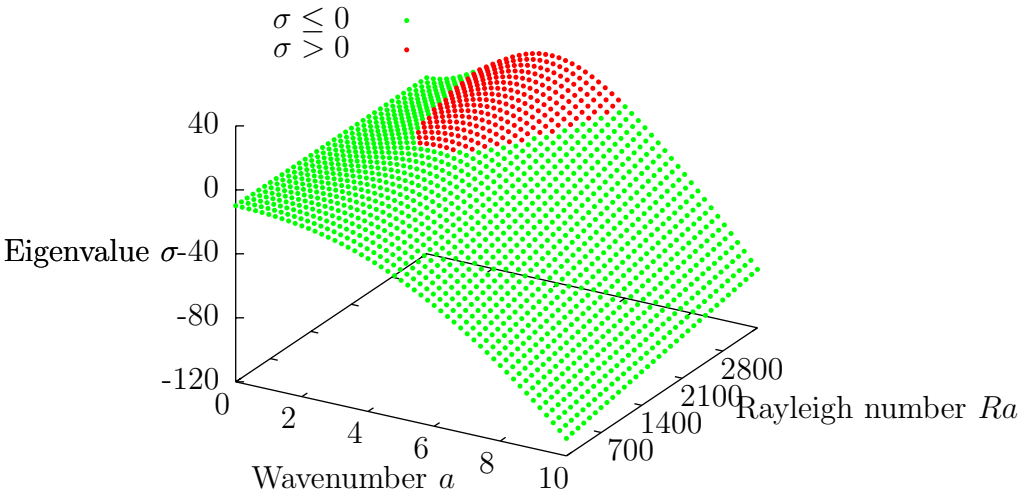

Figure 2.5: Spectrum for classical Boussinesq approximation and no-slip boundary condition

We can see that for the values of $a \approx 3$ and $Ra \approx 1700$ the first positive eigenvalues emerge. In Figure 2.6 we depicted the values of σ for $a \in [3.106, 3.128]$ with a step size of 0.0005 and $Ra \in [1707.75, 1707.78]$ with a step size of 0.001. Again, Prandtl number was set to $Pr = 10^9$.

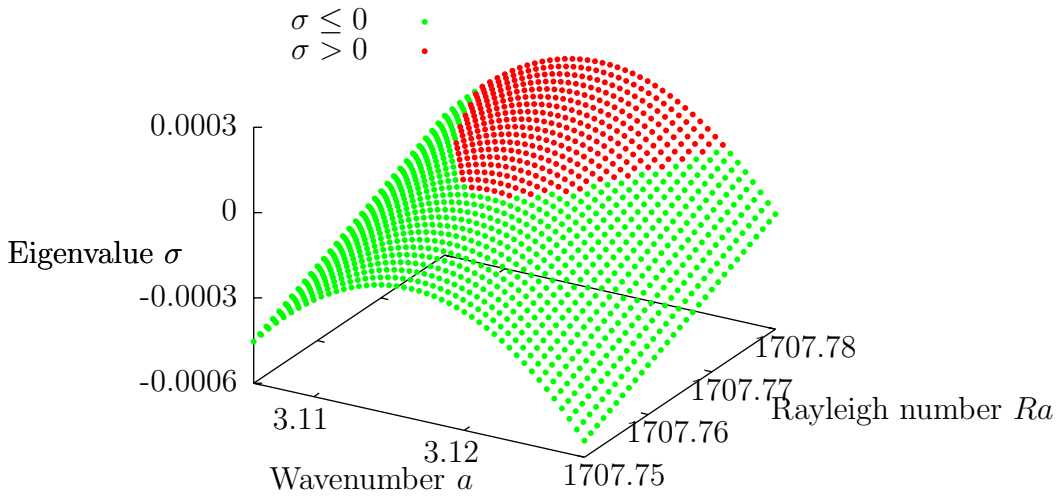

Figure 2.6: Magnification of spectrum near the critical point for classical Boussinesq approximation and free-slip boundary condition

We also include quantitatively more accessible depiction of the curves for specific values of maximum eigenvalues σ. This is shown in Figure 2.7 where we chose the values $\sigma = -5$ (green line), $\sigma = 0$ (gray line) and $\sigma = 5$ (red line).

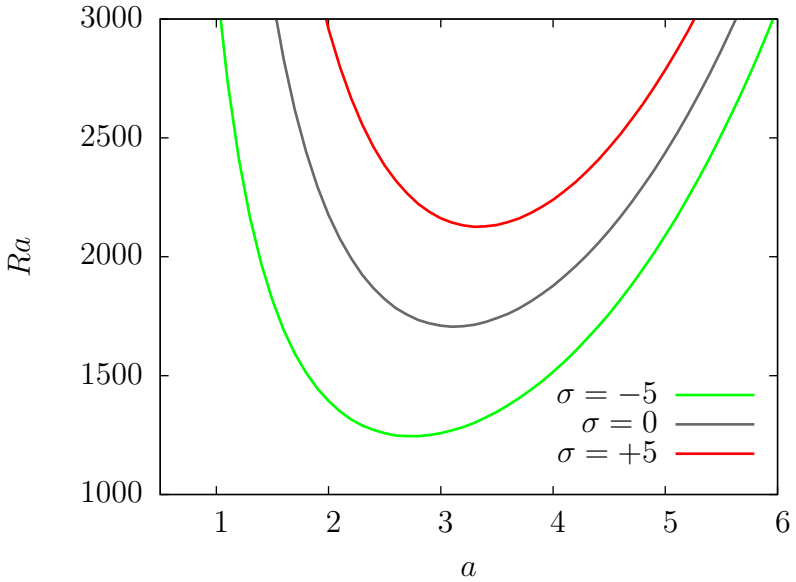

Figure 2.7: Curves for specific values of maximum eigenvalue σ, no-slip boundary condition

Similarly as for the free-slip boundary conditions, in Table 2.8 we investigated the numerical dependence of the critical pair a_{crit} and Ra_{crit} on Prandtl number.

Pr	Ra_{crit}	a_{crit}
0.1	1707.76177	3.1163
1	1707.76175	3.1164
10	1707.76170	3.116
100	1707.76169	3.1163
1000	1707.76173	3.1163
10^9	1707.76171	3.1163
∞	1707.76171	3.1163

Figure 2.8: The influence of Prandtl number on critical values of wave-number and Rayleigh number, no-slip boundary condition

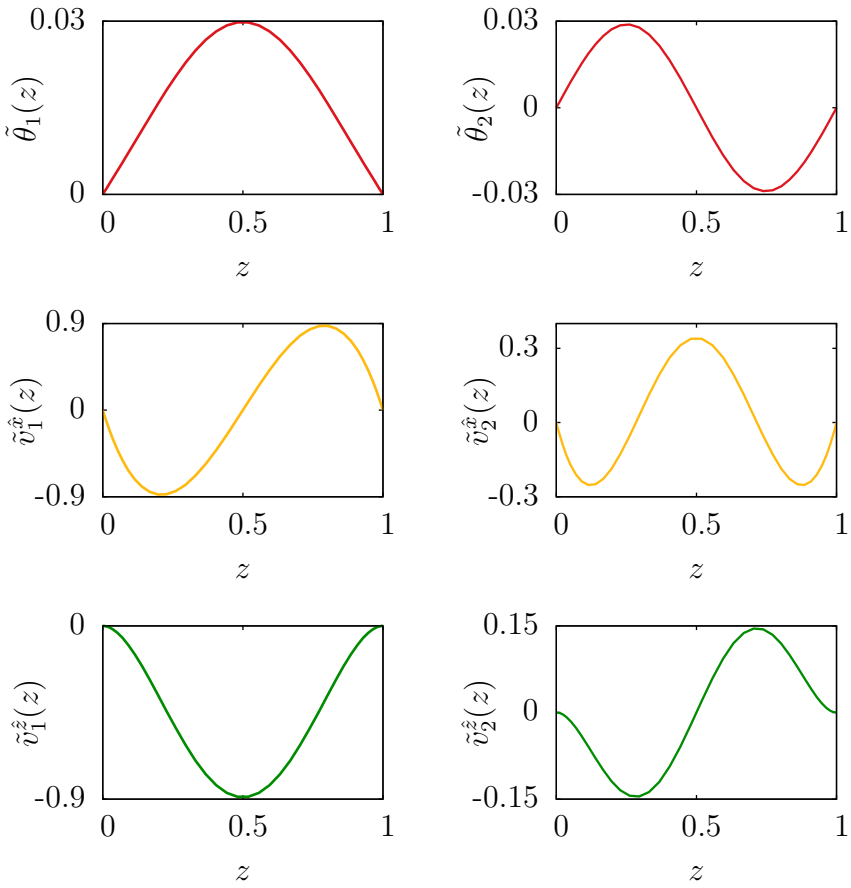

Figure 2.9: First two eigenfunctions for classical Boussinesq approximation and no-slip boundary condition in case of single rolls,, $Pr = 10^9$, $Ra = 2400$, $a = a_{\text{crit}} = 3.116$

This time we can see that the influence of Prandtl number is more significant. Moreover, the spectrum becomes distorted earlier than in the case of free-slip boundary condition and thus the precision of the critical values is not as high. Based on the obtained results, we set the critical values of wave-number and Rayleigh number to be $a_{\text{crit}} = 3.116$ and $Ra_{\text{crit}} = 1707.762$. This gives a relative difference of approximately 3.208×10^{-4} and 0 compared to the critical values of wave-number and Rayleigh number from Chandrasekhar (1961). However, we should bear in mind that these values were also obtained numerically.

Again, in the case of infinite longitudinal cells we can compute the x-component of velocity for specific values of a and Ra using the eigenfunctions $\tilde{v}^{\hat{z}}$ obtained numerically. We depicted the functions $\tilde{\theta}$, $\tilde{v}^{\hat{x}}$ and $\tilde{v}^{\hat{z}}$ in Figure 2.9 where we have taken the imaginary part of $\tilde{v}^{\hat{x}}$ and used the same scaling as in the free-slip case.

Depicting the velocity field and temperature field in the convecting layer will be again postponed to the next chapter where we are going to derive the time evolution of the unstable mode for slightly supercritical values of Ra.

2.2 Extended Boussinesq approximation

Let us now consider extended Boussinesq approximation. We follow exactly the same steps as for classical Boussinesq approximation up to the point of formulating generalized eigenvalue problem analogous to (2.43). We assume that the coefficients of thermal expansivity, dynamic viscosity and thermal conductivity are functions of depth and temperature, i.e. $\alpha = \alpha(z, T)$, $\mu = \mu(z, T)$ a $k = k(z, T)$. Explicit formulae for material parameters considered in this thesis are given in section 2.2.1.

We consider system of equations

$$\operatorname{div} \mathbf{v} = 0,$$

$$\varrho_0 \left[\frac{\partial \mathbf{v}}{\partial t} + (\mathbf{v} \cdot \nabla)\, \mathbf{v} \right] = -\varrho_0 \alpha (T - T_0) \mathbf{g}_0 - \nabla \Pi + \operatorname{div}(2\mu \mathbb{D}),$$

$$\varrho_0 c_p \frac{\partial T}{\partial t} = \operatorname{div}(k \nabla T) - \varrho_0 c_p \mathbf{v} \cdot \nabla T - \varrho_0 v^{\hat{r}} \alpha T g + 2\mu \mathbb{D} : \mathbb{D} + Q,$$

where, for the sake of simplicity, the reference gravitational acceleration $\mathbf{g}_0$ and the heat sources Q are assumed constant. Let us introduce dimensionless variables denoted again by stars

$$\mathbf{x} = d\mathbf{x}^*, \quad t = \frac{d^2}{\kappa_s} t^*, \quad \mathbf{v} = \frac{\kappa_s}{d} \mathbf{v}^*, \quad \Pi = \frac{\mu_s \kappa_s}{d^2} \Pi^*,$$

$$T = T_s + (T_b - T_s) T^*, \quad \alpha = \alpha_s \alpha^*, \quad \mu = \mu_s \mu^*, \quad k = k_s k^*,$$

where d is characteristic dimension of the system (e.g. the thickness of the Earth's mantle), $\kappa = k/\varrho_0 c_p$ and the subscript s denotes surface values of corresponding quantities, whereas subscript b denotes their bottom values.

Dimensionless form of the equations above then reads

$$\operatorname{div}^* \mathbf{v}^* = 0, \tag{2.48}$$

$$\frac{1}{Pr_s}\left[\frac{\partial \mathbf{v}^*}{\partial t^*} + (\mathbf{v}^* \cdot \nabla^*)\,\mathbf{v}^*\right] = Ra_s \alpha^* (T^* - T_0^*)\mathbf{e}_{\hat{r}} - \nabla^* \Pi^* + \operatorname{div}^* \left(\mu^* \left[\nabla^* \mathbf{v}^* + (\nabla^* \mathbf{v}^*)^T\right]\right), \tag{2.49}$$

$$\frac{\partial T^*}{\partial t^*} = \operatorname{div}^* (k^* \nabla^* T^*) - \mathbf{v}^* \cdot \nabla^* T^* - Di_s \alpha^* \left(T^* + \frac{Ra_s^{T_s}}{Ra_s}\right)(v^{\hat{r}})^* + \frac{Di_s}{Ra_s}\mu^* \left[\nabla^* \mathbf{v}^* + (\nabla^* \mathbf{v}^*)^T\right] : \nabla^* \mathbf{v}^* + \frac{Raq_s}{Ra_s}, \tag{2.50}$$

where we introduced dimensionless numbers

$$\begin{aligned}
&\textit{Prandtl number} && Pr_s = \frac{\mu_s}{\varrho_0 \kappa_s}\\
&\textit{Rayleigh number} && Ra_s = \frac{\varrho_0 \alpha_s (T_b - T_s) g_0 d^3}{\mu_s \kappa_s}\\
&\textit{Rayleigh number for heat sources} && Raq_s = \frac{\varrho_0 \alpha_s g_0 Q d^5}{\mu_s \kappa_s k_s}\\
&\textit{dissipation number} && Di_s = \frac{\alpha_s g_0 d}{c_p}\\
&\textit{auxiliary number} && Ra_s^{T_s} = \frac{\varrho_0 \alpha_s T_s g_0 d^3}{\mu_s \kappa_s}.
\end{aligned}$$

Let us now rewrite equations (2.1) - (2.3) in Cartesian coordinates (x^*, y^*, z^*), where x^* and y^* are dimensionless horizontal coordinates and z^* denotes dimensionless depth, $z^* \in [0, 1]$, $z = 0$ at the surface and $z = 1$ at the bottom of the convecting layer. The new system of equations reads (from now on we omit denoting the dimensionless variables by star, unless misunderstanding may arise)

$$\operatorname{div} \mathbf{v} = 0, \tag{2.51}$$

$$\frac{1}{Pr_s}\left[\frac{\partial \mathbf{v}}{\partial t} + (\mathbf{v} \cdot \nabla)\,\mathbf{v}\right] = -Ra_s \alpha (T - T_0)\mathbf{e}_{\hat{z}} - \nabla \Pi + \operatorname{div} \left(\mu \left[\nabla \mathbf{v} + (\nabla \mathbf{v})^T\right]\right), \tag{2.52}$$

$$\frac{\partial T}{\partial t} = \operatorname{div} (k \nabla T) - \mathbf{v} \cdot \nabla T + Di_s \alpha \left(T + \frac{Ra_s^{T_s}}{Ra_s}\right) v^{\hat{z}} + \frac{Di_s}{Ra_s}\mu \left[\nabla \mathbf{v} + (\nabla \mathbf{v})^T\right] : \nabla \mathbf{v} + \frac{Raq_s}{Ra_s}. \tag{2.53}$$

Reference state

Again, we assume that in the reference state the fluid is in quiescent state, i.e. $\mathbf{v} \equiv \mathbf{0}$, and the temperature is only function of depth, i.e. $T_0 = T_0(z)$. Equation (2.53) in the reference state then reads

$$0 = \operatorname{div}\left(k(z, T_0)\nabla T_0\right) + \frac{Raq_s}{Ra_s}. \tag{2.54}$$

Perturbation equations

Let us now assume that the reference state is perturbed slightly. We denote these perturbations of velocity, temperature and pressure by $\mathbf{v}$, θ and π, respectively. The perturbed state is then described by the quantities denoted by the prime

$$\begin{aligned}
\mathbf{v}' &= \mathbf{0} + \mathbf{v} = \mathbf{v}, \\
T' &= T_0 + \theta, \\
\Pi' &= 0 + \pi = \pi.
\end{aligned}$$

Putting these into equations (2.4) - (2.6) yields (with the aid of (2.54))

$$\operatorname{div}\mathbf{v} = 0, \tag{2.55}$$

$$\begin{aligned}
\frac{1}{Pr_s}\left[\frac{\partial \mathbf{v}}{\partial t} + (\mathbf{v}\cdot\nabla)\,\mathbf{v}\right] &= -Ra_s\alpha(z, T_0+\theta)\theta\mathbf{e}_{\hat{z}} - \nabla\pi \\
&\quad + \operatorname{div}\left(\mu(z, T_0+\theta)\left[\nabla\mathbf{v} + (\nabla\mathbf{v})^T\right]\right),
\end{aligned} \tag{2.56}$$

$$\begin{aligned}
\frac{\partial\theta}{\partial t} &= \operatorname{div}\left[k(z, T_0+\theta)\nabla(T_0+\theta) - k(z, T_0)\nabla T_0\right] - v^{\hat{z}}\frac{\mathrm{d}T_0}{\mathrm{d}z} - \mathbf{v}\cdot\nabla\theta \\
&+ Di_s\alpha(z, T_0+\theta)\left(T_0 + \theta + \frac{Ra_s^{T_s}}{Ra_s}\right)v^{\hat{z}} + \frac{Di_s}{Ra_s}\mu(z, T_0+\theta)\left[\nabla\mathbf{v} + (\nabla\mathbf{v})^T\right] : \nabla\mathbf{v}.
\end{aligned} \tag{2.57}$$

If we Taylor expand the coefficients k, α and μ and neglect the non-linear terms, we arrive at

$$\operatorname{div}\mathbf{v} = 0, \tag{2.58}$$

$$\frac{1}{Pr_s}\frac{\partial\mathbf{v}}{\partial t} = -Ra_s\alpha(z, T_0)\theta\mathbf{e}_{\hat{z}} - \nabla\pi + \operatorname{div}\left(\mu(z, T_0)\left[\nabla\mathbf{v} + (\nabla\mathbf{v})^T\right]\right), \tag{2.59}$$

$$\begin{aligned}
\frac{\partial\theta}{\partial t} &= \operatorname{div}\left(\frac{\partial k}{\partial T}(z, T_0)\frac{\mathrm{d}T_0}{\mathrm{d}z}\theta\mathbf{e}_{\hat{z}} + k(z, T_0)\nabla\theta\right) \\
&\quad - v^{\hat{z}}\frac{\mathrm{d}T_0}{\mathrm{d}z} + Di_s\alpha(z, T_0)\left(T_0 + \frac{Ra_s^{T_s}}{Ra_s}\right)v^{\hat{z}}.
\end{aligned} \tag{2.60}$$

Let us now apply the operator div to equation (2.59). We get

$$0 = -Ra_s \operatorname{div}\left(\alpha(z,T_0)\theta \mathbf{e}_{\hat{z}}\right) - \Delta\pi + \operatorname{div}\left(\operatorname{div}\left(\mu(z,T_0)\left[\nabla\mathbf{v} + (\nabla\mathbf{v})^T\right]\right)\right). \quad (2.61)$$

Applying of the operator Δ to equation (2.59) yields

$$\frac{1}{Pr_s}\frac{\partial}{\partial t}(\Delta\mathbf{v}) = -Ra_s\Delta\left(\alpha(z,T_0)\theta\right)\mathbf{e}_{\hat{z}} - \nabla(\Delta\pi) + \Delta\left(\operatorname{div}\left(\mu(z,T_0)\left[\nabla\mathbf{v} + (\nabla\mathbf{v})^T\right]\right)\right). \quad (2.62)$$

Putting the expression $\Delta\pi$ from (2.61) into (2.62) further yields

$$\frac{1}{Pr_s}\frac{\partial}{\partial t}(\Delta\mathbf{v}) = -Ra_s\Delta\left(\alpha(z,T_0)\theta\right)\mathbf{e}_{\hat{z}} + Ra_s\nabla\left(\operatorname{div}\left(\alpha(z,T_0)\theta\mathbf{e}_{\hat{z}}\right)\right) - \nabla\left(\operatorname{div}\left(\operatorname{div}\left(\mu(z,T_0)\left[\nabla\mathbf{v} + (\nabla\mathbf{v})^T\right]\right)\right)\right) + \Delta\left(\operatorname{div}\left(\mu(z,T_0)\left[\nabla\mathbf{v} + (\nabla\mathbf{v})^T\right]\right)\right).$$

This can be written in more compact form with the aid of identity $\operatorname{curl}(\operatorname{curl}\mathbf{u}) = \nabla(\operatorname{div}\mathbf{u}) - \Delta\mathbf{u}$ [4]

$$\frac{1}{Pr_s}\frac{\partial}{\partial t}(\Delta\mathbf{v}) = Ra_s\begin{bmatrix}\alpha(z,T_0)\frac{\partial^2\theta}{\partial x\partial z} + \frac{\mathrm{d}\alpha}{\mathrm{d}z}(z,T_0)\frac{\partial\theta}{\partial x}\\ \alpha(z,T_0)\frac{\partial^2\theta}{\partial y\partial z} + \frac{\mathrm{d}\alpha}{\mathrm{d}z}(z,T_0)\frac{\partial\theta}{\partial y}\\ -\alpha(z,T_0)\left(\frac{\partial^2\theta}{\partial x^2} + \frac{\partial^2\theta}{\partial y^2}\right)\end{bmatrix} - \operatorname{curl}\left(\operatorname{curl}\left(\operatorname{div}\left(\mu(z,T_0)\left[\nabla\mathbf{v} + (\nabla\mathbf{v})^T\right]\right)\right)\right). \quad (2.63)$$

Let us go back to equation (2.59) again and apply the operator curl to it. With the aid of the identity $\operatorname{curl}\nabla\varphi = 0$, we obtain

$$\frac{1}{Pr_s}\frac{\partial}{\partial t}(\operatorname{curl}\mathbf{v}) = Ra_s\begin{bmatrix}-\alpha(z,T_0)\frac{\partial\theta}{\partial y}\\ \alpha(z,T_0)\frac{\partial\theta}{\partial x}\\ 0\end{bmatrix} + \operatorname{curl}\left(\operatorname{div}\left(\mu(z,T_0)\left[\nabla\mathbf{v} + (\nabla\mathbf{v})^T\right]\right)\right). \quad (2.64)$$

Computing the vector operators in equations (2.63) and (2.64) and expressing the $\mathbf{e}_{\hat{z}}$-components from them yields (we are using the notation $\boldsymbol{\eta} \equiv \operatorname{curl}\mathbf{v}$)

$$\frac{1}{Pr_s}\frac{\partial}{\partial t}(\Delta v^{\hat{z}}) = -Ra_s\alpha(z,T_0)\left(\frac{\partial^2\theta}{\partial x^2} + \frac{\partial^2\theta}{\partial y^2}\right) + \mu(z,T_0)\Delta(\Delta v^{\hat{z}}) + 2\frac{\mathrm{d}\mu}{\mathrm{d}z}(z,T_0)\frac{\partial}{\partial z}\left(\Delta v^{\hat{z}}\right) - \frac{\mathrm{d}^2\mu}{\mathrm{d}z^2}(z,T_0)\left(\Delta v^{\hat{z}} - 2\frac{\partial^2 v^{\hat{z}}}{\partial z^2}\right), \quad (2.65)$$

$$\frac{1}{Pr_s}\frac{\partial\eta^{\hat{z}}}{\partial t} = \mu(z,T_0)\Delta\eta^{\hat{z}} + \frac{\mathrm{d}\mu}{\mathrm{d}z}(z,T_0)\frac{\partial\eta^{\hat{z}}}{\partial z}. \quad (2.66)$$

[4] Symbol $\frac{\mathrm{d}\alpha}{\mathrm{d}z}(z,T_0)$ denotes the total derivative of α with respect to z. Specifically,

$$\frac{\mathrm{d}\alpha}{\mathrm{d}z}(z,T_0) = \frac{\partial\alpha}{\partial z}(z,T_0) + \frac{\partial\alpha}{\partial T}(z,T_0)\frac{\mathrm{d}T_0}{\mathrm{d}z}(z).$$

We define the symbols $\frac{\mathrm{d}\mu}{\mathrm{d}z}(z,T_0)$, $\frac{\mathrm{d}k}{\mathrm{d}z}(z,T_0)$ analogously (along with higher derivatives which will appear later on).

Let us apply the div operator in equation (2.60) too

$$\frac{\partial\theta}{\partial t} = k(z,T_0)\Delta\theta + \left(\frac{\mathrm{d}k}{\mathrm{d}z}(z,T_0) + \frac{\partial k}{\partial T}(z,T_0)\frac{\mathrm{d}T_0}{\mathrm{d}z}\right)\frac{\partial\theta}{\partial z} + \frac{\mathrm{d}}{\mathrm{d}z}\left(\frac{\partial k}{\partial T}(z,T_0)\frac{\mathrm{d}T_0}{\mathrm{d}z}\right)\theta - \frac{\mathrm{d}T_0}{\mathrm{d}z}v^{\hat{z}} + Di_s\alpha(z,T_0)\left(T_0 + \frac{Ra_s^{T_s}}{Ra_s}\right)v^{\hat{z}}. \quad (2.67)$$

We now consider the perturbations in the form of normal modes

$$\begin{aligned}\mathbf{v}(t,\mathbf{x}) &= \tilde{\mathbf{v}}(z)\exp\left[\mathrm{i}(a_x x + a_y y) + \sigma t\right],\\ \boldsymbol{\eta}(t,\mathbf{x}) &= \tilde{\boldsymbol{\eta}}(z)\exp\left[\mathrm{i}(a_x x + a_y y) + \sigma t\right],\\ \theta(t,\mathbf{x}) &= \tilde{\theta}(z)\exp\left[\mathrm{i}(a_x x + a_y y) + \sigma t\right].\end{aligned}$$

Equations (2.65)–(2.67) can then be written in the form (we are using the notation $a^2 = a_x^2 + a_y^2$)

$$\frac{\sigma}{Pr_s}\left(\frac{\mathrm{d}^2}{\mathrm{d}z^2} - a^2\right)\tilde{v}^{\hat{z}} = a^2 Ra_s\alpha(z,T_0)\tilde{\theta} + \mu(z,T_0)\left(\frac{\mathrm{d}^2}{\mathrm{d}z^2} - a^2\right)^2\tilde{v}^{\hat{z}} + 2\frac{\mathrm{d}\mu}{\mathrm{d}z}(z,T_0)\left(\frac{\mathrm{d}^2}{\mathrm{d}z^2} - a^2\right)\frac{\mathrm{d}\tilde{v}^{\hat{z}}}{\mathrm{d}z} + \frac{\mathrm{d}^2\mu}{\mathrm{d}z^2}(z,T_0)\left(\frac{\mathrm{d}^2}{\mathrm{d}z^2} + a^2\right)\tilde{v}^{\hat{z}}, \quad (2.68)$$

$$\frac{\sigma}{Pr_s}\tilde{\eta}^{\hat{z}} = \mu(z,T_0)\left(\frac{\mathrm{d}^2}{\mathrm{d}z^2} - a^2\right)\tilde{\eta}^{\hat{z}} + \frac{\mathrm{d}\mu}{\mathrm{d}z}(z,T_0)\frac{\mathrm{d}\tilde{\eta}^{\hat{z}}}{\mathrm{d}z}, \quad (2.69)$$

$$\sigma\tilde{\theta} = k(z,T_0)\left(\frac{\mathrm{d}^2}{\mathrm{d}z^2} - a^2\right)\tilde{\theta} + \left(\frac{\mathrm{d}k}{\mathrm{d}z}(z,T_0) + \frac{\partial k}{\partial T}(z,T_0)\frac{\mathrm{d}T_0}{\mathrm{d}z}\right)\frac{\mathrm{d}\tilde{\theta}}{\mathrm{d}z} + \frac{\mathrm{d}}{\mathrm{d}z}\left(\frac{\partial k}{\partial T}(z,T_0)\frac{\mathrm{d}T_0}{\mathrm{d}z}\right)\tilde{\theta} - \frac{\mathrm{d}T_0}{\mathrm{d}z}\tilde{v}^{\hat{z}} + Di_s\alpha(z,T_0)\left(T_0 + \frac{Ra_s^{T_s}}{Ra_s}\right)\tilde{v}^{\hat{z}}. \quad (2.70)$$

This is again an eigenvalue problem - finding the eigenvalues determines the onset of convection for extended Boussinesq approximation. To be able to solve this problem we need to consider specific functions k, α, μ and set specific values of the dimensionless numbers Pr_s, Raq_s, Di_s and $Ra_s^{T_s}$.

2.2.1 Material properties of Earth's mantle

In this section, we distinguish between the variables with units and the dimensionless variables by using the no-star/star notation. The references used for writing this section include the monograph G. Schubert (2001) and the papers of Tosi et al. (2013), Hirth and Kohlstedt (2003), Kameyama et al. (1999), Čížková et al. (2012) and Matyska and Yuen (2007).

We assume that we know the functions k, α, μ along with all the material properties of the Earth's mantle (namely ϱ_0, g_0, c_p and d). To determine the critical Rayleigh number characterizing the onset of convection we will assume that we

know the surface temperature $T_s = 300\,\mathrm{K}$ and the bottom temperature T_b will represent free variable (in reality $T_b = 4000\,\mathrm{K}$). This approach simulates the experimental setting when one varies the bottom temperature in order to determine the onset of convection.

We also assume that we have fixed values of the dimensionless numbers Pr_s, Raq_s, Di_s and $Ra_s^{T_s}$. Specifically, for Earth's mantle: $Pr \approx 10^{22}$ (and thus we may use the infinite Prandtl number approximation), $Di_s = 0.5$, $Raq_s = 10^6$ and $Ra_s^{T_s} = 8.1 \times 10^5$ (see Matyska and Yuen (2007)). The authors of the referenced paper are using higher Rayleigh number for heat sources, namely $Raq_s = 3 \times 10^7$. However, this value is too high for our computations as will be discussed in section 2.2.3. We will also consider the cases when Raq_s is equal to zero or both Di_s and Raq_s are equal to zero.

Let us note that in Earth's mantle $Ra_s = 10^7$. This means that if our critical value of Ra_s is above this value, there is no convection in Earth's mantle. Surely, that is not what we expect. On contrary, Ra_{crit} should be way below the real value of Ra_s because we expect a chaotic (on geological timescale) behaviour far away from the steady convection cells.

Let us also note that from the knowledge of $Ra_s = 10^7$ and the bottom temperature $T_b = 4000\,\mathrm{K}$ we can express the constant ratio $r \equiv \frac{T_b - T_s}{Ra_s} = \frac{3700}{10^7}$. Lastly, let us set the thickness of the Earth's mantle to be $d = 2900\,\mathrm{km}$.

Concerning the material coefficients, for the sake of simplicity we consider these simple functions

$$\begin{aligned} k(z,T) &= (k_s + b_k z)\exp\left[-c_k(T - T_s)\right], \\ \alpha(z,T) &= \alpha_s \exp(-b_\alpha z), \\ \mu(z,T) &= \mu_s \exp[b_\mu z - c_\mu(T - T_s)], \end{aligned}$$

where the coefficients b, $c \in \mathbb{R}_0^+$ with corresponding subscripts will be chosen appropriately so that

- k is an increasing function of depth undergoing at most a change of order 1, or a decreasing function of temperature undergoing at most a change of order 1,
- α is a decreasing function of depth undergoing at most a change of order 1,
- μ is an increasing function of depth undergoing at most a change of order 2, or a decreasing function of temperature undergoing at most a change of order 2.

This behaviour of material parameters should roughly approximate the Earth's mantle's material properties. We refrain from investigating the temperature-dependence of thermal expansivity since this dependence is not very significant in geophysics. To investigate the influence of the material coefficients on the onset of convection, we always consider all the material coefficients being constant except for one being a z or T-dependent function.

In terms of dimensionless variables, the functions above can be written as

$$k^*(z^*, T^*) = \left(1 + \frac{b_k d z^*}{k_s}\right) \exp(-c_k r Ra_s T^*) = (1 + \tilde{b}_k z^*) \exp(-\tilde{c}_k Ra_s T^*),$$
$$\alpha^*(z^*, T^*) = \exp(-b_\alpha d z^*) = \exp(-\tilde{b}_\alpha z^*),$$
$$\mu^*(z^*, T^*) = \exp(b_\mu d z^* - c_\mu r Ra_s T^*) = \exp(\tilde{b}_\mu z^* - \tilde{c}_\mu Ra_s T^*),$$

where we denoted

$$\tilde{b}_k = b_k d/k_s, \quad \tilde{b}_\alpha = b_\alpha d, \quad \tilde{b}_\mu = b_\mu d,$$
$$\tilde{c}_k = c_k r, \quad \tilde{c}_\mu = c_\mu r.$$

We can see that the dimensionless form of functions k, α, μ are Ra_s-dependent.

Concerning the boundary conditions, we will be using free-slip case only, since this is a common boundary condition in geophysics. Let us mention that in laboratory experiments it is more common to consider the no-slip boundary condition.

2.2.2 Reference temperature

From now on we omit denoting the dimensionless variables by star again.

Since $k = k(z, T)$, equation (2.54) yields non-linear ordinary differential equation

$$k(z, T_0)\frac{\mathrm{d}^2 T_0}{\mathrm{d}z^2} + \frac{\mathrm{d}k}{\mathrm{d}z}(z, T_0)\frac{\mathrm{d}T_0}{\mathrm{d}z} + \frac{Raq_s}{Ra_s} = 0 \tag{2.71}$$

with the boundary conditions

$$T_0(0) = 0, \quad T_0(1) = 1. \tag{2.72}$$

Again, the solution T_0 will be for Raq_s non-zero Ra_s-dependent and hence we will have to solve (2.71) for every single value of Ra_s considered when determining the onset of convection. We solved equation (2.71) numerically using MATLAB and open-source package CHEBFUN.

As an illustrative example, in Figure 2.10 we depicted the reference temperature T_0 in two cases of the extended Boussinesq approximation along with the case of classical Boussinesq approximation. Using the notation in the figure

- EB1: depth-dependent thermal conductivity with nonzero heat sources ($\tilde{b}_k = 10$, $\tilde{c}_k = 0$, $Ra_s = 10^7$ and $Raq_s = 3 \times 10^7$),
- EB2: constant thermal conductivity with nonzero heat sources ($\tilde{b}_k = 0$, $\tilde{c}_k = 0$, $Ra_s = 10^7$ and $Raq_s = 3 \times 10^7$),
- CB: classical Boussinesq approximation ($k \equiv 1$, $Raq_s = 0$) .

Note that in the presence of heat sources the reference temperature can rise above the boundary value 1 as in the case EB2. Non-constant thermal conductivity can reduce this effect as in the case EB1.

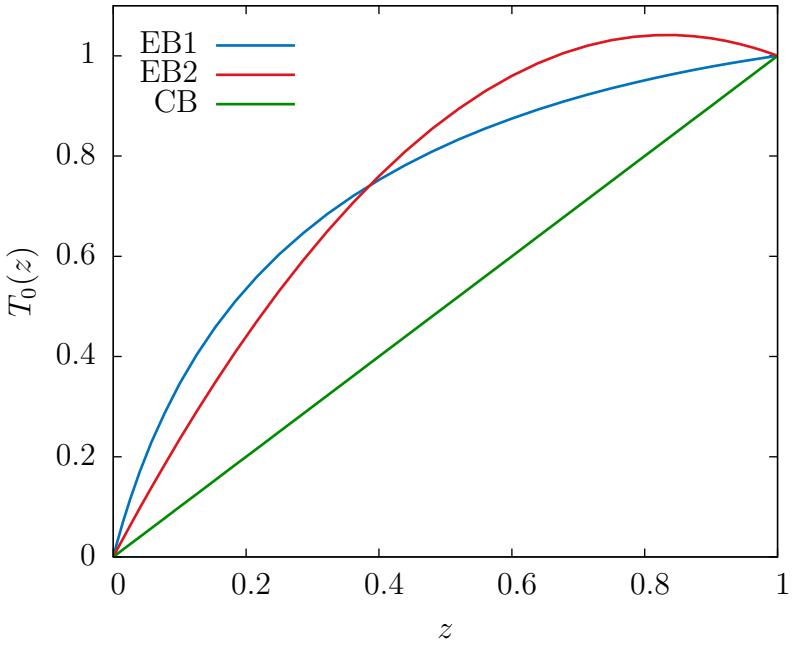

Figure 2.10: Reference temperature for extended (EB1, EB2) and classical (CB) Boussinesq approximation

2.2.3 Numerical solution

Let us reformulate equations (2.68)–(2.70) into an eigenvalue problem

$$\sigma\mathcal{A}\begin{bmatrix}\tilde{v}^{\hat{z}}\\ \tilde{\eta}^{\hat{z}}\\ \tilde{\theta}\end{bmatrix} = \mathcal{B}\begin{bmatrix}\tilde{v}^{\hat{z}}\\ \tilde{\eta}^{\hat{z}}\\ \tilde{\theta}\end{bmatrix}, \tag{2.73}$$

where

$$\mathcal{A} = \begin{bmatrix}\frac{1}{Pr_s}\left(\frac{\mathrm{d}^2}{\mathrm{d}z^2} - a^2\right) & 0 & 0\\ 0 & \frac{1}{Pr_s} & 0\\ 0 & 0 & 1\end{bmatrix}, \quad \mathcal{B} = \begin{bmatrix}B_{11} & 0 & B_{13}\\ 0 & B_{22} & 0\\ B_{31} & 0 & B_{33}\end{bmatrix},$$

and

$$B_{11} = \mu(z,T_0)\left(\frac{\mathrm{d}^2}{\mathrm{d}z^2} - a^2\right)^2 + 2\frac{\mathrm{d}\mu}{\mathrm{d}z}(z,T_0)\left(\frac{\mathrm{d}^2}{\mathrm{d}z^2} - a^2\right)\frac{\mathrm{d}}{\mathrm{d}z} + \frac{\mathrm{d}^2\mu}{\mathrm{d}z^2}(z,T_0)\left(\frac{\mathrm{d}^2}{\mathrm{d}z^2} + a^2\right),$$

$$B_{13} = a^2 Ra_s\alpha(z,T_0),$$

$$B_{22} = \mu(z,T_0)\left(\frac{\mathrm{d}^2}{\mathrm{d}z^2} - a^2\right) + \frac{\mathrm{d}\mu}{\mathrm{d}z}(z,T_0)\frac{\mathrm{d}}{\mathrm{d}z}$$

$$B_{31} = -\frac{\mathrm{d}T_0}{\mathrm{d}z} + Di_s\alpha(z,T_0)\left(T_0 + \frac{Ra_s^{T_s}}{Ra_s}\right),$$

$$B_{33} = k(z,T_0)\left(\frac{\mathrm{d}^2}{\mathrm{d}z^2} - a^2\right) + \left(\frac{\mathrm{d}k}{\mathrm{d}z}(z,T_0) + \frac{\partial k}{\partial T}(z,T_0)\frac{\mathrm{d}T_0}{\mathrm{d}z}\right)\frac{\mathrm{d}}{\mathrm{d}z} + \frac{\mathrm{d}}{\mathrm{d}z}\left(\frac{\partial k}{\partial T}(z,T_0)\frac{\mathrm{d}T_0}{\mathrm{d}z}\right).$$

Where for free-slip boundary conditions we have

$$\tilde{v}^{\hat{z}}\big|_{z=0,1} = \left.\frac{\mathrm{d}^2\tilde{v}^{\hat{z}}}{\mathrm{d}z^2}\right|_{z=0,1} = 0, \quad \left.\frac{\mathrm{d}\tilde{\eta}^{\hat{z}}}{\mathrm{d}z}\right|_{z=0,1} = 0, \quad \tilde{\theta}\Big|_{z=0,1} = 0$$

while for no-slip

$$\tilde{v}^{\hat{z}}\big|_{z=0,1} = \left.\frac{\mathrm{d}\tilde{v}^{\hat{z}}}{\mathrm{d}z}\right|_{z=0,1} = 0, \quad \tilde{\eta}^{\hat{z}}\big|_{z=0,1} = 0, \quad \tilde{\theta}\Big|_{z=0,1} = 0.$$

Our goal is to find eigenvalues σ. If for specific Ra and a there exists an eigenvalue with positive real part, then the perturbation will grow in time and the state is unstable. On the other hand, if all the eigenvalues are negative, then the state is stable and the perturbations will decay.

Let us first show that we can again eliminate equation (2.69) as in the case of classical Boussinesq approximation. We can write (2.69) in the form

$$\frac{\sigma}{Pr_s}\tilde{\eta}^{\hat{z}} = \frac{\mathrm{d}}{\mathrm{d}z}\left(\mu(z,T_0)\frac{\mathrm{d}\tilde{\eta}^{\hat{z}}}{\mathrm{d}z}\right) - a^2\mu(z,T_0)\tilde{\eta}^{\hat{z}}.$$

Multiplying the equation above by $\overline{\tilde{\eta}^{\hat{z}}}$, taking the real part of the resulting equality and integrating yields

$$\frac{\sigma_{\mathrm{Re}}}{Pr_s}\int_0^1 |\tilde{\eta}^{\hat{z}}|^2\,\mathrm{d}z = \int_0^1 \mathrm{Re}\left[\frac{\mathrm{d}}{\mathrm{d}z}\left(\mu(z,T_0)\frac{\mathrm{d}\tilde{\eta}^{\hat{z}}}{\mathrm{d}z}\right)\overline{\tilde{\eta}^{\hat{z}}}\right]\mathrm{d}z - a^2\int_0^1 \mu(z,T_0)|\tilde{\eta}^{\hat{z}}|^2\,\mathrm{d}z.$$

Integrating by parts and using either free-slip, or no-slip boundary conditions then yields

$$\frac{\sigma_{\mathrm{Re}}}{Pr_s}\int_0^1 |\tilde{\eta}^{\hat{z}}|^2\,\mathrm{d}z = -\int_0^1 \mu(z,T_0)\left|\frac{\mathrm{d}\tilde{\eta}^{\hat{z}}}{\mathrm{d}z}\right|^2\mathrm{d}z - a^2\int_0^1 \mu(z,T_0)|\tilde{\eta}^{\hat{z}}|^2\,\mathrm{d}z.$$

Since μ is a positive function it follows that $\sigma_{\mathrm{Re}} < 0$ for $\tilde{\eta}^{\hat{z}} \neq 0$. Hence, we can eliminate equation (2.69) and consider the reduced eigenvalue problem without this equation.

$$\sigma\mathcal{A}\begin{bmatrix}\tilde{v}^{\hat{z}}\\ \tilde{\theta}\end{bmatrix} = \mathcal{B}\begin{bmatrix}\tilde{v}^{\hat{z}}\\ \tilde{\theta}\end{bmatrix}, \tag{2.74}$$

with operators $\mathcal{A}$ and $\mathcal{B}$ appropriately modified.

Until now we were considering both free-slip or no-slip boundary conditions. As we stated in section 2.2.1 we will be using geophysically more relevant free-slip

case only. It is worth mentioning though that we can obtain results for both boundary conditions (if we wanted to test the numerical results via laboratory experiments, we would probably be using no-slip boundary conditions).

The numerical model used for solving (2.74) is principally the same as the one used in the classical case. Let us note that the open-source package CHEBFUN is also incorporated in the MATLAB code – we use this to solve differential equation (2.71). The spectra of problem (2.74) look qualitatively the same as for classical Boussinesq approximation. Thus, to save space we only give one illustrative example of the spectrum along with the eigenfunctions in the following section for depth-dependent thermal conductivity and dissipation and heat sources included.

Let us discuss the value of Raq_s as was mentioned in section 2.2.1. Depth- and temperature-dependent behaviour of the material coefficients mostly yields higher critical Rayleigh number, i.e. it has stabilizing effect, at least in the case of dissipation excluded. Heat sources on the other hand destabilize – the higher the value Raq_s is, the lower Ra_{crit} we get. Since we consider only one of the material coefficients non-constant at a time, the destabilizing effect for $Raq_s = 3 \times 10^7$ (the value from Matyska and Yuen (2007)) is so significant that there wouldn't be any reference state at all (more precisely, for heat sources this high the reference state is unstable for an arbitrarily small value of Ra_s). Thus, to get finite positive values of Ra_{crit} we set for our purposes $Raq_s = 10^6$.

Let us also mention that dissipation has a large stabilizing effect. The results of the following sections show that the value $Di_s = 0.5$ makes the critical Rayleigh number rise significantly ($Ra_{\text{crit}} \sim 10^5$). Since we used a rather large value of the dissipation number we also tried varying the dissipation number for the case of all the material parameters being constant and for several values of Raq_s. We investigated the cases when Di_s is equal to 0, 0.05, 0.1, 0.2 and 0.5. However, for larger values of Raq_s there are no stable conductive states for small dissipation numbers; for example if Raq_s is greater than approximately 2×10^4 there is no stable conductive state for constant material parameters and $Di_s = 0$. We considered the cases when Raq_s is equal to 0, 2×10^5, 3.5×10^5 and 6.5×10^5. The resulting critical values of wave-number and Rayleigh number can be found in Table 2.2.

We depicted the obtained dependence of critical Rayleigh number on dissipation number in Figure 2.11. Note the approximately linear profile in all the cases considered. As expected the heat sources only shift the critical values downwards and don't have substantial influence on the profiles.

Concerning the precision of the obtained critical values of wave-number and Rayleigh number, we should mention that again we experience some influence of Prandtl number on the critical values. This along with distortion of the spectrum for large magnifications restricts the precision of the obtained critical values. We round the values of a_{crit} to 4 significant digits and the values of Ra_{crit} to 6 significant digits – this precision is achievable in all the cases considered.

An important property of the eigenvalues in the classical case was that they were real. This was proven in section 2.1.2. However, in the case of extended

$Raq_s = 0$

Di_s	a_{crit}	Ra_{crit}
0	2.221	657.511
0.05	2.236	42 204.1
0.1	2.474	85 798.2
0.2	3.712	177 473
0.5	5.362	475 670

$Raq_s = 2 \times 10^5$

Di_s	a_{crit}	Ra_{crit}
0	–	–
0.05	5.189	2 935.01
0.1	5.224	45 385.0
0.2	5.352	133 457
0.5	6.054	422 491

$Raq_s = 3.5 \times 10^5$

Di_s	a_{crit}	Ra_{crit}
0	–	–
0.05	–	–
0.1	5.822	5235.43
0.2	5.907	93 003.4
0.5	6.423	379 560

$Raq_s = 6.5 \times 10^5$

Di_s	a_{crit}	Ra_{crit}
0	–	–
0.05	–	–
0.1	–	–
0.2	6.628	4 877.67
0.5	6.978	289 023

Table 2.2: Dependence of the critical Rayleigh number on dissipation number, constant material parameters and free-slip boundary condition

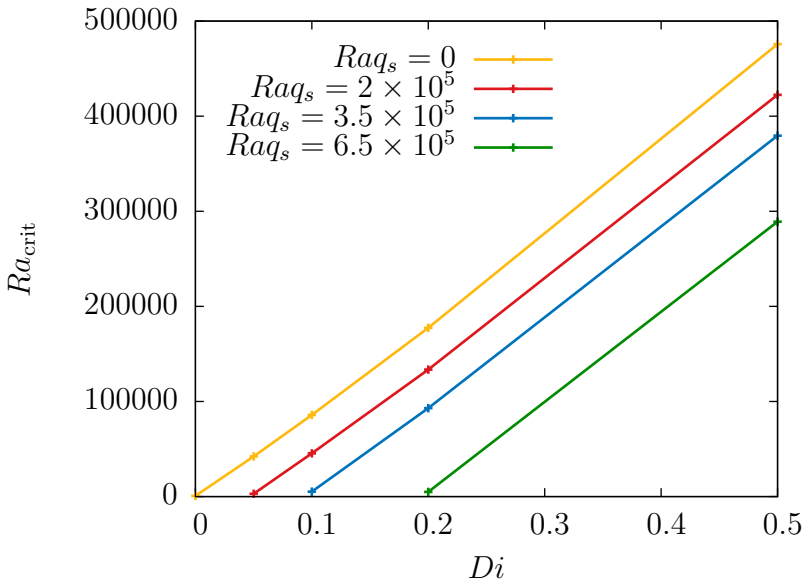

Figure 2.11: Dependence of the critical Rayleigh number on dissipation number, constant material parameters and free-slip boundary condition

Boussinesq approximation we rely on the numerical results only. For Prandtl numbers high enough (more than 10^3) the numerically obtained (and thus finite) spectrum for specific a and Ra is real for all the cases considered below. For $Pr < 10^3$ there are complex eigenvalues in some of the cases (when the depth- or temperature-dependence is significant, i.e. far from the classical case). The fact that the spectrum of problem (2.74) is real is a crucial property which will be useful in the next chapter and thus we will be using the value $Pr = 10^9$ there.

2.2.4 Non-constant thermal conductivity k

We assume that thermal expansivity α and dynamic viscosity μ are constant and thermal conductivity k is either depth-, or temperature-dependent.

Depth-dependent k

We assume that

$$k(z, T) = 1 + \tilde{b}_k z,$$

where $\tilde{b}_k \in \{1, 5, 10\}$. Numerical solution of (2.74) yields critical values of wavenumber and Rayleigh number that are summarized in Table 2.3. We considered three different cases - no dissipation or heat sources included, dissipation included and both dissipation and heat sources included (we use this pattern in all of the remaining cases of non-constant material coefficients).

$\tilde{b}_k$	Di_s	Raq_s	a_{crit}	Ra_{crit}
1	0	0	2.221	976.933
5	0	0	2.220	2 210.40
10	0	0	2.218	3 767.83
1	0.5	0	6.334	404 688
5	0.5	0	7.086	344 453
10	0.5	0	7.155	342 840
1	0.5	10^6	7.565	225 133
5	0.5	10^6	7.612	274 150
10	0.5	10^6	7.465	303 949

Table 2.3: Depth-dependent thermal conductivity, free-slip boundary condition

For the case of $Di_s = 0.5$ and $Raq_s = 0$, raising the coefficient $\tilde{b}_k$ has a destabilizing effect. Apparently, the dissipation number has a large influence on the behaviour of the material coefficients. We further investigated this for smaller values of Di_s. We can see in Table 2.4 that for $Di_s = 0.05$ the property of thermal conductivity being a stabilizing parameter is preserved (at least for the values of $\tilde{b}_k$ considered here). However, raising the dissipation number to $Di_s = 0.1$ yields a drop in Ra_{crit} for $\tilde{b}_k = 5$ compared to the value of Ra_{crit} for $\tilde{b}_k = 1$.

Most likely, for $Di_s > 0$ the value of Ra_{crit} first decreases as the coefficient $\tilde{b}_k$ rises and then for $\tilde{b}_k$ sufficiently high Ra_{crit} starts increasing. Based on the results we

$Di_s = 0.05$, $Raq_s = 0$

$\tilde{b}_k$	a_{crit}	Ra_{crit}
1	3.402	41 532.4
5	3.789	42 668.9
10	3.636	46 557.7

$Di_s = 0.1$, $Raq_s = 0$

$\tilde{b}_k$	a_{crit}	Ra_{crit}
1	4.108	80 800.0
5	4.565	78 171.2
10	4.503	83 024.5

Table 2.4: (De)stabilizing effect of thermal conductivity for smaller values of dissipation number, heat sources excluded, free-slip boundary condition

have we suspect that the higher the dissipation number is the higher the critical value of $\tilde{b}_k$ for which stabilizing effect of thermal conductivity sets in is. Of course, heat sources also influence the behaviour of thermal conductivity. We can see in Table 2.3 that for $Raq_s = 10^6$ thermal conductivity has the expected stabilizing property again.

The promised illustrative example of spectrum of eigenvalue problem (2.74) is depicted in Figure 2.12. We used following values $\tilde{b}_k = 1$, $Raq_s = 10^6$, $Di_s = 0.5$ with $a \in [0, 20]$ and the step size of 0.5 and $Ra_s \in [50\,000, 500\,000]$ and the step size of 15 000. We can see that the critical values of wave-number and Rayleigh number are approximately $a_{\text{crit}} \approx 8$ and $Ra_{\text{crit}} \approx 225\,000$ (more precise results can be found in Table 2.3).

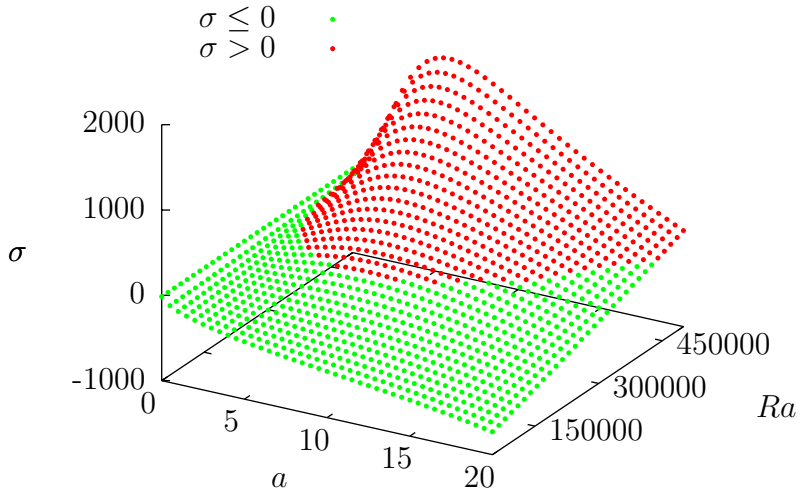

Figure 2.12: Spectrum for extended Boussinesq approximation, free-slip boundary condition and depth-dependent k ($\tilde{b}_k = 1$, $Raq_s = 10^6$, $Di_s = 0.5$)

We also include quantitatively more accessible depiction of the curves for specific values of maximum eigenvalues σ. This is shown in Figure 2.13 where we chose the values $\sigma = -100$ (green line), $\sigma = 0$ (gray line) and $\sigma = 100$ (red line).

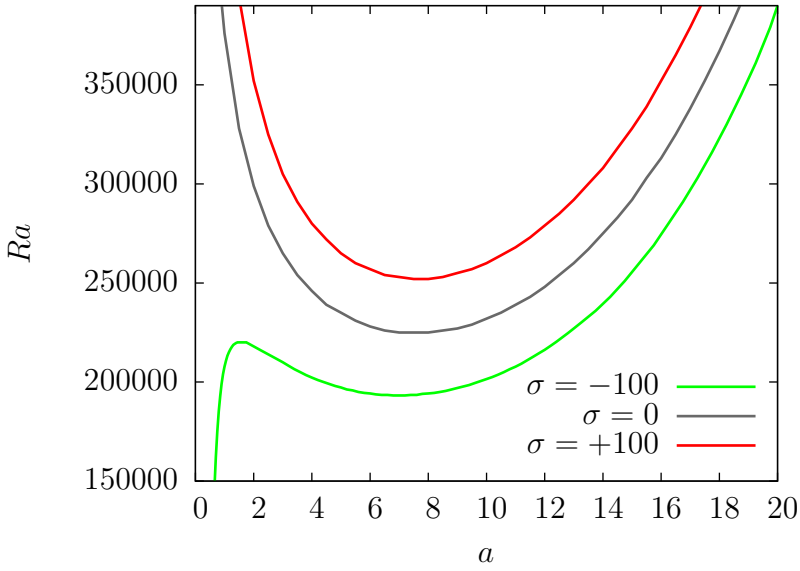

Figure 2.13: Curves for specific values of maximum eigenvalue σ, free-slip boundary condition and depth-dependent k ($\tilde{b}_k = 1$, $Raq_s = 10^6$, $Di_s = 0.5$)

In Figure 2.14 we depicted the eigenfunctions of (2.74). Note that they are very different from the classical case (see Figure 2.4) – this will yield different behaviour of convection cells as we will see in the following chapter.

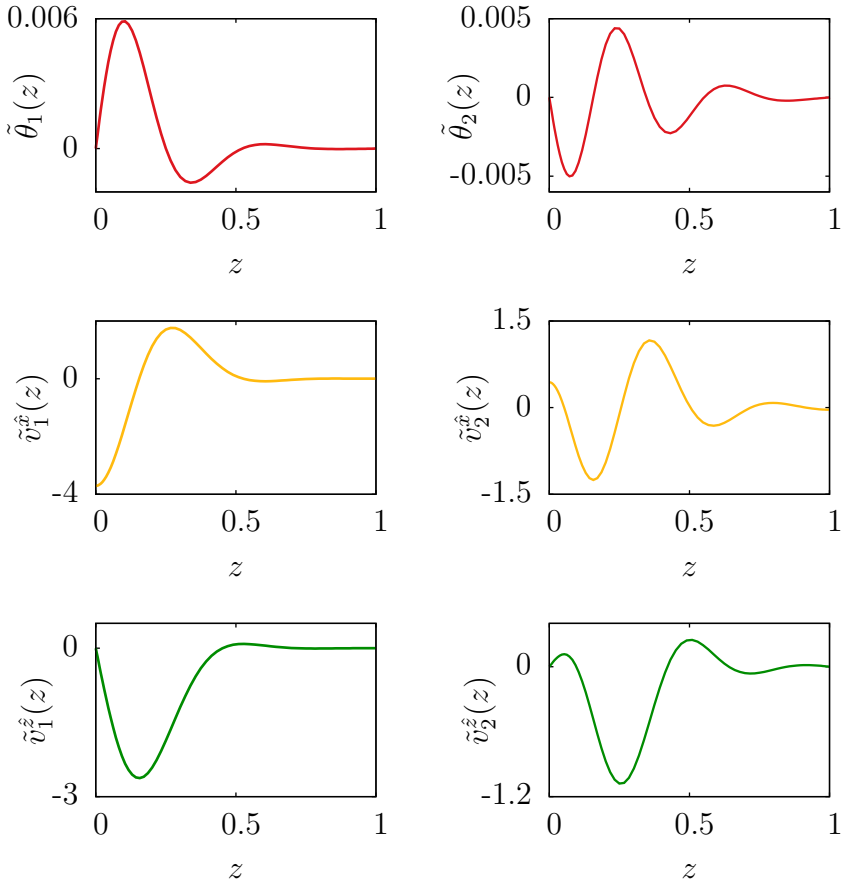

Figure 2.14: First two eigenfunctions for extended Boussinesq approximation and free-slip boundary condition in case of single rolls, $Pr_s = 10^9$, $Ra_s = 230\,000$, $Raq_s = 10^6$, $Di_s = 0.5$, $a = a_{\text{crit}} = 7.565$

Temperature-dependent k

We assume that

$$k(z,T) = \exp(-\tilde{c}_k Ra_s T),$$

where $\tilde{c}_k \in \{0.5 \times 10^{-7}, 1.0 \times 10^{-7}, 2.0 \times 10^{-7}\}$. Table 2.5 shows critical pairs of wave-number and Rayleigh number.

As in the case of depth-dependent k, we can see that for $Di_s = 0.5$ and heat sources excluded thermal conductivity lacks the expected stabilizing effect. However, for heat sources sufficiently large, the stabilizing property is restored again as can be seen in Table 2.5 when $Raq_s = 10^6$.

$\tilde{c}_k$	Di_s	Raq_s	a_{crit}	Ra_{crit}
0.5×10^{-7}	0	0	2.221	657.500
1.0×10^{-7}	0	0	2.221	657.489
2.0×10^{-7}	0	0	2.221	657.468
0.5×10^{-7}	0.5	0	5.416	472 859
1.0×10^{-7}	0.5	0	5.467	470 158
2.0×10^{-7}	0.5	0	5.564	465 054
0.5×10^{-7}	0.5	10^6	7.473	179 733
1.0×10^{-7}	0.5	10^6	7.486	181 198
2.0×10^{-7}	0.5	10^6	7.513	184 055

Table 2.5: Temperature-dependent thermal conductivity, free-slip boundary condition

2.2.5 Non-constant thermal expansivity α

We assume that thermal conductivity k and dynamic viscosity μ are constant and thermal expansivity α is depth-dependent.

Depth-dependent α

We assume that

$$\alpha(z,T) = \exp(-\tilde{b}_\alpha z),$$

where $\tilde{b}_\alpha \in \{0.5, 1.0, 2.0\}$. Table 2.6 shows critical pairs of wave-number and Rayleigh number.

We can see that the assumption of thermal expansivity being a stabilizing factor is violated even when the heat sources are present. We investigated in more detail the influence of dissipation on the critical value of Ra_s and we found that thermal expansivity has a destabilizing behaviour even for smaller values of Di_s. We can see in Table 2.7 that for a tiny value $Di_s = 0.001$ the stabilizing effect is still preserved but even for $Di_s = 0.01$ the destabilization occurs. Hence, for a rather large value $Di_s = 0.5$ we don't observe the expected stabilizing behaviour even when the heat sources are present.

$\tilde{b}_\alpha$	Di_s	Raq_s	a_{crit}	Ra_{crit}
0.5	0	0	2.222	840.560
1.0	0	0	2.223	1 065.19
2.0	0	0	2.227	1 666.83
0.5	0.5	0	3.639	387 573
1.0	0.5	0	4.294	258 856
2.0	0.5	0	3.854	138 156
0.5	0.5	10^6	7.068	139 911
1.0	0.5	10^6	6.694	103 769
2.0	0.5	10^6	6.067	39 607.8

Table 2.6: Depth-dependent thermal expansivity, free-slip boundary condition

$Di_s = 0.001$, $Raq_s = 0$

$\tilde{b}_\alpha$	a_{crit}	Ra_{crit}
0.5	2.220	1 476.74
1.0	2.219	1 572.19
2.0	2.221	2 003.81

$Di_s = 0.01$, $Raq_s = 0$

$\tilde{b}_\alpha$	a_{crit}	Ra_{crit}
0.5	2.227	7 210.85
1.0	2.218	6 122.01
2.0	2.192	5 013.65

Table 2.7: (De)stabilizing effect of thermal expansivity for smaller values of dissipation number, heat sources excluded, free-slip boundary condition

2.2.6 Non-constant dynamic viscosity μ

We assume that thermal conductivity k and thermal expansivity α are constant and dynamic viscosity α is either depth-, or temperature-dependent.

Depth-dependent μ

We assume that

$$\mu(z, T) = \exp(\tilde{b}_\mu z),$$

where $\tilde{b}_\mu \in \{1.0, 2.5, 4.5\}$. Table 2.8 shows critical pairs of wave-number and Rayleigh number.

We can see that in this case the stabilizing effect of viscosity is present in all the settings considered. Thus, we obtain the expected behaviour of viscosity.

$\tilde{b}_\mu$	Di_s	Raq_s	a_{crit}	Ra_{crit}
1.0	0	0	2.199	1 113.68
2.5	0	0	2.093	2 679.48
4.5	0	0	1.921	9 520.92
1.0	0.5	0	5.225	478 900
2.5	0.5	0	4.961	485 309
4.5	0.5	0	4.479	498 954
1.0	0.5	10^6	7.325	186 361
2.5	0.5	10^6	7.080	201 026
4.5	0.5	10^6	6.645	227 321

Table 2.8: Depth-dependent dynamic viscosity, free-slip boundary condition

Temperature-dependent μ

We assume that

$$\mu(z, T) = \exp(-\tilde{c}_\mu Ra_s T),$$

where $\tilde{c}_\mu \in \{1.0 \times 10^{-7}, 2.5 \times 10^{-7}, 4.5 \times 10^{-7}\}$. Table 2.5 shows critical pairs of wave-number and Rayleigh number.

We can see that viscosity as a decreasing function of temperature has destabilizing effect in all the cases considered.

$\tilde{c}_\mu$	Di_s	Raq_s	a_{crit}	Ra_{crit}
1.0×10^{-7}	0	0	2.221	657.490
2.5×10^{-7}	0	0	2.221	657.457
4.5×10^{-7}	0	0	2.222	657.414
1.0×10^{-7}	0.5	0	5.368	475 530
2.5×10^{-7}	0.5	0	5.376	475 325
4.5×10^{-7}	0.5	0	5.386	475 055
1.0×10^{-7}	0.5	10^6	7.466	177 821
2.5×10^{-7}	0.5	10^6	7.476	177 193
4.5×10^{-7}	0.5	10^6	7.490	176 369

Table 2.9: Temperature-dependent dynamic viscosity, free-slip boundary condition

2.3 Summary of Chapter 2

The main result of this chapter is the development of a numerical model which serves to compute the critical values of wave-number and Rayleigh number in the general case of the extended Boussinesq approximation.

We quantified these for various depth, or temperature dependences of the material coefficients, dissipation and heat sources both excluded and included. This was

done under the assumption of the free-slip boundary condition. However, the numerical model is not restricted to this case and we are able to reproduce similar results for the no-slip boundary condition as well.

We verified that for the classical Boussinesq approximation the method yields the well known analytical results and compared them to the ones obtained for the extended case. The noticeable difference causes the dissipation number which for the value $Di_s = 0.5$ makes the critical Rayleigh number rise up to the order of 5 (see Tables 2.3,2.5, 2.6, 2.8 and 2.9).

Also, the dissipation number has apparently large influence on the stabilizing/destabilizing effect of thermal conductivity and thermal expansivity as was investigated in Tables 2.4 and 2.7. In the case of depth-dependent thermal expansivity and temperature-dependent viscosity, the stabilizing effect is violated even when the heat sources are included. In all other cases the stabilizing behaviour of material coefficients is preserved (upon including the heat sources possibly), meaning that raising the coefficients of material parameters yields higher critical Rayleigh numbers (see Tables 2.3,2.5, 2.8 and 2.9).

Raising the dissipation number represents raising the influence of dissipation and adiabatic cooling/heating (see equation (2.53)). Since the dissipation term is divided by Ra_s, we assume that for higher values of Rayleigh number the main factor causing the critical threshold of convection rise is the adiabatic cooling/heating term.

The influence of Rayleigh number for heat sources lies in lowering the critical Rayleigh number (for all the other parameters fixed) and balancing the impact of higher dissipation number on (de)stabilizing effect of the material parameters (see again Tables 2.3,2.5, 2.6, 2.8 and 2.9).

Chapter 3

Weakly non-linear analysis

For the sake of simplicity, we consider only two-dimensional convection in this chapter, i.e. the case of single rolls. Since we are going to portray the convection cells let us remind the reader that the vertical axis z of the coordinate system is pointing downwards, i.e. $z = 0$ at the surface and $z = 1$ at the bottom of the convecting layer (z represents the dimensionless variable).

The sources for writing this chapter include the papers of Cross (1980) and Fujimura (1997) as well as the papers by Cross and Hohenberg (1993), Newell and Whitehead (1969) and Stuart (1958) and the monograph Haken (1983).

3.1 Classical Boussinesq approximation

Let us consider the classical Boussinesq approximation of the basic laws again. We have the system of equations (see (2.8)–(2.10))

$$\operatorname{div} \mathbf{v} = 0,$$

$$\frac{1}{Pr}\left[\frac{\partial \mathbf{v}}{\partial t} + (\mathbf{v}\cdot\nabla)\mathbf{v}\right] = -Ra\theta \mathbf{e}_{\hat{z}} - \nabla\pi + \Delta\mathbf{v},$$

$$\frac{\partial \theta}{\partial t} = \Delta\theta - v^{\hat{z}} - \mathbf{v}\cdot\nabla\theta.$$

We can rewrite this system in the form

$$\frac{\partial \boldsymbol{\psi}}{\partial t} = \mathcal{L}(Ra)(\boldsymbol{\psi}) - Pr\boldsymbol{\delta}\pi + \mathcal{N}(\boldsymbol{\psi},\boldsymbol{\psi}), \tag{3.1}$$

where

$$\boldsymbol{\psi} = \begin{bmatrix} \theta \\ v^{\hat{x}} \\ v^{\hat{z}} \end{bmatrix},$$

$\mathcal{L}(Ra)$ is a linear operator defined as

$$\mathcal{L}(Ra) = \begin{bmatrix} \Delta & 0 & -1 \\ 0 & Pr\Delta & 0 \\ -PrRa & 0 & Pr\Delta \end{bmatrix},$$

and $\mathcal{N}$ is a quadratic non-linear operator defined as

$$\mathcal{N}(\boldsymbol{\phi}, \boldsymbol{\psi}) = \mathcal{N}\left(\begin{bmatrix} \theta_\phi \\ v_\phi^{\hat{x}} \\ v_\phi^{\hat{z}} \end{bmatrix}, \begin{bmatrix} \theta_\psi \\ v_\psi^{\hat{x}} \\ v_\psi^{\hat{z}} \end{bmatrix} \right) = \begin{bmatrix} -\left(v_\phi^{\hat{x}} \frac{\partial}{\partial x} + v_\phi^{\hat{z}} \frac{\partial}{\partial z} \right) \theta_\psi \\ -\left(v_\phi^{\hat{x}} \frac{\partial}{\partial x} + v_\phi^{\hat{z}} \frac{\partial}{\partial z} \right) v_\psi^{\hat{x}} \\ -\left(v_\phi^{\hat{x}} \frac{\partial}{\partial x} + v_\phi^{\hat{z}} \frac{\partial}{\partial z} \right) v_\psi^{\hat{z}} \end{bmatrix}.$$

We also introduced operator $\boldsymbol{\delta} = [0, \nabla]^{\mathrm{T}}$.

We assume that $\boldsymbol{\psi}$ contains only divergence-free velocity field, i.e. $\boldsymbol{\delta} \cdot \boldsymbol{\psi} = 0$. We also assume that either free-slip or no-slip boundary conditions are imposed on $\boldsymbol{\psi}$ and that it is periodic in the x-direction with period denoted by D. Thus we investigate our problem in the cell $[0, D] \times [0, 1]$ only. We prescribe the period to match the critical wave-numbers found in Chapter 2 via $D = {}^{2\pi}/_{a_{\mathrm{crit}}}$ where a_{crit} corresponds to the specific case of boundary conditions considered (free-slip or no-slip).[1] Instead of a_{crit} we henceforth denote the critical wave-number simply by a.

3.1.1 Expansion into Fourier series and eigenfunctions of the linearized operator

First of all, we consider the linear eigenvalue problem

$$\mathcal{L}(Ra)\boldsymbol{\psi}^{(i)} = \sigma^{(i)}\boldsymbol{\psi}^{(i)},$$

where $\sigma^{(i)}$ is the i-th eigenvalue and $\boldsymbol{\psi}^{(i)}$ corresponding eigenfunction. We can show easily that $\mathcal{L}(Ra)$ is a self-adjoint operator and hence all the eigenvalues are real and simple and the eigenfunctions form an orthogonal and complete set in a Hilbert space denoted by H which consists of functions from $[W^{1,2}([0, D] \times [0, 1])]^3$ where appropriate boundary conditions are imposed. Let us introduce the inner product $\langle \cdot, \cdot \rangle$ in H by

$$\langle \boldsymbol{\phi}, \boldsymbol{\psi} \rangle := \int_0^1 \int_0^{\frac{2\pi}{a}} \boldsymbol{\phi}(x, z) \cdot \mathbb{M}\overline{\boldsymbol{\psi}(x, z)} \, \mathrm{d}x\mathrm{d}z \qquad \text{for} \qquad \boldsymbol{\phi}, \boldsymbol{\psi} \in H,$$

where

$$\mathbb{M} = \begin{bmatrix} Ra_s & 0 & 0 \\ 0 & Pr_s^{-1} & 0 \\ 0 & 0 & Pr_s^{-1} \end{bmatrix}.$$

We denote the induced norm by $\| \cdot \|$.

[1] Similarly, in the derivation of the amplitude equation for the extended Boussinesq approximation below, we always take the critical wave-number a_{crit} which determines the period D according to the specific choice of material parameters and dimensionless numbers.

Also, we let the eigenvalues be ordered in a descending manner (we know that in the classical case the eigenvalues are real)

$$\sigma^{(1)} > \sigma^{(2)} > \sigma^{(3)} > \dots$$

Let us note that for the critical value of Ra, we have $\sigma^{(1)} = 0$ and $\sigma^{(i)} < 0$ for $i \geq 2$.

Since we assumed x-periodicity, we can expand the eigenfunction to its Fourier series

$$\boldsymbol{\psi}^{(i)}(x,z) = \sum_{n=-\infty}^{+\infty} \boldsymbol{\psi}_n^{(i)}(z) e^{\mathrm{i}n\frac{2\pi}{D}x} = \sum_{n=-\infty}^{+\infty} \boldsymbol{\psi}_n^{(i)}(z) e^{\mathrm{i}nax}. \tag{3.2}$$

Functions $\boldsymbol{\psi}_n^{(i)}$ satisfy

$$\mathcal{L}_n(Ra)\boldsymbol{\psi}_n^{(i)} = \sigma_n^{(i)}\boldsymbol{\psi}_n^{(i)}, \tag{3.3}$$

where $\mathcal{L}_n$ is the Fourier transformed version of $\mathcal{L}$, i.e. $\mathcal{L}_n = \mathcal{L}|_{\frac{\partial}{\partial x}\to \mathrm{i}na, \frac{\partial}{\partial z}\to\frac{\mathrm{d}}{\mathrm{d}z}}$. The modified operator $\mathcal{L}_n$ is still normal and thus the eigenvalues $\sigma_n^{(i)}$ for specific n, a and Ra are simple and eigenfunctions $\boldsymbol{\psi}_n^{(i)}$ are orthogonal and complete in a Hilbert space denoted by $\widetilde{H}$ which consists of functions from $[W^{1,2}([0,1])]^3$ where appropriate boundary conditions are imposed. The inner product $\langle\langle\cdot,\cdot\rangle\rangle$ in $\widetilde{H}$ is defined as

$$\langle\langle\boldsymbol{\phi},\boldsymbol{\psi}\rangle\rangle := \int_0^1 \boldsymbol{\phi}(z)\cdot\mathbb{M}\overline{\boldsymbol{\psi}(z)}\,\mathrm{d}z \qquad \text{for} \qquad \boldsymbol{\phi},\boldsymbol{\psi}\in\widetilde{H}, \tag{3.4}$$

and the induced norm denoted by $|||\cdot|||$.

We can now expand any function $\boldsymbol{\psi}(t,\mathbf{x})$ into Fourier series and linear eigenfunctions as

$$\boldsymbol{\psi}(t,x,z) = \sum_{i=1}^{+\infty}\sum_{n=-\infty}^{+\infty} A_n^{(i)}(t)\boldsymbol{\psi}_n^{(i)}(z)e^{\mathrm{i}nax}. \tag{3.5}$$

We require that $\boldsymbol{\psi}(t,\mathbf{x})$ is a real function, hence $A_{-n}^{(i)} = \overline{A_n^{(i)}}$ and $\boldsymbol{\psi}_{-n}^{(i)} = \overline{\boldsymbol{\psi}_n^{(i)}}$.

Furthermore, we can assume that $A_n^{(i)} \in \mathbb{R}$. This follows from the specific form of $\boldsymbol{\psi}_n^{(i)}$ – we know that $\theta_n^{(i)}, (\tilde{v}_n^{(i)})^{\hat{z}}$ are real-valued and $(\tilde{v}_n^{(i)})^{\hat{x}}$ is imaginary-valued. Writing out the corresponding terms for n and $-n$ in the expansion above component-wise yields that real part of $A_n^{(i)}$ gives even modes of $\theta_n^{(i)}, (\tilde{v}_n^{(i)})^{\hat{z}}$ and odd modes of $(\tilde{v}_n^{(i)})^{\hat{x}}$. The imaginary part then gives the opposite modes for corresponding functions. We can transform odd modes into even ones simply by the change of horizontal coordinates, hence without loss of generality we simplify the analysis below by setting the imaginary part of $A_n^{(i)}$ zero.

3.1.2 Projection onto the eigenfunctions

Substituting the expansion (3.5) into (3.1) yields

$$\sum_{i=1}^{+\infty}\sum_{n=-\infty}^{+\infty}\frac{\mathrm{d}A_n^{(i)}}{\mathrm{d}t}(t)\boldsymbol{\psi}_n^{(i)}(z)e^{\mathrm{i}nax}=\sum_{i=1}^{+\infty}\sum_{n=-\infty}^{+\infty}A_n^{(i)}(t)\mathcal{L}\left(\boldsymbol{\psi}_n^{(i)}(z)e^{\mathrm{i}nax}\right)-Pr\boldsymbol{\delta}\pi$$
$$+\mathcal{N}\left(\sum_{i=1}^{+\infty}\sum_{n=-\infty}^{+\infty}A_n^{(i)}(t)\boldsymbol{\psi}_n^{(i)}(z)e^{\mathrm{i}nax},\sum_{j=1}^{+\infty}\sum_{m=-\infty}^{+\infty}A_m^{(j)}(t)\boldsymbol{\psi}_m^{(j)}(z)e^{\mathrm{i}max}\right),\quad(3.6)$$

We will now take the inner product of (3.6) with function $\boldsymbol{\psi}_l^{(k)}(z)e^{\mathrm{i}lax}$, where $k\in\mathbb{N}$ and $l\in\mathbb{Z}$. Let us treat the individual terms of the resulting equation separately. For the sake of clarity, we will omit writing the arguments of functions.

Using the definition of inner product in H we obtain quite easily

$$\begin{aligned}\left\langle\frac{\partial\boldsymbol{\psi}}{\partial t},\boldsymbol{\psi}_l^{(k)}e^{\mathrm{i}lax}\right\rangle&=\left\langle\sum_{i=1}^{+\infty}\sum_{n=-\infty}^{+\infty}\frac{\mathrm{d}A_n^{(i)}}{\mathrm{d}t}\boldsymbol{\psi}_n^{(i)}e^{\mathrm{i}nax},\boldsymbol{\psi}_l^{(k)}e^{\mathrm{i}lax}\right\rangle\\&=\sum_{i=1}^{+\infty}\sum_{n=-\infty}^{+\infty}\frac{\mathrm{d}A_n^{(i)}}{\mathrm{d}t}\int_0^1\int_0^{\frac{2\pi}{a}}\boldsymbol{\psi}_n^{(i)}\cdot\mathbb{M}\overline{\boldsymbol{\psi}_l^{(k)}}e^{\mathrm{i}(n-l)ax}\,\mathrm{d}x\mathrm{d}z\\&=\sum_{i=1}^{+\infty}\sum_{n=-\infty}^{+\infty}\frac{\mathrm{d}A_n^{(i)}}{\mathrm{d}t}\int_0^{\frac{2\pi}{a}}e^{\mathrm{i}(n-l)ax}\,\mathrm{d}x\int_0^1\boldsymbol{\psi}_n^{(i)}\cdot\mathbb{M}\overline{\boldsymbol{\psi}_l^{(k)}}\,\mathrm{d}z.\end{aligned}$$

From the orthogonality of functions $\{e^{\mathrm{i}nax}\}_{n=-\infty}^{+\infty}$ in $L^2([0,\frac{2\pi}{a}])$ we get

$$\begin{aligned}\left\langle\frac{\partial\boldsymbol{\psi}}{\partial t},\boldsymbol{\psi}_l^{(k)}e^{\mathrm{i}lax}\right\rangle&=\sum_{i=1}^{+\infty}\sum_{n=-\infty}^{+\infty}\frac{\mathrm{d}A_n^{(i)}}{\mathrm{d}t}\frac{2\pi}{a}\delta_{nl}\int_0^1\boldsymbol{\psi}_n^{(i)}\cdot\mathbb{M}\overline{\boldsymbol{\psi}_l^{(k)}}\,\mathrm{d}z\\&=\frac{2\pi}{a}\sum_{i=1}^{+\infty}\frac{\mathrm{d}A_l^{(i)}}{\mathrm{d}t}\int_0^1\boldsymbol{\psi}_l^{(i)}\cdot\mathbb{M}\overline{\boldsymbol{\psi}_l^{(k)}}\,\mathrm{d}z.\end{aligned}$$

Using also the orthogonality of functions $\{\boldsymbol{\psi}_n^{(i)}\}_{i=1}^{+\infty}$ in $\widetilde{H}$ we finally arrive at

$$\left\langle\frac{\partial\boldsymbol{\psi}}{\partial t},\boldsymbol{\psi}_l^{(k)}e^{ilax}\right\rangle=\frac{2\pi}{a}\sum_{i=1}^{+\infty}\frac{\mathrm{d}A_l^{(i)}}{\mathrm{d}t}\langle\langle\boldsymbol{\psi}_l^{(i)},\boldsymbol{\psi}_l^{(k)}\rangle\rangle=\frac{2\pi}{a}|||\boldsymbol{\psi}_l^{(k)}|||^2\frac{\mathrm{d}A_l^{(k)}}{\mathrm{d}t}.$$

We can simplify the next term in a similar manner. Let us first note that $\mathcal{L}(\boldsymbol{\psi}_n^{(i)}e^{\mathrm{i}nax})=\sigma_n^{(i)}\boldsymbol{\psi}_n^{(i)}e^{\mathrm{i}nax}$. We can then write

$$\begin{aligned}\left\langle\mathcal{L}\left(\boldsymbol{\psi}\right),\boldsymbol{\psi}_l^{(k)}e^{\mathrm{i}lax}\right\rangle&=\left\langle\sum_{i=1}^{+\infty}\sum_{n=-\infty}^{+\infty}A_n^{(i)}\mathcal{L}\left(\boldsymbol{\psi}_n^{(i)}e^{\mathrm{i}nax}\right),\boldsymbol{\psi}_l^{(k)}e^{\mathrm{i}lax}\right\rangle\\&=\left\langle\sum_{i=1}^{+\infty}\sum_{n=-\infty}^{+\infty}A_n^{(i)}\sigma_n^{(i)}\boldsymbol{\psi}_n^{(i)}e^{\mathrm{i}nax},\boldsymbol{\psi}_l^{(k)}e^{\mathrm{i}lax}\right\rangle.\end{aligned}$$

Now using the same orthogonality arguments, we easily obtain

$$\begin{aligned}\left\langle \mathcal{L}\left(\boldsymbol{\psi}\right), \boldsymbol{\psi}_l^{(k)} e^{\mathrm{i}lax} \right\rangle &= \sum_{i=1}^{+\infty} \sum_{n=-\infty}^{+\infty} \sigma_n^{(i)} A_n^{(i)} \frac{2\pi}{a} \delta_{nl} \int_0^1 \boldsymbol{\psi}_n^{(i)} \cdot \mathbb{M}\overline{\boldsymbol{\psi}_l^{(k)}} \,\mathrm{d}z \\ &= \frac{2\pi}{a} \sum_{i=1}^{+\infty} \sigma_l^{(i)} A_l^{(i)} \langle\langle \boldsymbol{\psi}_l^{(i)}, \boldsymbol{\psi}_l^{(k)} \rangle\rangle = \frac{2\pi}{a} |||\boldsymbol{\psi}_l^{(k)}|||^2 \sigma_l^{(k)} A_l^{(k)}.\end{aligned}$$

The term with pressure π vanishes upon integrating by parts thanks to $\boldsymbol{\psi}_l^{(k)} e^{ilax}$ being divergence-free and its boundary conditions. Indeed,

$$\begin{aligned}\left\langle -Pr\boldsymbol{\delta}\pi, \boldsymbol{\psi}_l^{(k)} e^{ilax} \right\rangle &= \int_0^1 \int_0^{\frac{2\pi}{a}} -Pr\boldsymbol{\delta}\pi \cdot \mathbb{M}\overline{\boldsymbol{\psi}_l^{(k)}} e^{-\mathrm{i}lax} \,\mathrm{d}x\mathrm{d}z \\ &= \int_0^1 \int_0^{\frac{2\pi}{a}} Pr\pi\boldsymbol{\delta} \cdot (\boldsymbol{\psi}_{-l}^{(k)} e^{-\mathrm{i}lax}) \,\mathrm{d}x\mathrm{d}z = 0.\end{aligned}$$

Finally, the non-linear term reads

$$\begin{aligned}&\left\langle \mathcal{N}\left(\boldsymbol{\psi}, \boldsymbol{\psi}\right), \boldsymbol{\psi}_l^{(k)} e^{\mathrm{i}lax} \right\rangle \\ &= \left\langle \mathcal{N}\left(\sum_{i=1}^{+\infty} \sum_{n=-\infty}^{+\infty} A_n^{(i)} \boldsymbol{\psi}_n^{(i)} e^{\mathrm{i}nax}, \sum_{j=1}^{+\infty} \sum_{m=-\infty}^{+\infty} A_m^{(j)} \boldsymbol{\psi}_m^{(j)} e^{\mathrm{i}max} \right), \boldsymbol{\psi}_l^{(k)} e^{\mathrm{i}lax} \right\rangle \\ &= \left\langle \sum_{i=1}^{+\infty} \sum_{n=-\infty}^{+\infty} \sum_{j=1}^{+\infty} \sum_{m=-\infty}^{+\infty} A_n^{(i)} A_m^{(j)} \widetilde{\mathcal{N}}\left(\boldsymbol{\psi}_n^{(i)}, \boldsymbol{\psi}_m^{(j)}\right) e^{\mathrm{i}(n+m)ax}, \boldsymbol{\psi}_l^{(k)} e^{\mathrm{i}lax} \right\rangle,\end{aligned}$$

where we introduced operator $\widetilde{\mathcal{N}}(\cdot,\cdot)$ defined as

$$\widetilde{\mathcal{N}}(\boldsymbol{\psi}_n^{(i)}, \boldsymbol{\psi}_m^{(j)}) = \begin{bmatrix} \left(-(v_n^{(i)})^{\hat{x}} \mathrm{i}am - (v_n^{(i)})^{\hat{z}} \frac{\mathrm{d}}{\mathrm{d}z}\right) \theta_m^{(j)} \\ \left(-(v_n^{(i)})^{\hat{x}} \mathrm{i}am - (v_n^{(i)})^{\hat{z}} \frac{\mathrm{d}}{\mathrm{d}z}\right) (v_m^{(j)})^{\hat{x}} \\ \left(-(v_n^{(i)})^{\hat{x}} \mathrm{i}am - (v_n^{(i)})^{\hat{z}} \frac{\mathrm{d}}{\mathrm{d}z}\right) (v_m^{(j)})^{\hat{z}} \end{bmatrix}.$$

Let us further simplify the expression using the orthogonality arguments

$$\begin{aligned}&\left\langle \mathcal{N}\left(\boldsymbol{\psi}, \boldsymbol{\psi}\right), \boldsymbol{\psi}_l^{(k)} e^{\mathrm{i}lax} \right\rangle \\ &= \sum_{i=1}^{+\infty} \sum_{n=-\infty}^{+\infty} \sum_{j=1}^{+\infty} \sum_{m=-\infty}^{+\infty} A_n^{(i)} A_m^{(j)} \int_0^1 \int_0^{\frac{2\pi}{a}} \widetilde{\mathcal{N}}\left(\boldsymbol{\psi}_n^{(i)}, \boldsymbol{\psi}_m^{(j)}\right) \cdot \mathbb{M}\overline{\boldsymbol{\psi}_l^{(k)}} e^{\mathrm{i}(n+m-l)ax} \,\mathrm{d}x\mathrm{d}z \\ &= \sum_{i=1}^{+\infty} \sum_{n=-\infty}^{+\infty} \sum_{j=1}^{+\infty} \sum_{m=-\infty}^{+\infty} A_n^{(i)} A_m^{(j)} \frac{2\pi}{a} \delta_{n+m,l} \langle\langle \widetilde{\mathcal{N}}(\boldsymbol{\psi}_n^{(i)}, \boldsymbol{\psi}_m^{(j)}), \boldsymbol{\psi}_l^{(k)} \rangle\rangle \\ &= \frac{2\pi}{a} \sum_{i=1}^{+\infty} \sum_{n=-\infty}^{+\infty} \sum_{j=1}^{+\infty} A_n^{(i)} A_{l-n}^{(j)} \langle\langle \widetilde{\mathcal{N}}(\boldsymbol{\psi}_n^{(i)}, \boldsymbol{\psi}_{l-n}^{(j)}), \boldsymbol{\psi}_l^{(k)} \rangle\rangle.\end{aligned}$$

Let us summarize what we have derived so far. Taking the inner product of (3.6) with $\boldsymbol{\psi}_l^{(k)}(z)e^{ilax}$ yields

$$\frac{2\pi}{a}|||\boldsymbol{\psi}_l^{(k)}|||^2\frac{\mathrm{d}A_l^{(k)}}{\mathrm{d}t}(t) = \frac{2\pi}{a}|||\boldsymbol{\psi}_l^{(k)}|||^2\sigma_l^{(k)}A_l^{(k)}(t) + \frac{2\pi}{a}\sum_{i=1}^{+\infty}\sum_{j=1}^{+\infty}\sum_{n=-\infty}^{+\infty} A_n^{(i)}(t)A_{l-n}^{(j)}(t)\langle\langle\widetilde{\mathcal{N}}(\boldsymbol{\psi}_n^{(i)},\boldsymbol{\psi}_{l-n}^{(j)}),\boldsymbol{\psi}_l^{(k)}\rangle\rangle.$$

If we introduce notation

$$\lambda_{n,l-n}^{i,j,k} := |||\boldsymbol{\psi}_l^{(k)}|||^{-2}\langle\langle\widetilde{\mathcal{N}}(\boldsymbol{\psi}_n^{(i)},\boldsymbol{\psi}_{l-n}^{(j)}),\boldsymbol{\psi}_l^{(k)}\rangle\rangle,$$

we can write the resulting equation in the form

$$\boxed{\frac{\mathrm{d}A_l^{(k)}}{\mathrm{d}t} = \sigma_l^{(k)}A_l^{(k)} + \sum_{i=1}^{+\infty}\sum_{j=1}^{+\infty}\sum_{n=-\infty}^{+\infty}\lambda_{n,l-n}^{i,j,k}A_n^{(i)}A_{l-n}^{(j)}.} \tag{3.7}$$

This is an infinite-dimensional system of ordinary differential equations for quotients $A_l^{(k)}$. We would now like to simplify the non-linear term, or more precisely, provide a good approximation of it. In particular we are interested in evolution equation for the amplitude of the first unstable mode, i.e. the evolution equation for the term $A_1^{(1)}$. From now on let us use the notation

$$A \equiv A_1^{(1)}.$$

We are then concerned with simplifying the equation

$$\frac{\mathrm{d}A}{\mathrm{d}t} = \sigma_1^{(1)}A + \sum_{i=1}^{+\infty}\sum_{j=1}^{+\infty}\sum_{n=-\infty}^{+\infty}\lambda_{n,1-n}^{i,j,1}A_n^{(i)}A_{1-n}^{(j)}. \tag{3.8}$$

3.1.3 The amplitude equation

Let us rewrite equation (3.8) in terms of the unstable mode A only (we are using the fact that $A_n^{(i)} = A_{-n}^{(i)}$)

$$\frac{\mathrm{d}A}{\mathrm{d}t} = \sigma_1^{(1)}A + \sum_{i=1}^{+\infty}\lambda_{0,1}^{i,1,1}A_0^{(i)}A + \sum_{j=1}^{+\infty}\lambda_{1,0}^{1,j,1}AA_0^{(j)} + \sum_{i=1}^{+\infty}\lambda_{2,-1}^{i,1,1}A_2^{(i)}A + \sum_{j=1}^{+\infty}\lambda_{-1,2}^{1,j,1}AA_2^{(j)} + \dots \tag{3.9}$$

We will ignore all the remaining terms. We see that the unstable mode is allowed to interact with modes 0 and 2 only. We would like to approximate the terms $A_0^{(k)}$ and $A_2^{(k)}$, $k \in \mathbb{N}$, by using equation (3.7) where we set $l = 0$ or $l = 2$, respectively.

Let us approximate the term $A_0^{(k)}$ first. Since the modes not equal to ± 1 are damped, we consider only stationary states for these modes. Ignoring all the terms not containing the unstable mode, (3.7) with $l = 0$ yields

$$0 = \sigma_0^{(k)} A_0^{(k)} + \sum_{i=1}^{+\infty}\sum_{j=1}^{+\infty} \lambda_{1,-1}^{i,j,k} A_1^{(i)} A_{-1}^{(j)} + \sum_{i=1}^{+\infty}\sum_{j=1}^{+\infty} \lambda_{-1,1}^{i,j,k} A_{-1}^{(i)} A_1^{(j)} + \dots$$

We can now express the term $A_0^{(k)}$ and further approximate it by setting $i, j = 1$

$$A_0^{(k)} = -\frac{1}{\sigma_0^{(k)}} \sum_{i=1}^{+\infty}\sum_{j=1}^{+\infty} \left(\lambda_{1,-1}^{i,j,k} A_1^{(i)} A_{-1}^{(j)} + \lambda_{-1,1}^{i,j,k} A_{-1}^{(i)} A_1^{(j)} \right) \approx -\frac{1}{\sigma_0^{(k)}} \left(\lambda_{1,-1}^{1,1,k} + \lambda_{-1,1}^{1,1,k} \right) A^2 \tag{3.10}$$

Similarly, to approximate the term $A_2^{(k)}$, we take (3.7) and set $l = 2$. Considering the stationary state only and ignoring the higher modes, we obtain

$$0 = \sigma_2^{(k)} A_2^{(k)} + \sum_{i=1}^{+\infty}\sum_{j=1}^{+\infty} \lambda_{1,1}^{i,j,k} A_1^{(i)} A_1^{(j)} + \dots$$

Finally, we arrive at

$$A_2^{(k)} = -\frac{1}{\sigma_2^{(k)}} \sum_{i=1}^{+\infty}\sum_{j=1}^{+\infty} \lambda_{1,1}^{i,j,k} A_1^{(i)} A_1^{(j)} \approx -\frac{1}{\sigma_2^{(k)}} \lambda_{1,1}^{1,1,k} A^2. \tag{3.11}$$

Putting the obtained approximations (3.10) and (3.11) back into (3.9) yeilds

$$\frac{\mathrm{d}A}{\mathrm{d}t} = \sigma_1^{(1)} A + \sum_{i=1}^{+\infty} -\frac{1}{\sigma_0^{(i)}} \left(\lambda_{1,-1}^{1,1,i} + \lambda_{-1,1}^{1,1,i} \right) \left(\lambda_{0,1}^{i,1,1} + \lambda_{1,0}^{1,i,1} \right) A^3 + \sum_{i=1}^{+\infty} -\frac{1}{\sigma_2^{(i)}} \lambda_{1,1}^{1,1,i} \left(\lambda_{2,-1}^{i,1,1} + \lambda_{-1,2}^{1,i,1} \right) A^3. \tag{3.12}$$

The equation above is the desired amplitude equation. By computing the non-linear coefficients and corresponding eigenvalues for a fixed slightly supercritical Ra we obtain the amplitude A of the unstable mode. We are going to derive this equation for extended Boussinesq approximation similarly. However, in the classical case we can simplify the coefficient of the cubic term using some properties of $\lambda_{n,l-n}^{i,j,k}$. Let us first derive these properties.

3.1.4 Properties of the non-linear coefficient $\lambda_{n,l-n}^{i,j,k}$

Property I

$$\boxed{\lambda_{n,l-n}^{i,j,k} \in \mathbb{R}.} \tag{3.13}$$

This follows easily from the definition of $\lambda_{n,l-n}^{i,j,k}$ and of the non-linear operator $\widetilde{\mathcal{N}}$ and the fact that $\theta_n^{(i)}$, $(\tilde{v}_n^{(i)})^{\hat{z}}$ are always real-valued and $(\tilde{v}_n^{(i)})^{\hat{x}}$ is always imaginary-valued. Since all the eigenvalues are real the coefficient of the cubic term A^3 is hence also real. Moreover, we expect it to be less than zero, i.e. we expect supercritical pitchfork bifurcation.

Property II

$$\boxed{\lambda^{i,j,k}_{n,l-n} = \lambda^{i,j,k}_{-n,-(l-n)}.} \tag{3.14}$$

Definition of $\lambda^{i,j,k}_{n,l-n}$ yields

$$\begin{aligned}
\overline{\lambda^{i,j,k}_{n,l-n}} &= |||\boldsymbol{\psi}^{(k)}_l|||^{-2}\overline{\langle\langle\widetilde{\mathcal{N}}(\boldsymbol{\psi}^{(i)}_n, \boldsymbol{\psi}^{(j)}_{l-n}), \boldsymbol{\psi}^{(k)}_l\rangle\rangle} \\
&= |||\boldsymbol{\psi}^{(k)}_l|||^{-2}\overline{\int_0^1 \left(-(v^{(i)}_n)^{\hat{x}}\mathrm{i}(l-n)a\boldsymbol{\psi}^{(j)}_{l-n} - (v^{(i)}_n)^{\hat{z}}\frac{\mathrm{d}\boldsymbol{\psi}^{(j)}_{l-n}}{\mathrm{d}z}\right)\cdot\overline{\boldsymbol{\psi}^{(k)}_l}\,\mathrm{d}z} \\
&= |||\boldsymbol{\psi}^{(k)}_l|||^{-2}\int_0^1 \left(-(v^{(i)}_{-n})^{\hat{x}}\mathrm{i}[-(l-n)]a\boldsymbol{\psi}^{(j)}_{-(l-n)} - (v^{(i)}_{-n})^{\hat{z}}\frac{\mathrm{d}\boldsymbol{\psi}^{(j)}_{-(l-n)}}{\mathrm{d}z}\right)\cdot\overline{\boldsymbol{\psi}^{(k)}_{-l}}\,\mathrm{d}z \\
&= |||\boldsymbol{\psi}^{(k)}_{-l}|||^{-2}\langle\langle\widetilde{\mathcal{N}}(\boldsymbol{\psi}^{(i)}_{-n}, \boldsymbol{\psi}^{(j)}_{-(l-n)}), \boldsymbol{\psi}^{(k)}_{-l}\rangle\rangle = \lambda^{i,j,k}_{-n,-(l-n)}.
\end{aligned}$$

Property III

$$\boxed{\lambda^{i,j,k}_{0,n} = 0.} \tag{3.15}$$

By definition of $\lambda^{i,j,k}_{n,l-n}$ we have

$$\lambda^{i,j,k}_{0,n} = |||\boldsymbol{\psi}^{(j)}_n|||^{-2}\langle\langle\widetilde{\mathcal{N}}(\boldsymbol{\psi}^{(i)}_0, \boldsymbol{\psi}^{(j)}_n), \boldsymbol{\psi}^{(j)}_n\rangle\rangle.$$

Now, it suffices to realize that $\boldsymbol{\psi}^{(i)}_0$ makes the term vanish. Indeed, since the wavenumber is zero, horizontal velocity $(v^{(i)}_0)^{\hat{x}}$ must be zero and using the fact that the velocity field is divergence free, $(v^{(i)}_0)^{\hat{z}}$ must also be zero. Hence, from the definition of the operator $\widetilde{\mathcal{N}}$ we conclude (3.15).

Property IV

$$\boxed{\lambda^{i,j,k}_{2n,-n} = 0.} \tag{3.16}$$

Again, it suffices to show that

$$\langle\langle\widetilde{\mathcal{N}}(\boldsymbol{\psi}^{(i)}_{2n}, \boldsymbol{\psi}^{(j)}_{-n}), \boldsymbol{\psi}^{(k)}_n\rangle\rangle = 0.$$

We can write

$$\begin{aligned}
&\langle\langle\widetilde{\mathcal{N}}(\boldsymbol{\psi}^{(i)}_{2n}, \boldsymbol{\psi}^{(i)}_{-n}), \boldsymbol{\psi}^{(i)}_n\rangle\rangle \\
&= \int_0^1 \left((v^{(i)}_{2n})^{\hat{x}}nia\boldsymbol{\psi}^{(j)}_{-n} - (v^{(i)}_{2n})^{\hat{z}}\frac{\mathrm{d}\boldsymbol{\psi}^{(j)}_{-n}}{\mathrm{d}z}\right)\cdot\overline{\boldsymbol{\psi}^{(k)}_n}\,\mathrm{d}z \\
&= \int_0^1 \left((v^{(i)}_{2n})^{\hat{x}}nia\boldsymbol{\psi}^{(j)}_{-n} - (v^{(i)}_{2n})^{\hat{z}}\frac{\mathrm{d}\boldsymbol{\psi}^{(j)}_{-n}}{\mathrm{d}z}\right)\cdot\boldsymbol{\psi}^{(k)}_{-n}\,\mathrm{d}z \\
&= \int_0^1 \left((v^{(i)}_{2n})^{\hat{x}}nia\,\boldsymbol{\psi}^{(j)}_{-n}\cdot\boldsymbol{\psi}^{(k)}_{-n} - (v^{(i)}_{2n})^{\hat{z}}\frac{\mathrm{d}}{\mathrm{d}z}\left(\frac{1}{2}\boldsymbol{\psi}^{(j)}_{-n}\cdot\boldsymbol{\psi}^{(k)}_{-n}\right)\right)\mathrm{d}z.
\end{aligned}$$

Integrating by parts and using the divergence-free condition again yields

$$\begin{aligned}\langle\langle\widetilde{\mathcal{N}}(\boldsymbol{\psi}_{2n}^{(i)},\boldsymbol{\psi}_{-n}^{(i)}),\boldsymbol{\psi}_{n}^{(i)}\rangle\rangle &= \int_0^1\left((v_{2n}^{(i)})^{\hat{x}}nia\,\boldsymbol{\psi}_{-n}^{(j)}\cdot\boldsymbol{\psi}_{-n}^{(k)}+\frac{1}{2}\frac{\mathrm{d}(v_{2n}^{(i)})^{\hat{z}}}{\mathrm{d}z}\boldsymbol{\psi}_{-n}^{(j)}\cdot\boldsymbol{\psi}_{-n}^{(k)}\right)\mathrm{d}z\\ &= \int_0^1\left((v_{2n}^{(i)})^{\hat{x}}nia\,\boldsymbol{\psi}_{-n}^{(j)}\cdot\boldsymbol{\psi}_{-n}^{(k)}-nia(v_{2n}^{(i)})^{\hat{z}}\boldsymbol{\psi}_{-n}^{(j)}\cdot\boldsymbol{\psi}_{-n}^{(k)}\right)\mathrm{d}z\\ &= 0.\end{aligned}$$

Property V

$$\boxed{\lambda_{n,l-n}^{i,j,k}=-\frac{|||\boldsymbol{\psi}_{l-n}^{(j)}|||^2}{|||\boldsymbol{\psi}_{l}^{(k)}|||^2}\lambda_{-n,l.}^{i,k,j}} \tag{3.17}$$

Remembering the definition of $\lambda_{n,l-n}^{i,j,k}$, it suffices to show that

$$\langle\langle\widetilde{\mathcal{N}}(\boldsymbol{\psi}_{n}^{(i)},\boldsymbol{\psi}_{l-n}^{(j)}),\boldsymbol{\psi}_{l}^{(k)}\rangle\rangle=-\overline{\langle\langle\widetilde{\mathcal{N}}(\boldsymbol{\psi}_{-n}^{(i)},\boldsymbol{\psi}_{l}^{(k)}),\boldsymbol{\psi}_{l-n}^{(j)}\rangle\rangle}.$$

By definition of the inner product in $\widetilde{H}$ and the non-linear operator $\widetilde{\mathcal{N}}$ we have

$$\langle\langle\widetilde{\mathcal{N}}(\boldsymbol{\psi}_{n}^{(i)},\boldsymbol{\psi}_{l-n}^{(j)}),\boldsymbol{\psi}_{l}^{(k)}\rangle\rangle=\int_0^1\left(-(v_n^{(i)})^{\hat{x}}\mathrm{i}(l-n)a\boldsymbol{\psi}_{l-n}^{(j)}-(v_n^{(i)})^{\hat{z}}\frac{\mathrm{d}\boldsymbol{\psi}_{l-n}^{(j)}}{\mathrm{d}z}\right)\cdot\overline{\boldsymbol{\psi}_{l}^{(k)}}\,\mathrm{d}z.$$

This can be written in the form

$$\begin{aligned}&\langle\langle\widetilde{\mathcal{N}}(\boldsymbol{\psi}_{n}^{(i)},\boldsymbol{\psi}_{l-n}^{(j)}),\boldsymbol{\psi}_{l}^{(k)}\rangle\rangle\\ &=\int_0^1\left(-(v_n^{(i)})^{\hat{x}}\mathrm{i}(l-n)a\boldsymbol{\psi}_{l-n}^{(j)}\cdot\overline{\boldsymbol{\psi}_{l}^{(k)}}-(v_n^{(i)})^{\hat{z}}\frac{\mathrm{d}}{\mathrm{d}z}\left(\boldsymbol{\psi}_{l-n}^{(j)}\cdot\overline{\boldsymbol{\psi}_{l}^{(k)}}\right)+(v_n^{(i)})^{\hat{z}}\boldsymbol{\psi}_{l-n}^{(j)}\cdot\frac{\mathrm{d}\overline{\boldsymbol{\psi}_{l}^{(k)}}}{\mathrm{d}z}\right)\mathrm{d}z.\end{aligned}$$

Upon integrating by parts

$$\begin{aligned}&\langle\langle\widetilde{\mathcal{N}}(\boldsymbol{\psi}_{n}^{(i)},\boldsymbol{\psi}_{l-n}^{(j)}),\boldsymbol{\psi}_{l}^{(k)}\rangle\rangle\\ &=\int_0^1\left(-(v_n^{(i)})^{\hat{x}}\mathrm{i}(l-n)a\boldsymbol{\psi}_{l-n}^{(j)}\cdot\overline{\boldsymbol{\psi}_{l}^{(k)}}+\frac{\mathrm{d}(v_n^{(i)})^{\hat{z}}}{\mathrm{d}z}\boldsymbol{\psi}_{l-n}^{(j)}\cdot\overline{\boldsymbol{\psi}_{l}^{(k)}}+(v_n^{(i)})^{\hat{z}}\boldsymbol{\psi}_{l-n}^{(j)}\cdot\frac{\mathrm{d}\overline{\boldsymbol{\psi}_{l}^{(k)}}}{\mathrm{d}z}\right)\mathrm{d}z.\end{aligned}$$

The divergence-free condition $\boldsymbol{\delta}\cdot\boldsymbol{\psi}_n^{(i)}=0$ implies that $\frac{\mathrm{d}(v_n^{(i)})^{\hat{z}}}{\mathrm{d}z}=-\mathrm{i}na(v_n^{(i)})^{\hat{x}}$. Hence

$$\begin{aligned}&\langle\langle\widetilde{\mathcal{N}}(\boldsymbol{\psi}_{n}^{(i)},\boldsymbol{\psi}_{l-n}^{(j)}),\boldsymbol{\psi}_{l}^{(k)}\rangle\rangle\\ &=\int_0^1\left(-(v_n^{(i)})^{\hat{x}}\mathrm{i}(l-n)a\boldsymbol{\psi}_{l-n}^{(j)}\cdot\overline{\boldsymbol{\psi}_{l}^{(k)}}-\mathrm{i}na(v_n^{(i)})^{\hat{x}}\boldsymbol{\psi}_{l-n}^{(j)}\cdot\overline{\boldsymbol{\psi}_{l}^{(k)}}+(v_n^{(i)})^{\hat{z}}\boldsymbol{\psi}_{l-n}^{(j)}\cdot\frac{\mathrm{d}\overline{\boldsymbol{\psi}_{l}^{(k)}}}{\mathrm{d}z}\right)\mathrm{d}z.\end{aligned}$$

Tidying up yields the desired equivalence

$$\begin{aligned}\langle\langle\widetilde{\mathcal{N}}(\boldsymbol{\psi}_{n}^{(i)},\boldsymbol{\psi}_{l-n}^{(j)}),\boldsymbol{\psi}_{l}^{(k)}\rangle\rangle &= \int_0^1\left(-(v_n^{(i)})^{\hat{x}}\mathrm{i}la\boldsymbol{\psi}_{l-n}^{(j)}\cdot\overline{\boldsymbol{\psi}_{l}^{(k)}}+(v_n^{(i)})^{\hat{z}}\boldsymbol{\psi}_{l-n}^{(j)}\cdot\frac{\mathrm{d}\overline{\boldsymbol{\psi}_{l}^{(k)}}}{\mathrm{d}z}\right)\mathrm{d}z\\ &=\overline{\int_0^1\left((v_{-n}^{(i)})^{\hat{x}}\mathrm{i}la\overline{\boldsymbol{\psi}_{l-n}^{(j)}}\cdot\boldsymbol{\psi}_{l}^{(k)}+(v_{-n}^{(i)})^{\hat{z}}\overline{\boldsymbol{\psi}_{l-n}^{(j)}}\cdot\frac{\mathrm{d}\boldsymbol{\psi}_{l}^{(k)}}{\mathrm{d}z}\right)\mathrm{d}z}\\ &=-\overline{\langle\langle\widetilde{\mathcal{N}}(\boldsymbol{\psi}_{-n}^{(i)},\boldsymbol{\psi}_{l}^{(k)}),\boldsymbol{\psi}_{l-n}^{(j)}\rangle\rangle}.\end{aligned}$$

3.1.5 The amplitude equation for classical Boussinesq approximation

Firstly, upon using properties (3.15) and (3.16), the terms $\lambda_{0,1}^{i,1,1}$ and $\lambda_{2,-1}^{i,1,1}$ vanish from (3.12). Thus, we obtain

$$\frac{\mathrm{d}A}{\mathrm{d}t} = \sigma_1^{(1)} A + \sum_{i=1}^{+\infty} -\frac{1}{\sigma_0^{(i)}} \left(\lambda_{1,-1}^{1,1,i} + \lambda_{-1,1}^{1,1,i}\right) \lambda_{1,0}^{1,i,1} A^3 + \sum_{i=1}^{+\infty} -\frac{1}{\sigma_2^{(i)}} \lambda_{1,1}^{1,1,i} \lambda_{-1,2}^{1,i,1} A^3.$$

Property (3.17) applied on $\lambda_{1,0}^{1,i,1}$ and $\lambda_{-1,2}^{1,i,1}$ further yields

$$\frac{\mathrm{d}A}{\mathrm{d}t} = \sigma_1^{(1)} A + \sum_{i=1}^{+\infty} \frac{1}{\sigma_0^{(i)}} \frac{|||\boldsymbol{\psi}_0^{(i)}|||^2}{|||\boldsymbol{\psi}_1^{(1)}|||^2} \lambda_{-1,1}^{1,1,i} \left(\lambda_{1,-1}^{1,1,i} + \lambda_{-1,1}^{1,1,i}\right) A^3 + \sum_{i=1}^{+\infty} \frac{1}{\sigma_2^{(i)}} \frac{|||\boldsymbol{\psi}_2^{(i)}|||^2}{|||\boldsymbol{\psi}_1^{(1)}|||^2} (\lambda_{1,1}^{1,1,i})^2 A^3.$$

Finally, from property (3.14) applied on $\lambda_{-1,1}^{1,1,i}$ we obtain

$$\frac{\mathrm{d}A}{\mathrm{d}t} = \sigma_1^{(1)} A + \sum_{i=1}^{+\infty} \frac{2}{\sigma_0^{(i)}} \frac{|||\boldsymbol{\psi}_0^{(i)}|||^2}{|||\boldsymbol{\psi}_1^{(1)}|||^2} (\lambda_{1,-1}^{1,1,i})^2 A^3 + \sum_{i=1}^{+\infty} \frac{1}{\sigma_2^{(i)}} \frac{|||\boldsymbol{\psi}_2^{(i)}|||^2}{|||\boldsymbol{\psi}_1^{(1)}|||^2} (\lambda_{1,1}^{1,1,i})^2 A^3.$$

This can be written as

$$\frac{\mathrm{d}A}{\mathrm{d}t} = \sigma_1^{(1)} A + \Lambda_1 A^3, \tag{3.18}$$

where

$$\Lambda_1 = \sum_{i=1}^{+\infty} \frac{2}{\sigma_0^{(i)}} \frac{|||\boldsymbol{\psi}_0^{(i)}|||^2}{|||\boldsymbol{\psi}_1^{(1)}|||^2} (\lambda_{1,-1}^{1,1,i})^2 + \frac{1}{\sigma_2^{(i)}} \frac{|||\boldsymbol{\psi}_2^{(i)}|||^2}{|||\boldsymbol{\psi}_1^{(1)}|||^2} (\lambda_{1,1}^{1,1,i})^2.$$

We can see that Λ_1 is indeed negative (for small enough Rayleigh numbers so that eigenvalues $\sigma_0^{(i)}$ and $\sigma_2^{(i)}$ are negative) which means that there is a supercritical pitchfork bifurcation at Ra_{crit}.

Note that the use of equation (3.18) is limited – we can only evaluate Λ_1 for such Rayleigh numbers so that all the eigenvalues are negative except for $\sigma_1^{(1)}$ (we used this assumption in the derivation above). Thus, we need to find a second critical value of Rayleigh number for which $\sigma_0^{(1)}$ or $\sigma_2^{(1)}$ becomes positive (we will show that $\sigma_0^{(i)}$ is always negative for all $i \in \mathbb{N}$). We can then evaluate Λ_1 for Rayleigh numbers in between those two critical values. However, the influence of the eigenvalue $\sigma_2^{(1)}$ can be quite significant as it's getting near zero – this will be apparent in the case of extended Boussinesq approximation.

We are interested in evolution equation of the first unstable mode in the form of longitudinal rolls. The rolls are given by function $\boldsymbol{\psi}$

$$\boldsymbol{\psi}(t,x,z) = A(t)\boldsymbol{\psi}_1^{(1)}(z)e^{\mathrm{i}ax} + \overline{A(t)}\overline{\boldsymbol{\psi}_1^{(1)}(z)}e^{-\mathrm{i}ax}. \tag{3.19}$$

More specifically

$$\boldsymbol{\psi}(t,x,z) = 2A(t)\begin{bmatrix} \theta_1^{(1)}\cos(ax) \\ \mathrm{i}(v_1^{(1)})^{\hat{x}}\sin(ax) \\ (v_1^{(1)})^{\hat{z}}\cos(ax) \end{bmatrix}.$$

3.1.6 Normalization of the eigenfunctions

From the expansion (3.2) it is clear that for $i \in \mathbb{N}$ condition

$$\lim_{n\to+\infty} |||\boldsymbol{\psi}_n^{(i)}||| = 0,$$

must hold. Thus we cannot set $|||\boldsymbol{\psi}_n^{(i)}||| = 1$ for $i \in \mathbb{N}$ and $\forall n \in \mathbb{Z}$. However, we can set $|||\boldsymbol{\psi}_n^{(i)}||| = 1$ for every $i \in \mathbb{N}$ and for a finite number of indices n. Hence, let us use for $\forall i \in \mathbb{N}$ normalization

$$|||\boldsymbol{\psi}_0^{(i)}||| = |||\boldsymbol{\psi}_1^{(i)}||| = |||\boldsymbol{\psi}_2^{(i)}||| = 1. \tag{3.20}$$

We can then write the amplitude equation as

$$\frac{\mathrm{d}A}{\mathrm{d}t} = \sigma_1^{(1)}A + \Lambda_1 A^3, \tag{3.21}$$

where

$$\Lambda_1 := \sum_{i=1}^{+\infty} \frac{2}{\sigma_0^{(i)}}(\lambda_{1,-1}^{1,1,i})^2 + \frac{1}{\sigma_2^{(i)}}(\lambda_{1,1}^{1,1,i})^2,$$

and

$$\lambda_{1,-1}^{1,1,i} = \langle\langle\widetilde{\mathcal{N}}(\boldsymbol{\psi}_1^{(1)}, \boldsymbol{\psi}_{-1}^{(1)}), \boldsymbol{\psi}_0^{(i)}\rangle\rangle,$$
$$\lambda_{1,1}^{1,1,i} = \langle\langle\widetilde{\mathcal{N}}(\boldsymbol{\psi}_1^{(1)}, \boldsymbol{\psi}_1^{(1)}), \boldsymbol{\psi}_2^{(i)}\rangle\rangle.$$

3.1.7 Numerical results

The numerical model from the second chapter give us eigenvalues $\sigma_1^{(i)}$ and eigenvectors $\boldsymbol{\psi}_1^{(i)}$ (after computing the x-component of velocity from the z-component). For $n \neq 0$ we can obtain all the remaining eigenfunctions simply by substituting a by na in eigenvalue problem (2.44).

As for the case of $n = 0$, let us set $a = 0$ in (2.44). Then the problem is reduced to the following system of equations

$$\frac{\sigma}{Pr}\frac{\mathrm{d}^2\tilde{v}^{\hat{z}}}{\mathrm{d}z^2} = \frac{\mathrm{d}^4\tilde{v}^{\hat{z}}}{\mathrm{d}z^4}, \qquad \sigma\tilde{\theta} = -\tilde{v}^{\hat{z}} + \frac{\mathrm{d}^2\tilde{\theta}}{\mathrm{d}z^2},$$

with either free-slip

$$\tilde{v}^{\hat{z}}\big|_{z=0,1} = \left.\frac{\mathrm{d}^2\tilde{v}^{\hat{z}}}{\mathrm{d}z^2}\right|_{z=0,1} = 0, \quad \tilde{\theta}\Big|_{z=0,1} = 0,$$

or no-slip boundary conditions

$$\tilde{v}^{\hat{z}}\big|_{z=0,1} = \left.\frac{\mathrm{d}\tilde{v}^{\hat{z}}}{\mathrm{d}z}\right|_{z=0,1} = 0, \quad \tilde{\theta}\Big|_{z=0,1} = 0.$$

Since the the horizontal velocity must be zero (due to $a = 0$) and the velocity field is divergence-free, the vertical component of velocity must be also zero. Hence, from the second equation above, after substituting by $\tilde{v}^{\hat{z}} = 0$, we easily obtain for both types of boundary conditions the eigenvalues $\sigma_0^{(k)}$ and corresponding eigenfunctions $\boldsymbol{\psi}_0^{(k)}$ (properly normed)

$$\sigma_0^{(k)} = -k^2\pi^2, \qquad \boldsymbol{\psi}_0^{(k)} = \begin{bmatrix} \sqrt{2Ra_s^{-1}}\sin(k\pi z) \\ 0 \\ 0 \end{bmatrix}.$$

Free-slip

Firstly, we know from the analytical approach that the eigenfunctions of the modes ± 1 can be written as

$$\boldsymbol{\psi}_{\pm 1}^{(1)} = \begin{bmatrix} c_{1,\theta}^{(1)}\sin(\pi z) \\ \pm \mathrm{i}\frac{\pi}{a}c_{1,v^{\hat{z}}}^{(1)}\cos(\pi z) \\ c_{1,v^{\hat{z}}}^{(1)}\sin(\pi z) \end{bmatrix}, \tag{3.22}$$

where $c_{1,\theta}^{(1)}, c_{1,v^{\hat{z}}}^{(1)} \in \mathbb{R}$ are chosen appropriately so that (3.20) holds. Note that in the previous chapter we depicted the properly scaled eigenfunction $\boldsymbol{\psi}_1^{(1)}$ (along with $\boldsymbol{\psi}_1^{(2)}$) in Figure 2.4 for $Pr = 10^9$, $Ra = 1000$ and $a = a_{\mathrm{crit}} = 2.2214$.

Using (3.22) we can write the non-linear terms $\widetilde{\mathcal{N}}(\boldsymbol{\psi}_1^{(1)}, \boldsymbol{\psi}_{-1}^{(1)})$ and $\widetilde{\mathcal{N}}(\boldsymbol{\psi}_1^{(1)}, \boldsymbol{\psi}_1^{(1)})$ as

$$\widetilde{\mathcal{N}}(\boldsymbol{\psi}_1^{(1)}, \boldsymbol{\psi}_{-1}^{(1)}) = \begin{bmatrix} -\pi c_{1,\theta}^{(1)} c_{n,v^{\hat{z}}}^{(1)}\sin(2\pi z) \\ \mathrm{i}\frac{\pi^2}{a}(c_{1,v^{\hat{z}}}^{(1)})^2\cos(2\pi z) \\ -\pi(c_{1,v^{\hat{z}}}^{(1)})^2\sin(2\pi z) \end{bmatrix}, \qquad \widetilde{\mathcal{N}}(\boldsymbol{\psi}_1^{(1)}, \boldsymbol{\psi}_1^{(1)}) = \begin{bmatrix} 0 \\ \mathrm{i}\frac{\pi^2}{a}(c_{1,v^{\hat{z}}}^{(1)})^2 \\ 0 \end{bmatrix}.$$

Since

$$\lambda_{1,-1}^{1,1,i} = \langle\langle \widetilde{\mathcal{N}}(\boldsymbol{\psi}_1^{(1)}, \boldsymbol{\psi}_{-1}^{(1)}), \boldsymbol{\psi}_0^{(i)}\rangle\rangle = \int_0^1 -\sqrt{2Ra_s^{-1}}\pi c_{1,\theta}^{(1)} c_{1,v^{\hat{z}}}^{(1)}\sin(2\pi z)\sin(i\pi z)\,\mathrm{d}z,$$

we can see that the term $\lambda_{1,-1}^{1,1,i}$ is non-zero only for $i = 2$, in which case

$$\lambda_{1,-1}^{1,1,2} = -\frac{1}{2}\sqrt{2Ra_s^{-1}}\pi c_{1,\theta}^{(1)} c_{1,v^{\hat{z}}}^{(1)}.$$

The term $\lambda_{1,1}^{1,1,i}$ vanishes completely. Indeed, since we know that $(v_n^{(i)})^{\hat{z}} \sim \sin(k\pi z)$ for some $k \in \mathbb{N}$ and the velocity field is divergence free, it follows that $(v_n^{(i)})^{\hat{z}} \sim \cos(k\pi z)$ for some $k \in \mathbb{N}$. Hence for every $i \in \mathbb{N}$

$$\lambda_{1,1}^{1,1,i} = \langle\langle \widetilde{\mathcal{N}}(\boldsymbol{\psi}_1^{(1)}, \boldsymbol{\psi}_1^{(1)}), \boldsymbol{\psi}_2^{(i)} \rangle\rangle \sim \int_0^1 \cos(k\pi z)\,\mathrm{d}z = 0. \tag{3.23}$$

The amplitude equation for free-slip boundary condition thus simplifies substantially

$$\begin{aligned}\frac{\mathrm{d}A}{\mathrm{d}t} &= \sigma_1^{(1)} A + \frac{2}{\sigma_0^{(2)}} (\lambda_{1,-1}^{1,1,2})^2 A^3 \\ &= \sigma_1^{(1)} A - \frac{1}{4} Ra_s^{-1} (c_{1,\theta}^{(1)} c_{1,v^{\hat{z}}}^{(1)})^2 A^3.\end{aligned}$$

It can be shown analytically that for $Ra > 2Ra_{\mathrm{crit}}$ the eigenvalue $\sigma_2^{(1)}$ is positive and hence the use of amplitude equation is (at least formally) limited to the interval $Ra \in [\frac{27\pi^4}{4}, \frac{27\pi^4}{2}]$. We computed the coefficients $\sigma_1^{(1)}$, $c_{1,\theta}^{(1)}$, $c_{1,v^{\hat{z}}}^{(1)}$ for Ra in this interval using the numerical model from the previous chapter. In Figure 3.1 we depicted the stable solutions $|A|$ of the amplitude equation for different values of Pr.

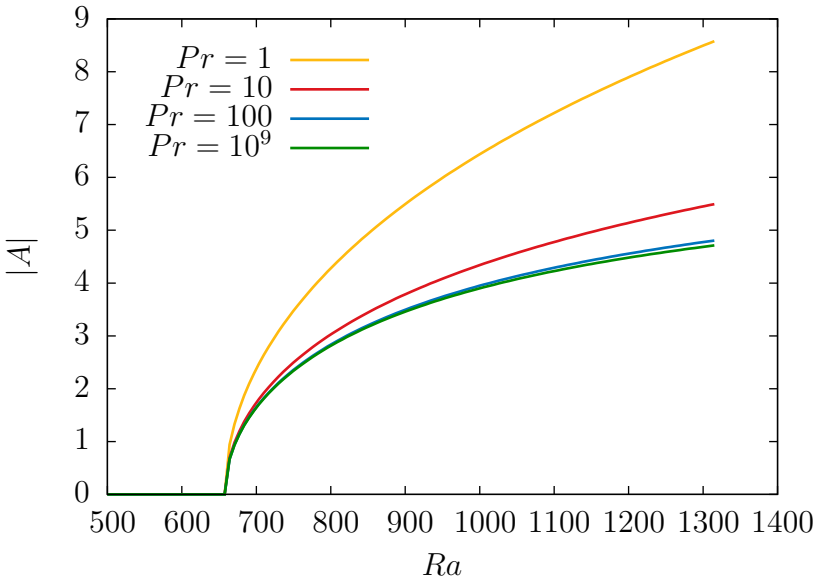

Figure 3.1: Stable solutions of amplitude equation for classical Boussinesq approximation, free-slip boundary conditions

After computing the amplitude A for specific supercritical value of Ra, we can portray the corresponding velocity and temperature field in the convection cell. This is shown in Figure 3.2 for $Pr = 10^9$ and $Ra = 1000$. The amplitude for such values is approximately $A = 3.900$.

Note: The velocity field is depicted mainly for qualitative evaluation and comparison with the extended Boussinesq approximation. We refrain from stating

the exact magnitude of the velocity vectors. However, we used the same scaling for all of the velocity field figures in this thesis to assure the comparison of their magnitudes.

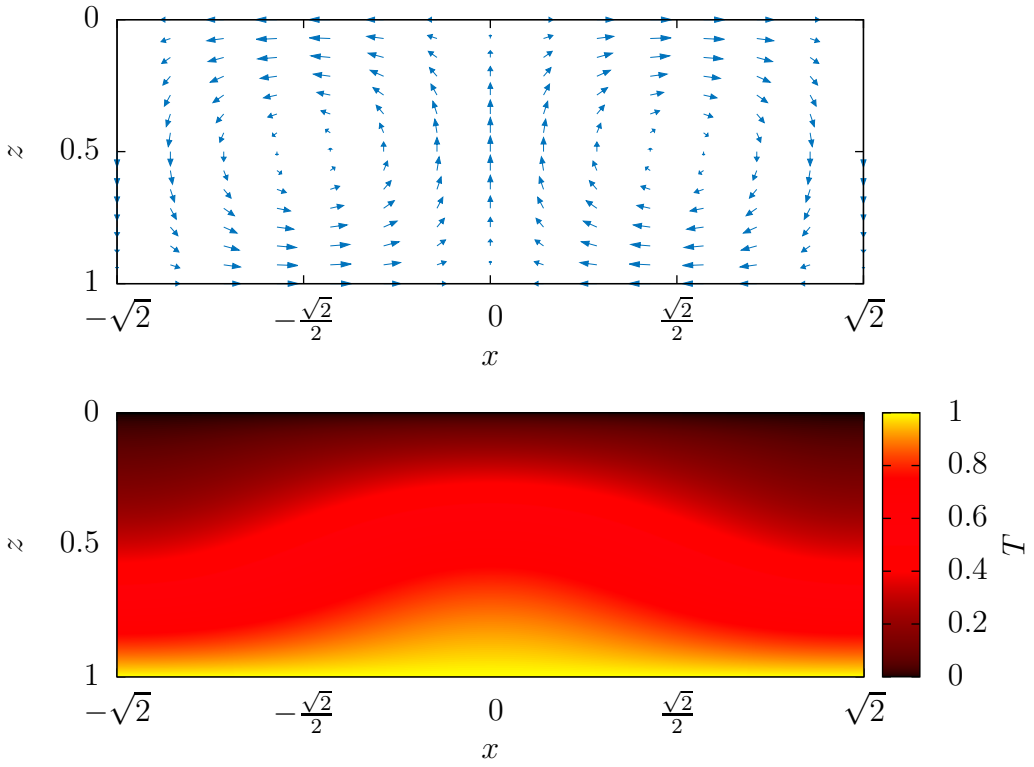

Figure 3.2: Convection cell for classical Boussinesq approximation and free-slip boundary condition in case of single rolls, $Pr = 10^9$, $Ra = 1000$

No-slip

For no-slip boundary conditions we don't have the analytical form of eigenfunctions as in the free-slip case and there will be no reduction of the infinite series in the term Λ_1. The evaluation of Λ_1 is thus slightly more complicated and we will have to truncate the series at $I_0 \in \mathbb{N}$, say.

We computed the required eigenvalues and eigenfunctions using the numerical model of the previous chapter (as an illustrative example we can see the properly scaled eigenfunctions $\boldsymbol{\psi}_1^{(1)}$ and $\boldsymbol{\psi}_1^{(2)}$ for $Pr = 10^9$, $Ra = 2400$ and $a = a_{\text{crit}} = 3.116$ in Figure 2.9).

For $Ra \approx 3715.777$ the eigenvalue $\sigma_2^{(1)}$ becomes positive and thus we can evaluate Λ_1 in the interval $[1707.762, 3715.777]$ only.

Table 3.1 shows the computed value of Λ_1 for different values of truncation level I_0. We can see that Λ_1 indeed converges to a finite value. To save computational time, for evaluating Λ_1 for many values of Ra we used the truncation level $I_0 = 12$ as the difference from $I_0 = 40$ is not very significant.

I_0	Λ_1
2	-0.44491135
4	-0.45161935
8	-0.45175444
12	-0.45175666
20	-0.45175685
40	-0.45175686

Table 3.1: Convergence of Λ_1 in terms of the truncation level I_0, no-slip boundary condition, $Pr = 10^9$, $Ra = 2400$, $a = a_{\text{crit}} = 3.116$

In Figure 3.3 we depicted the stable solutions $|A|$ of the amplitude equation for different values of Pr.

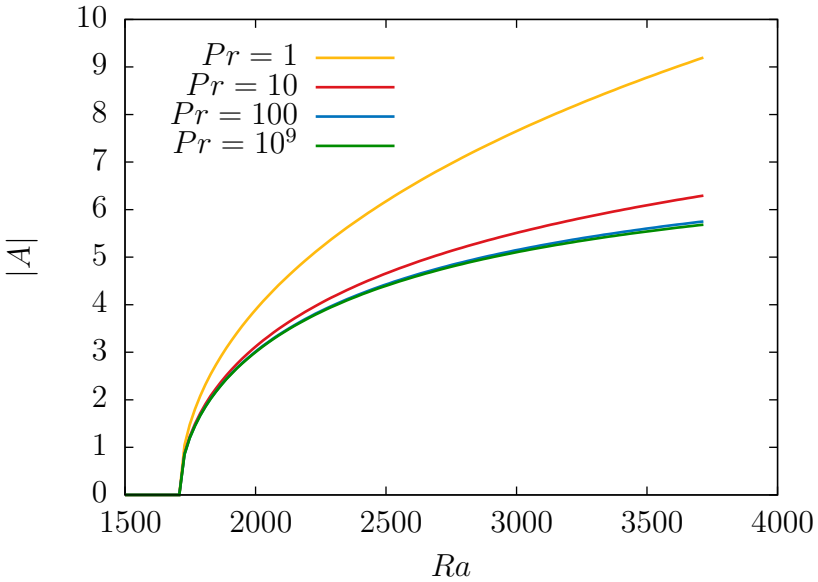

Figure 3.3: Stable solutions of amplitude equation for classical Boussinesq approximation, no-slip boundary conditions

We can portray the corresponding velocity and temperature field in the convection cell for specific supercritical Ra. This is shown in Figure 3.4 for $Pr = 10^9$ and $Ra = 2400$. The amplitude for such values is approximately $A = 4.201$.

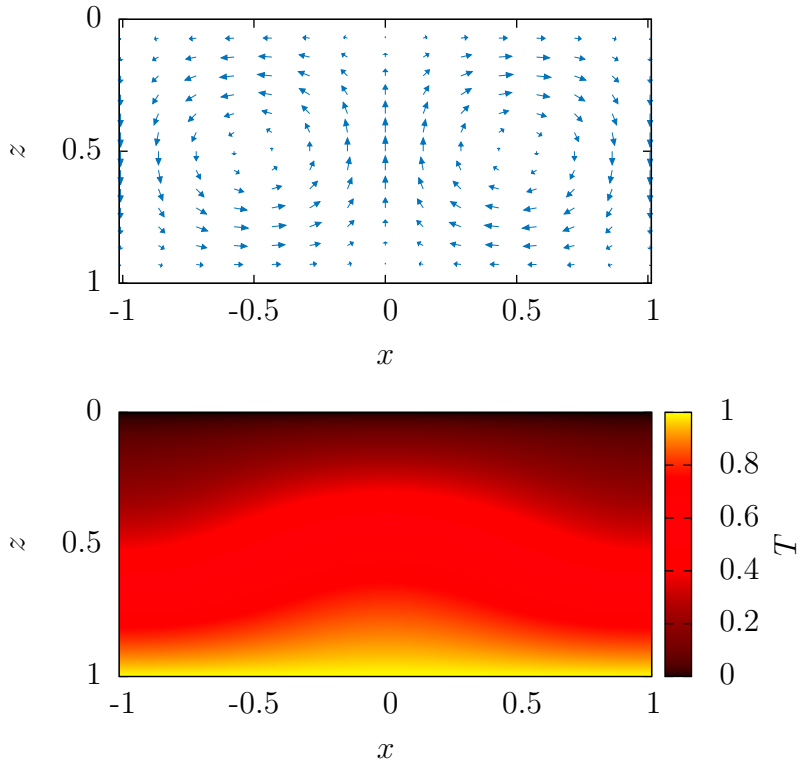

Figure 3.4: Convection cell for classical Boussinesq approximation and no-slip boundary condition, $Pr = 10^9$, $Ra = 2400$

3.2 Derivation of the amplitude equation for the extended Boussinesq approximation

Let us consider the extended Boussinesq approximation of the basic laws. In this case the perturbation equations read (see (2.55)–(2.57))

$$\operatorname{div} \mathbf{v} = 0,$$

$$\frac{1}{Pr_s}\left[\frac{\partial \mathbf{v}}{\partial t} + (\mathbf{v}\cdot\nabla)\,\mathbf{v}\right] = -Ra_s\alpha(z, T_0+\theta)\theta\mathbf{e}_{\hat{z}} - \nabla\pi + \operatorname{div}\left(\mu(z, T_0+\theta)\left[\nabla\mathbf{v} + (\nabla\mathbf{v})^T\right]\right),$$

$$\frac{\partial\theta}{\partial t} = \operatorname{div}\left[k(z, T_0+\theta)\nabla(T_0+\theta) - k(z, T_0)\nabla T_0\right] - v^{\hat{z}}\frac{\mathrm{d}T_0}{\mathrm{d}z} - \mathbf{v}\cdot\nabla\theta + Di_s\alpha(z, T_0+\theta)\left(T_0+\theta+\frac{Ra_s^{T_s}}{Ra_s}\right)v^{\hat{z}} + \frac{Di_s}{Ra_s}\mu(z, T_0+\theta)\left[\nabla\mathbf{v} + (\nabla\mathbf{v})^T\right] : \nabla\mathbf{v}.$$

We Taylor expand the material coefficients and keep the non-linearities of the second order only; we neglect all the higher terms. The system above is then transformed into

$$\operatorname{div} \mathbf{v} = 0,$$

$$\frac{1}{Pr_s}\left[\frac{\partial \mathbf{v}}{\partial t} + (\mathbf{v}\cdot\nabla)\,\mathbf{v}\right] = -Ra_s\left(\alpha(z,T_0) + \frac{\partial \alpha}{\partial T}(z,T_0)\theta\right)\theta \mathbf{e}_{\hat{z}} - \nabla\pi + \operatorname{div}\left(\left(\mu(z,T_0) + \frac{\partial \mu}{\partial T}(z,T_0)\theta\right)\left[\nabla\mathbf{v} + (\nabla\mathbf{v})^T\right]\right),$$

$$\frac{\partial \theta}{\partial t} = \operatorname{div}\left[k(z,T_0)\nabla\theta + \frac{\partial k}{\partial T}(z,T_0)\theta\nabla(T_0+\theta) + \frac{1}{2}\frac{\partial^2 k}{\partial T^2}(z,T_0)\theta^2\nabla T_0\right] - v^{\hat{z}}\frac{\mathrm{d}T_0}{\mathrm{d}z} - \mathbf{v}\cdot\nabla\theta + Di_s\alpha(z,T_0)\left(T_0+\theta+\frac{Ra_s^{T_s}}{Ra_s}\right)v^{\hat{z}} + Di_s\frac{\partial\alpha}{\partial T}(z,T_0)\left(T_0+\frac{Ra_s^{T_s}}{Ra_s}\right)\theta v^{\hat{z}} + \frac{Di_s}{Ra_s}\mu(z,T_0)\left[\nabla\mathbf{v} + (\nabla\mathbf{v})^T\right] : \nabla\mathbf{v}.$$

We can rewrite this in the form

$$\frac{\partial \boldsymbol{\psi}}{\partial t} = \mathcal{L}(Ra)(\boldsymbol{\psi}) - Pr\boldsymbol{\delta}\pi + \mathcal{N}(\boldsymbol{\psi},\boldsymbol{\psi}), \tag{3.24}$$

where

$$\boldsymbol{\psi} = \begin{bmatrix}\theta \\ v^{\hat{x}} \\ v^{\hat{z}}\end{bmatrix},$$

contains only divergence-free velocity field, i.e. $\boldsymbol{\delta}\cdot\boldsymbol{\psi} = 0$, $\mathcal{L}(Ra)$ denotes a linear operator

$$\mathcal{L} = \begin{bmatrix}L_{11} & 0 & L_{13} \\ 0 & L_{22} & L_{23} \\ L_{31} & 0 & L_{33},\end{bmatrix},$$

with

$$L_{11} = k(z,T_0)\Delta + \left(\frac{\mathrm{d}k}{\mathrm{d}z}(z,T_0) + \frac{\partial k}{\partial T}(z,T_0)\frac{\mathrm{d}T_0}{\mathrm{d}z}\right)\frac{\partial}{\partial z} + \frac{\mathrm{d}}{\mathrm{d}z}\left(\frac{\partial k}{\partial T}(z,T_0)\frac{\mathrm{d}T_0}{\mathrm{d}z}\right),$$

$$L_{13} = -\frac{\mathrm{d}T_0}{\mathrm{d}z} + Di_s\alpha(z,T_0)\left(T_0+\frac{Ra_s^{T_s}}{Ra_s}\right),$$

$$L_{22} = Pr_s\mu(z,T_0)\Delta + Pr_s\frac{\mathrm{d}\mu}{\mathrm{d}z}(z,T_0)\frac{\partial}{\partial z},$$

$$L_{23} = Pr_s\frac{\mathrm{d}\mu}{\mathrm{d}z}(z,T_0)\frac{\partial}{\partial x},$$

$$L_{31} = -Pr_s Ra_s\alpha(z,T_0),$$

$$L_{33} = Pr_s\mu(z,T_0)\Delta + 2Pr_s\frac{\mathrm{d}\mu}{\mathrm{d}z}(z,T_0)\frac{\partial}{\partial z},$$

and $\mathcal{N}$ denotes a quadratic non-linear operator

$$\mathcal{N}(\boldsymbol{\phi},\boldsymbol{\psi}) = \mathcal{N}\left(\begin{bmatrix}\theta_\phi \\ v_\phi^{\hat{x}} \\ v_\phi^{\hat{z}}\end{bmatrix}, \begin{bmatrix}\theta_\psi \\ v_\psi^{\hat{x}} \\ v_\psi^{\hat{z}}\end{bmatrix}\right) = \begin{bmatrix}N_1 \\ N_2 \\ N_3\end{bmatrix},$$

with

$$N_1 = -(\mathbf{v}_\phi \cdot \nabla)\theta_\psi + \operatorname{div}\left[\frac{\partial k}{\partial T}(z,T_0)\theta_\phi \nabla\theta_\psi + \frac{1}{2}\frac{\partial^2 k}{\partial T^2}(z,T_0)\nabla T_0\,\theta_\phi\theta_\psi\right] + Di_s\alpha(z,T_0)v_\phi^{\hat{z}}\theta_\psi + Di_s\frac{\partial\alpha}{\partial T}(z,T_0)\left(T_0 + \frac{Ra_s^{T_s}}{Ra_s}\right)v_\phi^{\hat{z}}\theta_\psi + \frac{Di_s}{Ra_s}\mu(z,T_0)[\nabla\mathbf{v}_\phi + (\nabla\mathbf{v}_\phi)^T] : \nabla\mathbf{v}_\psi$$

$$N_2 = -(\mathbf{v}_\phi \cdot \nabla)v_\psi^{\hat{x}} + Pr_s\left[\operatorname{div}\left(\frac{\partial\mu}{\partial T}(z,T_0)[\nabla\mathbf{v}_\phi + (\nabla\mathbf{v}_\phi)^T]\theta_\psi\right)\right]^{\hat{x}},$$

$$N_3 = -(\mathbf{v}_\phi \cdot \nabla)v_\psi^{\hat{z}} - Pr_s Ra_s\frac{\partial\alpha}{\partial T}(z,T_0)\theta_\phi\theta_\psi + Pr_s\left[\operatorname{div}\left(\frac{\partial\mu}{\partial T}(z,T_0)[\nabla\mathbf{v}_\phi + (\nabla\mathbf{v}_\phi)^T]\theta_\psi\right)\right]^{\hat{z}}.$$

3.2.1 Main issues

In the general case of all the coefficients being arbitrary functions of z and T, the formulae for operators $\mathcal{L}$ and $\mathcal{N}$ are quite long and untidy. However, we are interested in the six simple cases of only one of the material coefficients k, α and μ being a function of z, or T as stated in section 2.2.1. Thus, the corresponding operators simplify a little.

Even under these simplifications in none of the cases considered there is an inner product for which the linear operator $\mathcal{L}$ would be normal (let alone self-adjoint as for the classical Boussinesq approximation). Hence, we lose an important property of the eigenfunctions of the linear eigenvalue problem

$$\mathcal{L}(Ra)\boldsymbol{\psi}^{(i)} = \sigma^{(i)}\boldsymbol{\psi}^{(i)},$$

and that is that they form an orthogonal basis of the Hilbert space H (defined as in the case of the classical Boussinesq approximation). This will complicate the derivation and numerical evaluation of the amplitude equation. However, the numerical results show that for Prandtl numbers sufficiently large (greater than approximately 10^3) the eigenvalues of problem (2.74) are real and distinct. This leads us to the assumption that the eigenfunctions still form a complete set in H, i.e. an arbitrary function $\boldsymbol{\psi} \in H$ can be expanded in terms of $\boldsymbol{\psi}^{(i)}$.[2]

Then, as for the expansion into Fourier series and linear eigenfunctions, we can repeat the same steps as in the previous section. We will also be using the same notation and definition of the inner products and induced norms as in the classical case of Boussinesq approximation (see 3.1.1).

[2]We could also orthogonalize the presumably complete set $\{\boldsymbol{\psi}^{(i)}\}_{i=1}^{+\infty}$ to obtain an orthogonal complete set $\{\boldsymbol{\phi}^{(i)}\}_{i=1}^{+\infty}$ and consider the expansion in terms of the orthogonal functions $\boldsymbol{\phi}^{(i)}$. However, these functions are not the eigenfunctions of the operator $\mathcal{L}$ and that would cause more problems in deriving the amplitude equation than using the original non-orthogonal functions for the expansion.

3.2.2 Projection onto the eigenfunctions

As was mentioned above, we assume that we can expand any function $\boldsymbol{\psi}(t, \mathbf{x})$ into Fourier series and linear eigenfunctions as

$$\boldsymbol{\psi}(t, x, z) = \sum_{i=1}^{+\infty} \sum_{n=-\infty}^{+\infty} A_n^{(i)}(t) \boldsymbol{\psi}_n^{(i)}(z) e^{\mathrm{i}nax}, \tag{3.25}$$

where $A_{-n}^{(i)} = \overline{A_n^{(i)}}$ and $\boldsymbol{\psi}_{-n}^{(i)} = \overline{\boldsymbol{\psi}_n^{(i)}}$. Substituting this into (3.24) yields

$$\begin{aligned}\sum_{i=1}^{+\infty} \sum_{n=-\infty}^{+\infty} \frac{\mathrm{d}A_n^{(i)}}{\mathrm{d}t}(t) \boldsymbol{\psi}_n^{(i)}(z) e^{\mathrm{i}nax} = \sum_{i=1}^{+\infty} \sum_{n=-\infty}^{+\infty} A_n^{(i)}(t) \mathcal{L}\left(\boldsymbol{\psi}_n^{(i)}(z) e^{\mathrm{i}nax}\right) - Pr\boldsymbol{\delta}\pi \\ + \mathcal{N}\left(\sum_{i=1}^{+\infty} \sum_{n=-\infty}^{+\infty} A_n^{(i)}(t) \boldsymbol{\psi}_n^{(i)}(z) e^{\mathrm{i}nax}, \sum_{j=1}^{+\infty} \sum_{m=-\infty}^{+\infty} A_m^{(j)}(t) \boldsymbol{\psi}_m^{(j)}(z) e^{\mathrm{i}max}\right),\end{aligned} \tag{3.26}$$

Let us now take the inner product of the last equation with $\boldsymbol{\psi}_l^{(k)}(z) e^{\mathrm{i}lax}$, where $k \in \mathbb{N}$ and $l \in \mathbb{Z}$. Repeating the same steps as in the classical case, except for using the orthogonality of the eigenfunctions, we arrive at

$$\begin{aligned}\sum_{i=1}^{+\infty} \frac{\mathrm{d}A_l^{(i)}}{\mathrm{d}t} \langle\langle \boldsymbol{\psi}_l^{(i)}, \boldsymbol{\psi}_l^{(k)} \rangle\rangle = \sum_{i=1}^{+\infty} \sigma_l^{(i)} A_l^{(i)} \langle\langle \boldsymbol{\psi}_l^{(i)}, \boldsymbol{\psi}_l^{(k)} \rangle\rangle \\ + \sum_{i=1}^{+\infty} \sum_{j=1}^{+\infty} \sum_{n=-\infty}^{+\infty} A_n^{(i)} A_{l-n}^{(j)} \langle\langle \widetilde{\mathcal{N}}(\boldsymbol{\psi}_n^{(i)}, \boldsymbol{\psi}_{l-n}^{(j)}), \boldsymbol{\psi}_l^{(k)} \rangle\rangle,\end{aligned} \tag{3.27}$$

where $\widetilde{\mathcal{N}}$ is the Fourier transformed version of $\mathcal{N}$, i.e.

$$\widetilde{\mathcal{N}}(\boldsymbol{\psi}_n^{(i)}, \boldsymbol{\psi}_m^{(j)}) = \mathcal{N}(\boldsymbol{\psi}_n^{(i)}, \boldsymbol{\psi}_m^{(j)})\big|_{\frac{\partial}{\partial x}\boldsymbol{\psi}_n^{(i)} \to \mathrm{i}na\boldsymbol{\psi}_n^{(i)}, \frac{\partial}{\partial x}\boldsymbol{\psi}_m^{(i)} \to \mathrm{i}ma\boldsymbol{\psi}_m^{(i)}, \frac{\partial}{\partial z} \to \frac{\mathrm{d}}{\mathrm{d}z}}.$$

To be able to apply similar steps for deriving amplitude equation as in the previous section, we need to transform equation (3.27) into something similar to (3.7). To do so, let us restrict ourselves to a finite number of eigenfunctions (I_0, say). Equation (3.27) then reads

$$\begin{aligned}\sum_{i=1}^{I_0} \frac{\mathrm{d}A_l^{(i)}}{\mathrm{d}t} \langle\langle \boldsymbol{\psi}_l^{(i)}, \boldsymbol{\psi}_l^{(k)} \rangle\rangle = \sum_{i=1}^{I_0} \sigma_l^{(i)} A_l^{(i)} \langle\langle \boldsymbol{\psi}_l^{(i)}, \boldsymbol{\psi}_l^{(k)} \rangle\rangle \\ + \sum_{i=1}^{I_0} \sum_{j=1}^{I_0} \sum_{n=-\infty}^{+\infty} A_n^{(i)} A_{l-n}^{(j)} \langle\langle \widetilde{\mathcal{N}}(\boldsymbol{\psi}_n^{(i)}, \boldsymbol{\psi}_{l-n}^{(j)}), \boldsymbol{\psi}_l^{(k)} \rangle\rangle,\end{aligned}$$

This can also be written as

$$\mathbb{P}_l \frac{\mathrm{d}\mathbf{A}_l}{\mathrm{d}t} = \mathbb{P}_l \mathbb{D}_l \mathbf{A}_l + \sum_{i=1}^{I_0} \sum_{j=1}^{I_0} \sum_{n=-\infty}^{+\infty} A_n^{(i)} A_{l-n}^{(j)} \mathbf{N}_{n,l-n}^{i,j}, \tag{3.28}$$

where we introduced matrix $\mathbb{P}_l$ defined by

$$[\mathbb{P}_l]_{ki} = \langle\langle \boldsymbol{\psi}_l^{(i)}, \boldsymbol{\psi}_l^{(k)} \rangle\rangle,$$

diagonal matrix $\mathbb{D}_l$ with the diagonal entries $[\mathbb{D}_l]_{ii} = \sigma_l^{(i)}$ and vectors $\mathbf{A}_l$ and $\mathbf{N}_{n,l-n}^{i,j}$ defined by

$$[\mathbf{A}_l]_i = A_l^{(i)}, \qquad [\mathbf{N}_{n,l-n}^{i,j}]_k = \langle\langle \widetilde{\mathcal{N}}(\boldsymbol{\psi}_n^{(i)}, \boldsymbol{\psi}_{l-n}^{(j)}), \boldsymbol{\psi}_l^{(k)} \rangle\rangle.$$

The matrix $\mathbb{P}_l$ is in fact the Gramian matrix and since we assumed that the eigenfunctions are linearly independent, it is invertible.[3] Let us mention that since in all of the subsequent numerical computations $\mathbb{P}_l$ was non-singular, this is a confirmation that the linear independence of $\{\boldsymbol{\psi}^{(i)}\}_{i=1}^{+\infty}$ is a justifiable assumption.

Multiplying equation (3.28) by $\mathbb{P}_l^{-1}$ from the left yields

$$\frac{\mathrm{d}\mathbf{A}_l}{\mathrm{d}t} = \mathbb{D}_l \mathbf{A}_l + \sum_{i=1}^{I_0} \sum_{j=1}^{I_0} \sum_{n=-\infty}^{+\infty} A_n^{(i)} A_{l-n}^{(j)} \mathbb{P}_l^{-1} \mathbf{N}_{n,l-n}^{i,j},$$

which can be written component-wise as

$$\frac{\mathrm{d}A_l^{(k)}}{\mathrm{d}t} = \sigma_l^{(k)} A_l^{(k)} + \sum_{i=1}^{I_0} \sum_{j=1}^{I_0} \sum_{n=-\infty}^{+\infty} A_n^{(i)} A_{l-n}^{(j)} [\mathbb{P}_l^{-1} \mathbf{N}_{n,l-n}^{i,j}]_k.$$

If we introduce notation

$$\lambda_{n,l-n}^{i,j,k} \equiv [\mathbb{P}_l^{-1} \mathbf{N}_{n,l-n}^{i,j}]_k, \tag{3.29}$$

we can write the resulting equation in the form

$$\frac{\mathrm{d}A_l^{(k)}}{\mathrm{d}t} = \sigma_l^{(k)} A_l^{(k)} + \sum_{i=1}^{I_0} \sum_{j=1}^{I_0} \sum_{n=-\infty}^{+\infty} \lambda_{n,l-n}^{i,j,k} A_n^{(i)} A_{l-n}^{(j)}. \tag{3.30}$$

This is the equation which after repeating the same steps as in the classical case of Boussinesq approximation yields the amplitude equation in the form

$$\frac{\mathrm{d}A}{\mathrm{d}t} = \sigma_1^{(1)} A + \Lambda_1 A^3,$$

where

$$\Lambda_1 = \sum_{i=1}^{+\infty} -\frac{2}{\sigma_0^{(i)}} \lambda_{1,-1}^{1,1,i} \left(\lambda_{0,1}^{i,1,1} + \lambda_{1,0}^{1,i,1} \right) + \sum_{i=1}^{+\infty} -\frac{1}{\sigma_2^{(i)}} \lambda_{1,1}^{1,1,i} \left(\lambda_{2,-1}^{i,1,1} + \lambda_{-1,2}^{1,i,1} \right).$$

[3] Let us denote $V \equiv \mathrm{span}\{\boldsymbol{\psi}_l^{(1)}, \ldots, \boldsymbol{\psi}_l^{(n)}\}$. V is a finite-dimensional Hilbert space with the inner product $\langle\langle \cdot, \cdot \rangle\rangle$ and we can define the map $f : V \to \mathbb{R}^n$ via

$$f(v) = \begin{bmatrix} \langle\langle \boldsymbol{\psi}_l^{(1)}, v \rangle\rangle \\ \vdots \\ \langle\langle \boldsymbol{\psi}_l^{(n)}, v \rangle\rangle \end{bmatrix}, \qquad v \in V.$$

It follows easily that $\mathrm{Ker}\, f = \{0\}$ and hence the set of vectors $\{f(\boldsymbol{\psi}_l^{(1)}), \ldots, f(\boldsymbol{\psi}_l^{(n)})\} \subset \mathbb{R}^n$ is linearly independent. This implies that $\mathbb{P}_l = \left[f(\boldsymbol{\psi}_l^{(1)}), \ldots, f(\boldsymbol{\psi}_l^{(n)}) \right]$ is invertible.

The only difference is that this time the coefficient $\lambda_{n,l-n}^{i,j,k}$ given by (3.29) is quite complicated and in general it lacks the last three properties (3.15)–(3.17) which would simplify the term Λ_1. However, we can still show quite easily that $\lambda_{n,l-n}^{i,j,k} \in \mathbb{R}$, provided that the spectrum of the eigenvalue problem (2.74) is real and hence the eigenfunctions θ and $v^{\hat{z}}$ are real-valued. Also, property (3.14) still holds.

Again, let us mention that the use of the amplitude equation is limited to a certain interval of supercritical values of Rayleigh number. The influence of the eigenvalue $\sigma_2^{(1)}$ as it's getting smaller is quite significant compared to the classical case as we shall see on the examples below. Thus, Λ_1 can be evaluated formally for all Rayleigh numbers such that all the eigenvalues are negative except for $\sigma_1^{(1)}$, but we should always make a judicious estimate of its usage based on the shape of the obtained "pitchfork" curve of stable solutions.

3.2.3 Numerical results

For all the computations the value $Pr_s = 10^9$ was used to ensure the desired property of all the eigenvalues being real and distinct.

For $n \neq 0$ we can compute the eigenvalues $\sigma_n^{(k)}$ and eigenfunctions $\boldsymbol{\psi}_n^{(k)}$ directly using the numerical model of the previous chapter. Again, we simply put na instead of a in eigenvalue problem (2.74) and we compute the horizontal component of velocity from the divergence-free condition.

As for the case of $n = 0$, let us go back to eigenvalue problem (2.74) where we set $a = 0$. Then the problem is reduced to the following system of equations

$$\frac{\sigma}{Pr}\frac{\mathrm{d}^2\tilde{v}^{\hat{z}}}{\mathrm{d}z^2} = \mu(z,T_0)\frac{\mathrm{d}^4\tilde{v}^{\hat{z}}}{\mathrm{d}z^4} + 2\frac{\mathrm{d}\mu}{\mathrm{d}z}(z,T_0)\frac{\mathrm{d}^3\tilde{v}^{\hat{z}}}{\mathrm{d}z^3} + \frac{\mathrm{d}^2\mu}{\mathrm{d}z^2}(z,T_0)\frac{\mathrm{d}^2\tilde{v}^{\hat{z}}}{\mathrm{d}z^2},$$

$$\begin{aligned}\sigma\tilde{\theta} = &\left(-\frac{\mathrm{d}T_0}{\mathrm{d}z} + Di_s\alpha(z,T_0)\left(T_0 + \frac{Ra_s^{T_s}}{Ra_s}\right)\right)\tilde{v}^{\hat{z}} + k(z,T_0)\frac{\mathrm{d}^2\tilde{\theta}}{\mathrm{d}z^2} \\ &+ \left(\frac{\mathrm{d}k}{\mathrm{d}z}(z,T_0) + \frac{\partial k}{\partial T}(z,T_0)\frac{\mathrm{d}T_0}{\mathrm{d}z}\right)\frac{\mathrm{d}\tilde{\theta}}{\mathrm{d}z} + \frac{\mathrm{d}}{\mathrm{d}z}\left(\frac{\partial k}{\partial T}(z,T_0)\frac{\mathrm{d}T_0}{\mathrm{d}z}\right),\end{aligned}$$

with the free-slip boundary conditions being

$$\tilde{v}^{\hat{z}}\big|_{z=0,1} = \left.\frac{\mathrm{d}^2\tilde{v}^{\hat{z}}}{\mathrm{d}z^2}\right|_{z=0,1} = 0, \quad \tilde{\theta}\Big|_{z=0,1} = 0.$$

Since the horizontal velocity must be zero (due to $a = 0$) and the velocity field is divergence-free, the vertical component of velocity must be also zero. Hence, from the second equation above, after substituting by $\tilde{v}^{\hat{z}} = 0$, we obtain an eigenvalue problem for $\tilde{\theta}$

$$\sigma\tilde{\theta} = k(z,T_0)\frac{\mathrm{d}^2\tilde{\theta}}{\mathrm{d}z^2} + \left(\frac{\mathrm{d}k}{\mathrm{d}z}(z,T_0) + \frac{\partial k}{\partial T}(z,T_0)\frac{\mathrm{d}T_0}{\mathrm{d}z}\right)\frac{\mathrm{d}\tilde{\theta}}{\mathrm{d}z} + \frac{\mathrm{d}}{\mathrm{d}z}\left(\frac{\partial k}{\partial T}(z,T_0)\frac{\mathrm{d}T_0}{\mathrm{d}z}\right), \tag{3.31}$$

with homogeneous boundary conditions. For non-constant k, we solve this using the spectral method. For constant k, the problem reduces to the classical case of previous section and we have

$$\sigma_0^{(k)} = -k^2\pi^2, \qquad \boldsymbol{\psi}_0^{(k)} = \begin{bmatrix} \sqrt{2Ra_s^{-1}}\sin(k\pi z) \\ 0 \\ 0 \end{bmatrix}.$$

We are going to evaluate the term Λ_1 for various cases of material coefficients being non-constant. We have the critical values of wave-number and Rayleigh number from the previous chapter and we could investigate the supercritical behaviour of all of the cases covered in section 2.2.3. However, to save space, we only picked a few interesting examples – firstly, for the depth-dependent quantities we compare the supercritical behaviour of the classical Boussinesq approximation and of the extended one for $Di_s = 0$ and $Raq = 10^6$. In this case depicting the convection cells wouldn't be very informative as the velocity and temperature fields are only slightly different from the classical case. Thus, secondly, we depict one convection cell for each of the depth- and temperature-dependent material coefficients with dissipation and heat sources included. In this case the velocity and temperature fields are significantly different from the classical case (see Figure 3.2 for comparison).

To evaluate the coefficient Λ_1 we again extended the numerical code used in the second chapter. This time the implementation lied in tedious transcription of the unwieldy formulae for computing the non-linear coefficients $\lambda^{i,j,k}_{n,l-n}$ into the MATLAB code.

As for the evaluation itself, Table 3.2 shows the convergence of Λ_1 in terms of truncation level I_0 for depth-dependent k and dissipation and heat sources included (see the caption for details). Similar tables of convergence could be done for all the remaining cases. We can see that the convergence is not as fast as in the classical case for no-slip boundary conditions (see Table 3.1). However, to decrease the computational time, we again used the truncation level $I_0 = 12$ for all the evaluations, even though the precision is not as high as in the classical case.

I_0	Λ_1
2	−1.18219303
4	−2.32396270
8	−3.52020696
12	−3.44083661
20	−3.44074136
40	−3.44065954

Table 3.2: Convergence of Λ_1 in terms of the truncation level I_0, extended Boussinesq approximation and free-slip boundary condition, $k(z,T) = 1+5z$, $Pr_s = 10^9$, $Ra_s = 280\,000$, $Di_s = 0.5$, $Raq_s = 10^6$, $a = a_{\text{crit}} = 7.612$

We compute the term Λ_1 in appropriate intervals for which all the eigenvalues are negative expect for the first unstable mode. We refrain from listing all the critical values of Rayleigh number for which the eigenvalue $\sigma_2^{(1)}$ becomes positive – the values will be apparent from the appropriate figures.

Depth-dependent k

We assume that

$$k(z,T) = 1 + \tilde{b}_k z,$$

where $\tilde{b}_k \in \{1, 5, 10\}$.

Figure 3.5 shows the stable solutions of the amplitude equation where we excluded dissipation and heat sources so we could compare it to the classical Boussinesq approximation ($\tilde{b}_k = 0$). Note the influence of the eigenvalue $\sigma_2^{(1)}$ as it's getting smaller, i.e. Ra is getting closer to the second critical value when $\sigma_2^{(1)}$ becomes positive. We should use the amplitude equation for slightly supercritical values of Ra only and avoid the values for which the influence of the second mode becomes apparent.

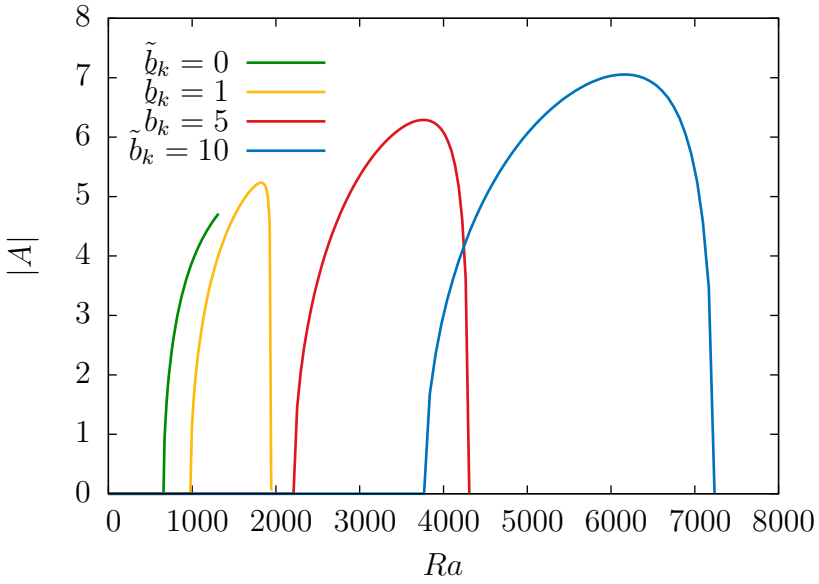

Figure 3.5: Extended Boussinesq approximation, free-slip boundary condition, $k(z,T) = 1 + \tilde{b}_k z$, $Pr_s = 10^9$, $Di_s = 0$, $Raq_s = 0$

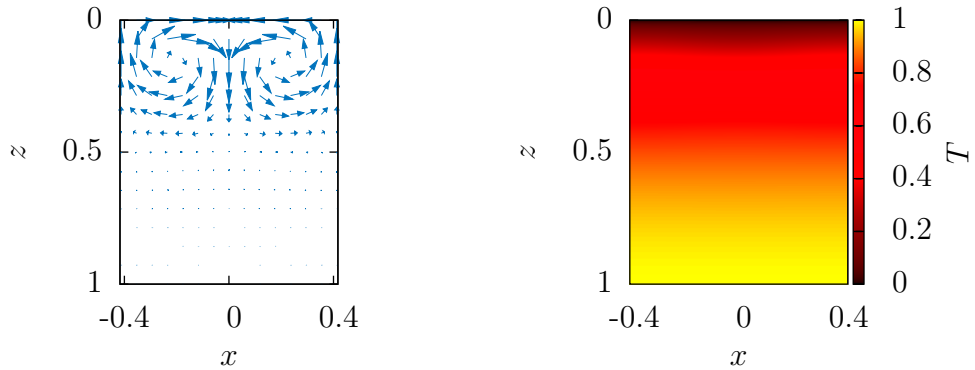

Figure 3.6: Convection cell for extended Boussinesq approximation and free-slip boundary condition, $k(z,T) = 1 + 5z$, $Pr_s = 10^9$, $Ra_s = 280\,000$, $Di_s = 0.5$, $Raq_s = 10^6$

In Figure 3.6 we depicted the velocity and temperature fields in convection cell for $\tilde{b}_k = 5$ and dissipation and heat sources included. In this case $a_{\text{crit}} = 7.612$ and $Ra_{\text{crit}} = 274\,150$. Note the different nature of the convection cell compared to the classical case depicted in Figure 3.2. The cell is narrower and the motion takes place mostly in the upper part of the layer.

Temperature-dependent k

We assume that

$$k(z,T) = \exp(-\tilde{c}_k Ra_s T),$$

where $\tilde{c}_k \in \{0.5 \times 10^{-7}, 1.0 \times 10^{-7}, 2.0 \times 10^{-7}\}$.

In Figure 3.7 we depicted the velocity and temperature fields in convection cell for $\tilde{c}_k = 1.0 \times 10^{-7}$ and dissipation and heat sources included. In this case $a_{\text{crit}} = 7.486$ and $Ra_{\text{crit}} = 181\,198$.

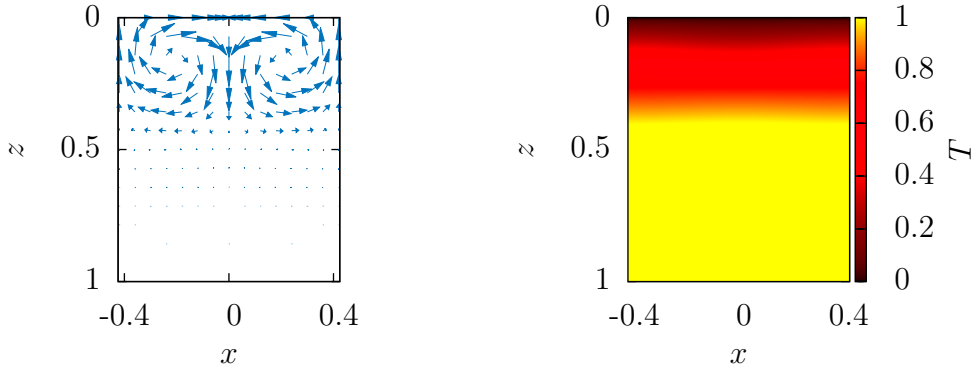

Figure 3.7: Convection cell for extended Boussinesq approximation and free-slip boundary condition, $k(z,T) = \exp(- \times 10^{-7} Ra_s T)$, $Pr_s = 10^9$, $Ra_s = 200\,000$, $Di_s = 0.5$, $Raq_s = 10^6$

Depth-dependent α

We assume that

$$\alpha(z,T) = \exp(-\tilde{b}_\alpha z),$$

where $\tilde{b}_\alpha \in \{0.5, 1.0, 2.0\}$.

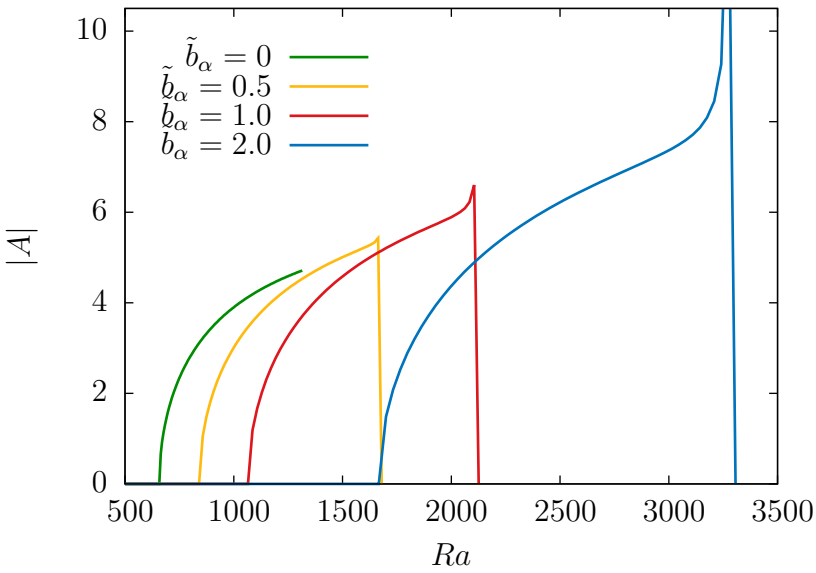

Figure 3.8: Extended Boussinesq approximation, free-slip boundary condition, $\alpha(z,T) = \exp(-\tilde{b}_\alpha z)$, $Pr_s = 10^9$, $Di_s = 0$, $Raq_s = 0$

Figure 3.8 shows the stable solutions of the amplitude equation where we excluded dissipation and heat sources so we could compare it to the classical Boussinesq approximation ($\tilde{b}_\alpha = 0$).

In Figure 3.9 we depicted the velocity and temperature fields in convection cell for $\tilde{b}_\alpha = 1$ and dissipation and heat sources included. In this case $a_{\text{crit}} = 6.694$ and $Ra_{\text{crit}} = 103\,769$.

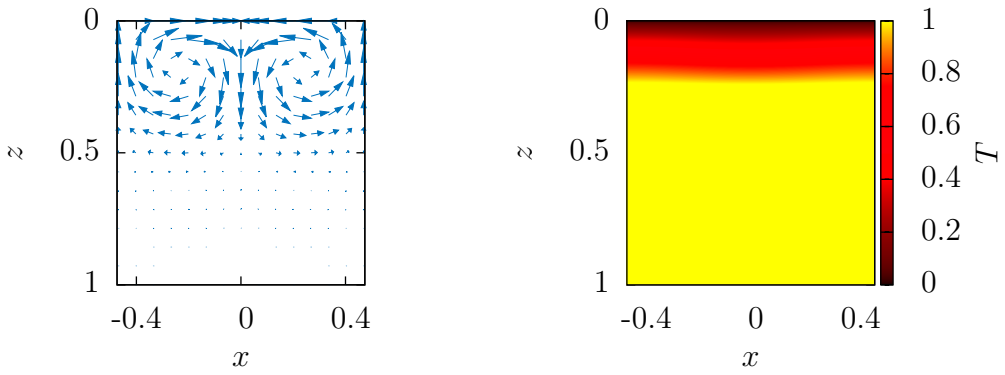

Figure 3.9: Convection cell for extended Boussinesq approximation and free-slip boundary condition, $\alpha(z,T) = \exp(-z)$, $Pr_s = 10^9$, $Ra_s = 120\,000$, $Di_s = 0.5$, $Raq_s = 10^6$

Depth-dependent μ

We assume that

$$\mu(z,T) = \exp(\tilde{b}_\mu z),$$

where $\tilde{b}_\mu \in \{1.0, 2.5, 4.5\}$.

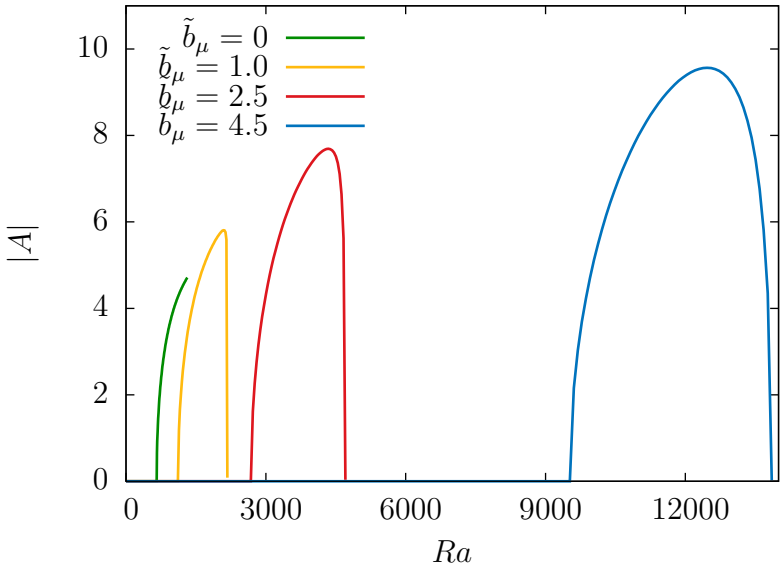

Figure 3.10: Extended Boussinesq approximation, free-slip boundary condition, $\mu(z,T) = \exp(\tilde{b}_\mu z)$, $Pr_s = 10^9$, $Di_s = 0$, $Raq_s = 0$

Figure 3.10 shows the stable solutions of the amplitude equation where we excluded dissipation and heat sources so we could compare it to the classical Boussinesq approximation ($\tilde{b}_\mu = 0$).

In Figure 3.9 we depicted the velocity and temperature fields in convection cell for $\tilde{b}_\mu = 1.0$ and dissipation and heat sources included. In this case $a_{\text{crit}} = 7.325$ and $Ra_{\text{crit}} = 186\,361$.

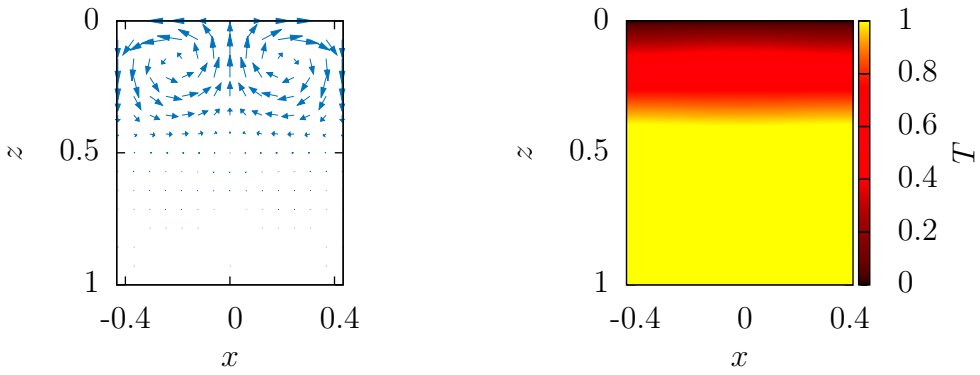

Figure 3.11: Convection cell for extended Boussinesq approximation and free-slip boundary condition, $\mu(z,T) = \exp(z)$, $Pr_s = 10^9$, $Ra_s = 200\,000$, $Di_s = 0.5$, $Raq_s = 10^6$

Temperature-dependent μ

We assume that

$$\mu(z,T) = \exp(-\tilde{c}_\mu Ra_s T),$$

where $\tilde{c}_\mu \in \{1.0 \times 10^{-7}, 2.5 \times 10^{-7}, 4.5 \times 10^{-7}\}$.

In Figure 3.9 we depicted the velocity and temperature fields in convection cell for $\tilde{c}_\mu = 2.5 \times 10^{-7}$ and dissipation and heat sources included. In this case $a_{\text{crit}} = 7.476$ and $Ra_{\text{crit}} = 177\,193$.

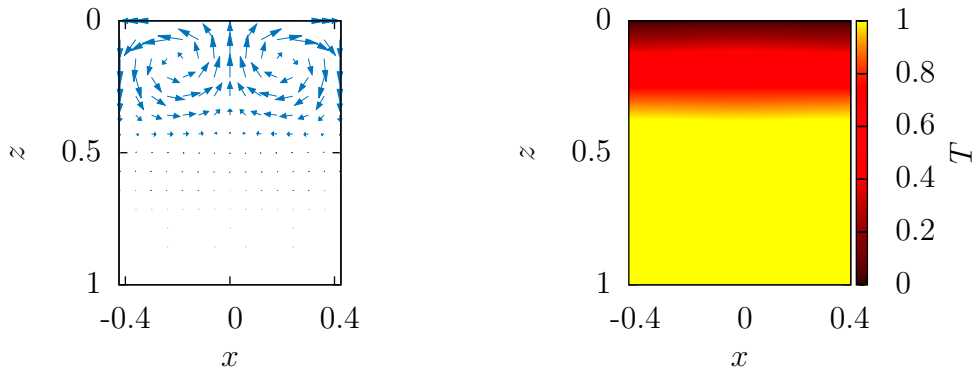

Figure 3.12: Convection cell for extended Boussinesq approximation and free-slip boundary condition, $\mu(z,T) = \exp(-2.5 \times 10^{-7} Ra_s T)$, $Pr_s = 10^9$, $Ra_s = 190\,000$, $Di_s = 0.5$, $Raq_s = 10^6$

3.3 Summary of Chapter 3

We derived the amplitude equation for the classical Boussinesq approximation in a two-dimensional layer following the works of Cross (1980) and Fujimura (1997) and we repeated the procedure for the extended Boussinesq approximation. However, we had to deal with a significant complication – the linearized operator corresponding to the extended Boussinesq approximation is not self-adjoint as in the classical case. Hence, the generalization is not trivial and relies on the completeness and linear independence of the operator's eigenfunctions. We verified the linear independence using the numerical computations only and did not proof the assertion analytically.

Numerical evaluation of the amplitude equation was done by extending the MATLAB program from the second chapter. The main part of the work lied in rewriting the unwieldy formulae of the non-linear operator to MATLAB code (especially in the case of the extended Boussinesq approximation).

For the classical Boussinesq approximation, we depicted the supercritical pitchfork bifurcation for various values of Prandtl number in the case of free-slip (Figure 3.1) and no-slip (Figure 3.3) boundary conditions. Corresponding convection cells (velocity and temperature fields) were portrayed in Figures 3.2 and 3.4.

For the extended Boussinesq approximation we depicted the supercritical pitchfork bifurcation for $Pr = 10^9$, free-slip boundary condition and various depth-dependent material coefficients (see Figures 3.5, 3.8 and 3.10). We also portrayed a few of the convection cells for a comparison with the classical case (see Figures 3.6, 3.7, 3.9, 3.11 and 3.12). The general trend is the same in all of the cases considered – the cells are narrower (which is due to the smaller value of wave-number), mass motion occurs mainly in the upper part of the cells and the temperature undergoes a significant change mainly in the upper part of the cells.

Chapter 4

Conclusion

We dealt with a generalized Rayleigh-Bénard problem. The standard approach assumes constant material parameters and does not take into account dissipation, adiabatic heating/cooling nor heat sources. Using the so called extended Boussinesq approximation we included these effects in the governing equations. The standard procedures examining the onset of convection and the supercritical regime of thermal convection were generalized for extended Boussinesq approximation. The material parameters used in our study are those approximately corresponding to the properties of the Earth's mantle.

Following the theory of linear stability analysis we linearized the governing equations in the vicinity of the basic state and we computed the spectrum of the corresponding linear operator. The computations were based on the discretization of the operator via the Chebyshev spectral collocation method. The critical Rayleigh number for the onset of convection was found in the extended as well as in the classical setting. The numerical results for the classical case are in accordance with the analytical ones which can be found in literature, e.g. see Chandrasekhar (1961). The results for the extended case are covered in sections 2.2.4, 2.2.5 nad 2.2.6 of Chapter 2. The main difference from the classical case is caused by the presence of adiabatic heating/cooling which significantly raises the critical threshold of convection. For a summary of the obtained results see section 2.3.

We further investigated the qualitative characteristics of the thermal convection for slightly supercritical values of Rayleigh number in a two-dimensional setting (we did not aim at a direct numerical simulation of convection). Via the weakly non-linear analysis we derived the amplitude equation for classical Boussinesq approximation following the works of Cross (1980) and Fujimura (1997) and we evaluated the corresponding coefficient of the amplitude equation for various combinations of Rayleigh and Prandtl numbers. We also identified the dominant velocity and temperature fields in the supercritical regimes (see section 3.1.7). The necessary computations were done in MATLAB, using again the Chebyshev spectral collocation method.

Generalizing of the weakly non-linear analysis for the case of the extended Boussi-

nesq approximation was not straightforward and we had to deal with the fact that the linearized operator is not self-adjoint and hence the eigenfunctions do not form an orthonormal basis. We overcame this difficulty with the assumption that the eigenfunctions form a complete and linearly independent set. This assumption was not verified analytically. However, strong numerical evidence supporting the assumption of the linear independence of the eigenfunctions was obtained. We then derived an amplitude equation for the extended Boussinesq approximation and evaluated the corresponding coefficient of the amplitude equation. We were hence able to identify the convection cells in the supercritical regimes for various combinations of the material dependences with the effects of dissipation, adiabatic cooling/heating and heat sources (see section 3.1.7). The dominating convection patterns substantially differ from the standard ones. For a summary of the obtained results for the weakly non-linear analysis see 3.3.

4.1 Open problems

Let us discuss the main issues that were left unresolved

- For the sake of simplicity we assumed exponential (or linear) profile of the material parameters. Even though we used values that roughly correspond to the data known about the Earth's mantle, the actual dependences are far more complicated and due to the phase changes even discontinuous. It would not be possible to implement such discontinuous behaviour in the Chebyshev method since it assumes smooth enough data.
- The derivation of the amplitude equation for the extended Boussinesq approximation was not rigorous because we did not formally prove that the eigenfunctions of the linearized operator form a complete and linearly independent set. Our assumption was based on the numerical results only – the eigenvalues were distinct and real for high enough Prandtl numbers (approximately 10^3).

Overall, the assumed simple depth- or temperature-dependent profile of material parameters was shown to substantially influence the character of convection. Consequently, it is desirable to further investigate the influence of material parameters with the actual depth-temperature-dependence seen in the Earth's mantle.

Bibliography

John P. Boyd. *Chebyshev and Fourier spectral methods*. Dover Publications Inc., Mineola, NY, second edition, 2001. ISBN 0-486-41183-4.

S. Chandrasekhar. *Hydrodynamic and Hydromagnetic Stability*. Oxford University Press, 1961. ISBN 9780198512370.

M. C. Cross. Derivation of the amplitude equation at the Rayleigh-Bénard instability. *Physics of Fluids*, 23:1727–1731, 1980.

M. C. Cross and P. C. Hohenberg. Pattern formation outside of equilibrium. *Rev. Mod. Phys.*, 65(3):851, 1993. doi: 10.1103/RevModPhys.65.851.

K. Fujimura. Centre manifold reduction and the Stuart-Landau equation for fluid motions. *Proceedings of the Royal Society of London A: Mathematical, Physical and Engineering Sciences*, 453:181–203, 1997.

P. Olson G. Schubert, D. L. Turcotte. *Mantle Convection in the Earth and Planets*. Cambridge Monographs on Mechanics. Cambridge University Press, 2001. ISBN 9780511612879.

H. Haken. *Synergetics, an Introduction: Nonequilibrium Phase Transitions and Self-Organization in Physics, Chemistry, and Biology*. Springer Series in Synergetics 1. Springer-Verlag Berlin Heidelberg, 3 edition, 1983. ISBN 978-3-642-88340-8.

G. Hirth and D. Kohlstedt. Rheology of the upper mantle and the mantle wedge: A view from the experimentalists. *Geophysical Monograph, 138: Inside the Subduction Factory*, pages 83–105, 2003.

M. Kameyama, D. A. Yuen, and S.-I. Karato. Thermal-mechanical effects of low-temperature plasticity (the Peierls mechanism) on the deformation of a viscoelastic shear zone. *Earth and Planetary Science Letters*, 168:159–172, 1999.

C. Matyska and D. A. Yuen. Lower mantle material properties and convection models of multiscale plumes. *Geological Society of America Special Papers*, pages 137–163, 2007.

Alan C. Newell and J. A. Whitehead. Finite bandwidth, finite amplitude convection. *Journal of Fluid Mechanics*, 38:279–303, 1969. ISSN 1469-7645.

S. C. Reddy and J. A. Weideman. A Matlab differentiation matrix suite. *Journal ACM Transactions on Mathematical Software*, 26:465–519, 2000.

J. T. Stuart. On the non-linear mechanics of hydrodynamic stability. *Journal of Fluid Mechanics*, 4:1–21, 1958.

N. Tosi, D. A. Yuen, N. de Koker, and R. M. Wentzcovitch. Mantle dynamics with pressure- and temperature-dependent thermal expansivity and conductivity. *Physics of the Earth and Planetary Interiors*, 217:48–58, 2013.

L. N. Trefethen. *Spectral Methods in Matlab*. SIAM: Society for Industrial and Applied Mathematics, 2001. ISBN 9780898714654.

H. Čížková, Arie P. van den Berg, W. Spakman, and C. Matyska. The viscosity of Earths lower mantle inferred from sinking speed of subducted lithosphere. *Physics of the Earth and Planetary Interiors*, 200201:56 – 62, 2012.

List of Figures

List of Tables